

The Synthesis and Characterization of Polystyrene Liquid Crystalline Siloxane Block Copolymers

By

Aaron Moment

Bachelor of Science, Chemical Engineering
Rensselaer Polytechnic Institute, Troy, NY, 1994

Master of Science in Chemical Engineering Practice
Massachusetts Institute of Technology, Cambridge, MA, 1996

SUBMITTED TO THE DEPARTMENT OF CHEMICAL ENGINEERING IN
PARTIAL FULFILLMENT OF THE REQUIREMENTS FOR THE DEGREE OF

DOCTOR OF PHILOSOPHY IN CHEMICAL ENGINEERING

AT THE

MASSACHUSETTS INSTITUTE OF TECHNOLOGY

FEBRUARY, 2000

© Massachusetts Institute of Technology – 2000

ARCHIVES

MASSACHUSETTS INSTITUTE
OF TECHNOLOGY

FEB 10 2000

LIBRARIES

Signature of Author: _____

Department of Chemical
Engineering
January 2000

Certified By: _____

Paula T. Hammond
Thesis Supervisor

Certified By: _____

Robert E. Cohen
St. Laurent Professor of Chemical Engineering
Chairman, Committee for Graduate Students

Acknowledgements

I would like to thank all those who helped me complete this thesis. My advisor Paula Hammond and the members of my thesis committee, Prof. Cohen, Prof. Thomas, and Prof. Merrill all provided me with valuable guidance, encouragement, and expertise. Special thanks to the support staff of the MIT Chemical Engineering Department, especially Elaine Aufiero, Janet Fischer, Tony Modestino, and Steve Wetzel for supporting me and my classmates throughout the years.

Ruben Miranda (an undergraduate UROP) worked with me on the synthesis of mesogens and their attachment to polymer backbones. Discussions with Anne Valerie Ruzette, a fellow graduate student, helped me understand some fundamental properties of the polymers I made. Chinedum Osuji helped with oscillatory shear experiments. And all the members of the Hammond Lab, past and present, were there in too many ways to list. Joe Adario and Peter Kloumann provided assistance with SAXS, and Mike Frongillo taught me TEM. The NSF provided most of the funding for this work. Finally, thanks to my family and friends for supporting me during my years at MIT.

Abstract

Diblock copolymers of polystyrene and side-chain liquid crystalline siloxanes have been prepared with a wide range of molecular weights (M_n total from 20,000 to 144,000) and liquid crystalline siloxane weight fractions (0.4 - 0.9). A new synthetic technique was developed to synthesize these materials, and is based on living anionic polymerization of a polystyrene-polyvinylmethysiloxane diblock copolymer followed by the attachment of side-chain mesogens to the siloxane via hydrosilylation chemistry. Two different types of block copolymers were prepared, each series having a different mesogen attached to the siloxane block. Both mesogens were selected to result in a smectic C* siloxane LCP block. Increasing the rigidity of the mesogen led to stronger microphase segregation between the PS and LCP blocks, and to a higher T_g and LC clearing point for the LCP block. Samples with large LCP weight fractions (>0.8) and low T_g ($< -25^\circ\text{C}$) LCP blocks were elastomeric at room temperature, presumably because of the high molecular weight (80-130K) and low T_g ($\sim -30^\circ\text{C}$) of the siloxane block. X-Ray measurements on these rubbery samples indicate that the mesogens orient perpendicular to the stretch direction. Mechano-optic effects were observed in these materials due to mesogen reorientation in a mechanical field. When stretched under crossed-polarizers, the optical textures could be dramatically altered, and in some cases light could be extinguished in particular regions of the film.

As the mesogen choice and the block lengths were varied, four types of morphologies were observed by TEM and SAXS: 1) alternating LCP and PS lamellae, 2) weakly ordered PS cylinders in a LCP matrix, 3) hexagonally packed PS cylinders in an LCP matrix, and 4) hexagonally packed LCP cylinders in a PS matrix. We found that the

length, rigidity, and chemical structure of the mesogen greatly influence the extent of phase segregation, the nature of the block copolymer interface, and the stability of the resulting LC phase.

The electro-optic properties of the LC block copolymers and their homopolymer analogues were studied, as the smectic C* phase is known to exhibit a fast bistable optical switching effect in the presence of an electric field. Electro-optic effects were found to be more facile in the homopolymers than in the block copolymers. Voltages as high as $\pm 30\text{V}/\mu\text{m}$ did not effect mesogen reorientation in the block copolymers from room temperature up to the LC clearing point. The homopolymers, on the other hand, were all electro-optically active at voltages not exceeding $\pm 10\text{V}/\mu\text{m}$, suggesting that the block copolymer morphology severely restricts the motion of the mesogens in an applied electric field.

Table of Contents

CHAPTER 1 INTRODUCTION AND BACKGROUND.....	11
1.1 BACKGROUND AND MOTIVATION	11
1.2 OBJECTIVES	12
1.3 SMALL MOLECULE LIQUID CRYSTALS AND THE SMECTIC C* PHASE.....	14
1.4 SIDE-CHAIN LC HOMOPOLYMERS	20
1.5 SSFLCS	21
1.6 SIDE-CHAIN LCP ELASTOMERS.....	22
1.7 AMORPHOUS-LCP BLOCK COPOLYMERS	24
1.8 DIBLOCK COPOLYMER MICROPHASE SEGREGATION	26
1.9 REFERENCES	28
CHAPTER 2 DESIGN AND SYNTHESIS.....	31
2.1 DESIGN OF LOW Tg LC BLOCK COPOLYMERS.....	31
2.2 EARLY SYNTHETIC ATTEMPTS	31
2.3 DESCRIPTION OF SYNTHETIC SCHEME	32
2.4 GENERAL PROCEDURE FOR POLYMER SYNTHESIS	33
2.5 INSTRUMENTATION.....	35
2.6 SYNTHESIS OF MESOGEN A.....	38
2.7 SYNTHESIS OF MESOGEN B	42
2.8 SYNTHESIS OF MESOGEN C.....	44
2.9 PS-PVMS BLOCK COPOLYMER SYNTHESIS	47
2.10 LCP SILOXANE HOMOPOLYMER SYNTHESIS	49
2.11 SUMMARY OF MATERIALS SYNTHESIZED.....	55
2.12 MOLECULAR WEIGHT DETERMINATION.....	58
2.12.1 A note about molecular weight measurements.....	60
2.13 REFERENCES	61
CHAPTER 3 MORPHOLOGY AND THERMAL PROPERTIES	63
3.1 BACKGROUND AND RELATED LITERATURE.....	63
3.2 EXPERIMENTAL.....	64
3.3 RESULTS AND DISCUSSION	66
3.4 MESOGEN A POLYMERS.....	66
3.5 MESOGEN B POLYMERS.....	86
3.6 APPENDIX: OSCILLATORY SHEAR OF PS39 – LCPA 30.....	93
3.7 CHAPTER 3 SUMMARY.....	95
3.8 REFERENCES	95
CHAPTER 4 ELECTRO-OPTIC AND MECHANO-OPTIC PROPERTIES OF LC HOMOPOLYMERS AND BLOCK COPOLYMERS.....	97
4.1 BACKGROUND AND MOTIVATION	97
4.2 EXPERIMENTAL.....	98
4.3 RESULTS AND DISCUSSION.....	99
4.4 MECHANO-OPTIC AND X-RAY STRETCHING INVESTIGATION OF MESOGEN A ELASTOMERS.....	107
4.5 CHAPTER 4 SUMMARY.....	114
4.6 REFERENCES	114
CHAPTER 5 BLENDS AND HOMOPOLYMER LC PROPERTIES.....	116
5.1 CONTEXT AND BACKGROUND	116
5.2 MIXTURES OF POLYSTYRENE WITH SMALL MOLECULE MESOGEN A'	116
5.3 MIXTURES OF POLYSTYRENE WITH LCPA 47.....	118

5.4	MIXTURES OF LC SILOXANES WITH SMALL MOLECULE MESOGEN.....	120
5.5	MIXTURES OF PS-LCP BLOCK COPOLYMERS WITH SMALL MOLECULE MESOGEN.....	121
5.6	THERMAL PROPERTIES OF LC HOMOPOLYMERS AND SMALL MOLECULE MESOGENS.....	122
5.7	CHAPTER 5 SUMMARY.....	125
5.8	REFERENCES	126
CHAPTER 6 CONCLUSIONS AND FUTURE DIRECTIONS.....		127
6.1	CONCLUSIONS.....	127
6.2	FUTURE DIRECTIONS	128
6.3	REFERENCES	130

Table of Figures

Figure 1.1 Schematic of poly(styrene-b-siloxane) liquid crystalline side-chain block copolymer. Rigid side-chain mesogens impart liquid crystallinity to the siloxane block.	14
Figure 1.2 Schematic of the molecules in a nematic liquid crystalline phase. The director is defined as the average direction in which the molecules align. The value theta varies for each molecule. Taken from 18.	16
Figure 1.3 Schematic of a chiral nematic liquid crystal. Taken from 19.	17
Figure 1.4 Schematic of smectic C and smectic A liquid crystal phases. The layers are perpendicular to the director in the smectic A phase, and are tilted with respect to the director in the smectic C phase. Taken from 18.	18
Figure 1.5 Schematic of the smectic C* phase. The planes represent the smectic layers. The director takes the same angle with respect each layer, but rotates around an axis normal to the layers. Taken from 18.	19
Figure 1.6 Triangular relationship between mesogen orientation, spontaneous polarization, and stress in smectic C* LC elastomers.	24
Figure 1.7 Equilibrium morphologies in AB diblock copolymers as the fraction of A block increases. Taken from A.S. Argon, R.E. Cohen, et al. 45.	26
Figure 1.8 The well known Liebler weak segregation phase diagram for AB diblock copolymers, taken from 50.	28
Figure 2.1 Two initial synthetic schemes towards α,ω difunctional siloxane side-chain LCPS using cationic and step-growth polymerization.	32
Figure 2.2 Synthetic route to polystyrene siloxane liquid crystalline block copolymers, using anionic polymerization followed by the attachment of side-chain mesogens via hydrosilylation.	36
Figure 2.3 Variation of synthetic route to polystyrene siloxane liquid crystalline block copolymers. THF is added along with D3 in order to accelerate the conversion from carbanion to siloxanolate anion. Rigorously speaking, the result is a triblock copolymer with a small PDMS block as the middle block.	37
Figure 2.4 Chemical structures of two mesogens used in the PS-LCP block copolymers. Mesogen B has a shorter alkyl spacer and a more rigid core.	38
Figure 2.5 Synthetic scheme to mesogen A. Mesogens B, C, and A' were synthesized with the same general scheme.	39
Figure 2.6 Chemical structure of mesogen A'. Synthesis is the same as for mesogen A, substituting pentamethyldisiloxane for tetramethyldisiloxane in the preparation of 4A. Mesogen A' has a single Sc* to isotropic transition at 26°C.	40
Figure 2.7 Chemical structure of mesogen C. Synthesis scheme is the same as that as that for mesogen A, substituting 3-bromo-1-propene for 8-bromo-1-octene in preparation of 2A, and 4'-hydroxy-4-biphenyl carboxylic acid for 4-hydroxybenzoic acid in preparation of 2A.	40
Figure 2.8 Anionic synthesis of siloxane side-chain LCP using a monofunctional initiator.	49
Figure 2.9 Anionic synthesis of PVMS using a difunctional initiator and endcapping agent.	51
Figure 2.10 Synthesis of VID2 monomer.	52
Figure 2.11 Repeat unit structure of LCPC 19. A PVMS backbone was synthesized substituting VID2 monomer for V3, using a difunctional initiator and a benzyl chloride end capping agent as shown in Figure 2.8.	55
Figure 2.12 1H NMR spectra of PS-PVMS block copolymer before mesogen attachment. The composition of this polymer is estimated from the labeled peaks. For this sample, PS Mn GPC = 14,100; Siloxane Mn GPC = 29,100; Siloxane Mn NMR = 21,200.	57
Figure 2.13 1H NMR spectra of PS 14 - LCPA 129 block copolymer after mesogen A attachment. The block copolymer substrate is the same as that shown in Figure 2.6.	59
Figure 3.1 OM image of PS 39 - LCPA 30 taken between crossed polarizers at room temperature.	68
Figure 3.2 DSC heating trace at 20°C/min of PS 14 - LCPA 129 showing two Tg's and a single smectic liquid crystalline clearing point.	69
Figure 3.3 Clearing point (°C) and smectic d-spacing (Å) vs. wt. fraction PS in LCPA block copolymers.	70

Figure 3.4 Clearing point ($^{\circ}\text{C}$) vs. % mesogen substitution in the LCP block.	71
Figure 3.5 Normalized clearing transition enthalpy ($SC^* - I$) in PS-LCP block copolymers vs. wt. fraction PS.	74
Figure 3.6 Normalized clearing point enthalpy vs. % mesogen substitution in LCPA block copolymers.	75
Figure 3.7 1D SAXS plot of $\log(I)$ vs. q (\AA^{-1}) for PS 39 - LCPA 30. Sample was toluene cast, then annealed at 80°C for 24hr. A first order peak at 286\AA and a second peak at 150\AA are observed. The morphology of the sample is lamellar as observed in TEM (Figure 3.5).	76
Figure 3.8 TEM image of PS 39 - LCPA 30.	77
Figure 3.9 Schematic of the morphology, and temperature path for morphology development in sample PS 39 - LCPA 30. The dimensions are estimates from the TEM image shown in Figure 3.6.	78
Figure 3.10 TEM image of PS 13 - LCPA 81.	80
Figure 3.11 TEM image of PS 14 - LCPA 129.	80
Figure 3.12 1D SAXS profiles of PS 13 - LCPA 81 and PS 14 - LCPA 129. Samples were cast from toluene and annealed at 90°C for 12 hr prior to X-ray measurements.	81
Figure 3.13 Experimentally determined phase diagram for polymers made with mesogen A.	85
Figure 3.14 1D and 2D SAXS patterns of PS 12 - LCPB 8 after casting from toluene and annealing at 110°C	88
Figure 3.15 TEM image of PS 12 - LCPB 8. The sample was toluene cast and annealed at 110°C overnight. The RuO ₄ stain is preferentially absorbed by the polystyrene, making these regions appear dark in the image. Also note the small grain sizes in this sample.	89
Figure 3.16 Schematic illustration of LCP cylinder morphology in PS 12 - LCPB 8. The cartoon is drawn approximately to scale.	89
Figure 3.17 1D SAXS plot for PS 14 - LCPB 111.	91
Figure 3.18 TEM image of PS 14 - LCPB 111. The sample was toluene cast and annealed at 110°C overnight. The RuO ₄ stain is preferentially absorbed by the polystyrene, making these regions appear dark in the image.	91
Figure 3.19 2D SAXS pattern of oriented sample of PS 39 - LCPA 30.	93
Figure 3.20 Integration of 1st order lamellar peak and 1st order smectic peak in the 2D SAXS pattern of PS 39 - LCPA 30 shown in Figure 3.18.	94
Figure 4.1 Ferroelectric bistable electro-optic switching of LCPA 47 at room temperature. The white arrow points to the same domain in both images.	100
Figure 4.2 Chemical structure of mesogen A', which has a Sc^* to isotropic transition at 26°C	100
Figure 4.3 Room temperature bistable switching of small molecule mesogen A' at room temperature. The white arrow points to the same domain, which switches from light to dark. Domains switch from light to dark in a well defined circular pattern.	102
Figure 4.4 Room temperature bistable switching of LCPC 19. Positive and negative voltages result in a region that is uniformly brighter than regions with no voltage. In the images above the light regions are treated with ITO, the dark regions are untreated.	104
Figure 4.5 Spontaneous polarizaion of two LCP siloxanes taken from the literature. These LCPs are analogous to LCP blocks used in this thesis and in Mao et al.'s demonstration of switching in amorphous-LCP block copolymers ¹⁰	106
Figure 4.6 Mechano-optic effect in PS 13 - LCPA 81, on stretching to 12.5% strain. The LC domains in this polydomain sample change color on stretching.	108
Figure 4.7 Optical microscope image of a mechano-optic effect in PS 14 - LCPA 129. The 0.25mm film was stretched to 8% strain between crossed polarizers; the result is the extinguishing of light.	109
Figure 4.8 Schematic of SAXS stretching experiments showing scattering pattern when mesogens are aligned a) perpendicular and b) parallel to the stretch direction.	110
Figure 4.9 SAXS scattering pattern and integration around the smectic peak in a stretched sample (20% strain) of PS 13 LCPA 81. The results indicate that the mesogens reorient perpendicular to the stretch direction.	110
Figure 4.10 Schematic illustrating that mesogen orientation perpendicular to the stretch direction is not uniquely specified. The angle theta in the figure can take any value between 0 and 2π	111
Figure 5.1 Schematic of polystyrene blended with mesogen A', forming a 2 phase system with LC droplets in equilibrium at room temperature with plasticized polystyrene.	118

Figure 5.2 DSC heating traces illustrating the miscibility of mesogen A' and its polymer analogue LCPA 47.	120
Figure 5.3 Table of some smectic C* LC siloxane homopolymers and their smectic clearing points.	123
Figure 5.4 LC clearing points of materials as they progress from vinyl mesogen to Si-H tipped mesogen, and finally to the side chain liquid crystalline siloxane homopolymer.	125

Table of Tables

Table 2.1 Summary of polymers made with mesogen A.....	56
Table 2.2 Polydispersity index of polymers made with mesogen A.....	56
Table 2.3 Summary of polymers made with mesogen B.....	57
Table 2.4 Polydispersity index of polymers made with mesogen B.....	57
Table 3.1 Molecular weight characterization of polymers made with mesogen A.....	67
Table 3.2 Thermal properties of polymers made with mesogen A. Values taken from DSC heating scans at 20°C/min heating rate.....	67
Table 3.3 SAXS and TEM observations of mesogen A containing polymers.....	73
Table 3.4 Comparison of TEM measured domain dimensions and theoretical domain dimensions for perfect segregation in PS 39 - LCPA 30.....	79
Table 3.5 Molecular weight characterization of mesogen B polymers.....	86
Table 3.6 Thermal properties of polymers made with mesogen B. Values taken from DSC heating scans at 20°C/ min.....	86
Table 3.7 Summary of SAXS and TEM observations of mesogen B containing polymers.....	92
Table 5.1 Thermal data before and after annealing a mixture of polystyrene (47wt%) and mesogen A' (53wt%).....	117
Table 5.2 Thermal properties of a 50/50 mixture of polystyrene and LCPA 47 before and after annealing treatments.....	119
Table 5.3 Thermal data and SAXS measurements of a mixture of mesogen A' and PS 39 – LCPA 30 compared to the pure block copolymer PS 39 – LCPA 30.....	122
Table 5.4 LC properties of mesogens and LC homopolymers.....	124

Chapter 1 Introduction and Background

1.1 Background and Motivation

AB diblock copolymers that contain a side-chain liquid crystalline block coupled to an amorphous block have become an active area investigation in the past several years¹⁻⁷, as they offer a unique combination of liquid crystalline and block copolymer properties. This combination is derived from the coexistence of block copolymer morphology and liquid crystallinity within the microphase segregated domains formed by the liquid crystalline block. Such materials have unique properties and ordered structures that are of scientific and technical interest. For example, these block copolymers form liquid crystalline films whose mechanical properties can be changed by varying the block sizes in the diblock copolymer. In addition, conventional thermal and solution processing techniques can be used to macroscopically orient the morphological elements in addition to the LC director. Because all applications of LC materials rely on controlling the orientation of the LC director, a strong motivation for amorphous-LCP diblocks is explore how block copolymer morphology can be used as an orienting tool for the liquid crystal domains.

Liquid crystalline blocks exhibiting the smectic C* phase are of particular interest^{5, 6}, as the block copolymer morphology can be used to stabilize the ferroelectric smectic C* phase⁸. The resulting materials exhibit the bistable electro-optic switching phenomena of small molecule Sc* and side-chain siloxane Sc* homopolymers, in addition to having the mechanical integrity and processability of block copolymers.

Thus, one can imagine using these materials as display elements, piezoelectric sensors, or as mechano-optic elements.

A number of traditional triblock and segmented copolymers exhibit elastomeric mechanical properties. Covalently crosslinked liquid crystalline siloxane networks have been studied extensively^{9, 10}, and continue to receive attention¹¹ as they show promise as piezo-elements¹² and mechano-optical systems. The incorporation of side chain mesogens within a phase segregated thermoplastic elastomer matrix should produce crystalline thermoplastic elastomers (LCTPE's) with unique mechano-optical properties, which can be altered and enhanced through processing. If a ferroelectric smectic C* mesogen is chosen, it should be possible to observe a response to electrical field with mechanical deformation in a well ordered sample; this sort of piezoelectric effect may provide a route to new electromechanical systems.

1.2 Objectives

The objectives of this thesis have been: 1) to prepare AB block copolymers where the A block is amorphous polystyrene and the B block is a side-chain Sc* liquid crystalline block whose T_g is well below room temperature; 2) to conduct conventional chemical, thermal, and morphological characterization of these polymers in order to establish their structure and phase behavior, and 3) to conduct electro-optic and mechano-optic measurements on some of these materials.

The successful synthesis of these AB block copolymers has provided an LC block whose mesogens are mobile at room temperature. Many of the reported PS-LCP diblocks have LCP block T_gs above or slightly below room temperature, making elastomers and room temperature electro-optic and ferroelectric properties impossible.

The materials synthesized for this thesis address this drawback by providing the lowest reported T_g for a side-chain LCP block. In addition, LCP siloxane homopolymers have been the most successful polymer analogues to small molecule LCs to date, precisely because of their low T_g which allows the mesogens mobility^{13, 14}.

A schematic of the block copolymer structure appears in Figure 1.1, showing an amorphous polystyrene block linked to a smectic liquid crystalline siloxane block with side chain mesogens attached. The side chain mesogens were chosen to effect the formation of the smectic C* liquid crystalline phase and hence yield electro-optic and ferroelectric properties. Because of their low T_g , the field dependent properties of liquid crystalline siloxanes, such as electro-optic switching, may be accessed at room temperature¹³⁻¹⁶. The low T_g of the siloxane block in the block copolymer also allows for the synthesis of soft rubbery materials when the siloxane volume fraction is high. When the polystyrene block is the majority block, hard films are formed.

Extension of the diblock system described here to PS-LCP-PS triblocks should give true liquid crystalline elastomers with non-covalent crosslinks. These materials would differ from the covalently crosslinked LC elastomers synthesized by Finkelmann¹⁰ in that the polystyrene domains would act as physical crosslinks, and the material could be solution and heat processed.

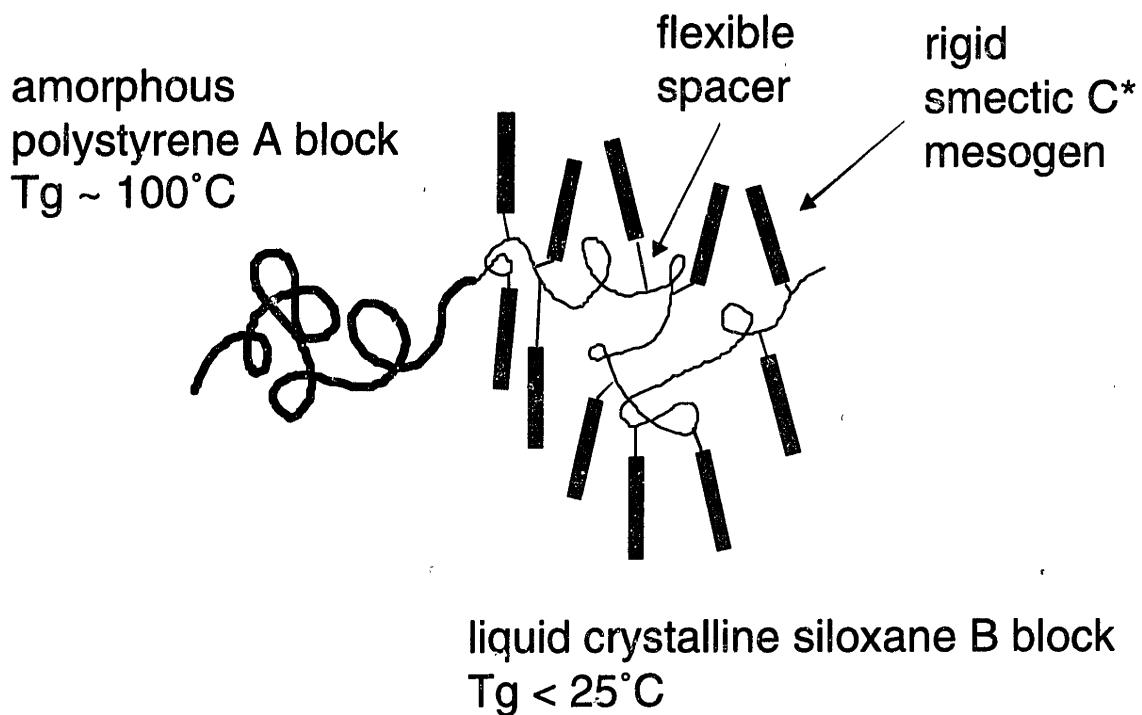


Figure 1.1 Schematic of poly(styrene-b-siloxane) liquid crystalline side-chain block copolymer. Rigid side-chain mesogens impart liquid crystallinity to the siloxane block.

1.3 Small molecule liquid crystals and the smectic C* phase

Organic molecules in crystalline solids are constrained to rest in fixed positions (positional order) and in addition are oriented with respect to one another (orientational order). Upon melting to an isotropic liquid, the molecules lose both their positional and orientational order. Some crystalline materials do not immediately melt to an isotropic liquid upon heating, but progress through various liquid crystalline phases before becoming an isotropic liquid. In the liquid crystalline phases, the molecules may maintain some time and space *average* positional and orientational order, but are not constrained in space and are free to move about similar to an isotropic liquid. In fact, small molecule liquid crystalline phases flow like liquids, but maintain some average molecular order.

The direction of preferred orientation in a liquid crystal is called the director. Molecules that possess rigid portions with high aspect ratios tend to form liquid crystals, and a small molecule known to be liquid crystalline is termed a mesogen.

Many different liquid crystalline phases are known to exist; all are characterized by the degree and nature of the molecular orientation and positional order. A single liquid crystalline substance may exhibit more than one liquid crystalline phase, depending on the temperature and/or composition. The simplest liquid crystalline phase is the *nematic* phase, in which the molecules tend to line up parallel to each other as shown in Figure 1.2. Each molecule has a vector associated with its orientation (at a fixed point in time), and the average of these vectors is the director. The degree of order in the sample is quantified by an order parameter, which takes a value between 1 and $-1/2$, and is defined as the average of $(3\cos^2\theta-1)/2$, where θ is the angle between a given molecule and the director¹⁷. An order parameter of 0 represents an isotropic collection of molecules, whereas a perfectly ordered sample has an order parameter of 1 or $-1/2$.

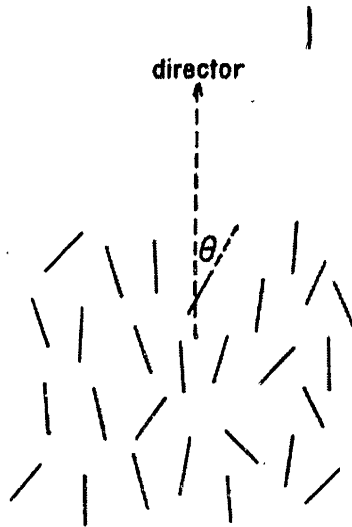


Figure 1.2 Schematic of the molecules in a nematic liquid crystalline phase. The director is defined as the average direction in which the molecules align. The value theta varies for each molecule. Taken from **18**.

An important variant of the nematic phase is the chiral nematic phase, in which the director rotates throughout the sample, as shown in Figure 1.3. The distance it takes for the director to make a full rotation is known as the pitch of the liquid crystal. Chiral nematics are formed by chiral molecules and the handedness of the helix is directly related to the handedness of the molecule. Many chiral nematics have pitches on the order of visible light, and therefore selectively reflect circularly polarized light of a given wavelength¹⁷.

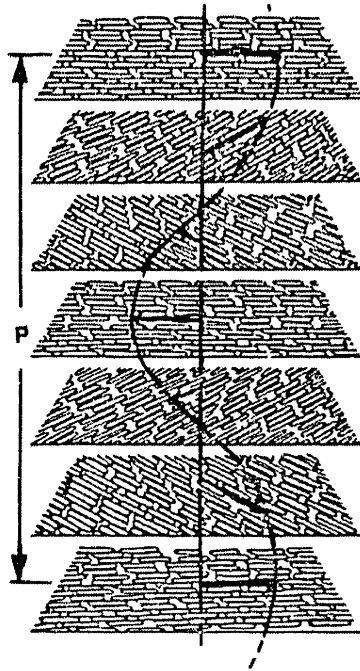


Figure 1.3 Schematic of a chiral nematic liquid crystal. Taken from¹⁹

Another class of liquid crystal phases are the smectic phases in which the molecules have some positional and orientational order. In these cases, the molecules tend to point along a director and to arrange themselves in layers. Figure 1.3 shows the two most common smectic phases, the smectic A and the smectic C. In smectic A, the molecules are on average oriented perpendicular to the layers and in smectic C, the molecules are on average oriented at some angle with respect to the layers.

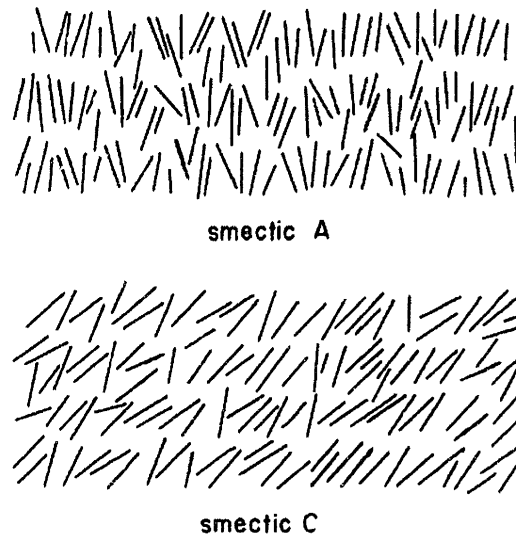


Figure 1.4 Schematic of smectic C and smectic A liquid crystal phases. The layers are perpendicular to the director in the smectic A phase, and are tilted with respect to the director in the smectic C phase. Taken from **18**.

A variant of the smectic C phase, termed the smectic C* phase is important to this proposed work since it is known to be ferroelectric²⁰ when the sample is properly confined. By definition, a ferroelectric material is one that displays an electric polarization in the absence of an externally applied field. Moreover, the direction of this polarization may be reversed by the application of an electric field²¹. Ferroelectric materials are inherently piezoelectric, as an application of stress can induce a switch in the direction of polarization.

A schematic of the smectic C* phase is shown in Figure 1.4. Within each of the layers, the mesogens are tilted, and from layer to layer this tilt angle rotates about an axis normal to the layers. The distance it takes for the director to make a full rotation is known as the pitch, and is on the order of 2-3 μm for smectic C* LCs²².

Ferroelectric liquid crystals were first predicted in organic liquid crystals by Meyer in 1975²⁰, who showed by a crystallographic argument the smectic C* phase can be ferroelectric if the molecule contains a chiral center. In order for a sample to possess a macroscopic spontaneous polarization that is bistable, the pitch of the helix must be “unwound” so that the phase resembles a smectic C* phase with no helix²³. This is the principle behind the surface stabilized Sc* LCs discussed in section 1.5.

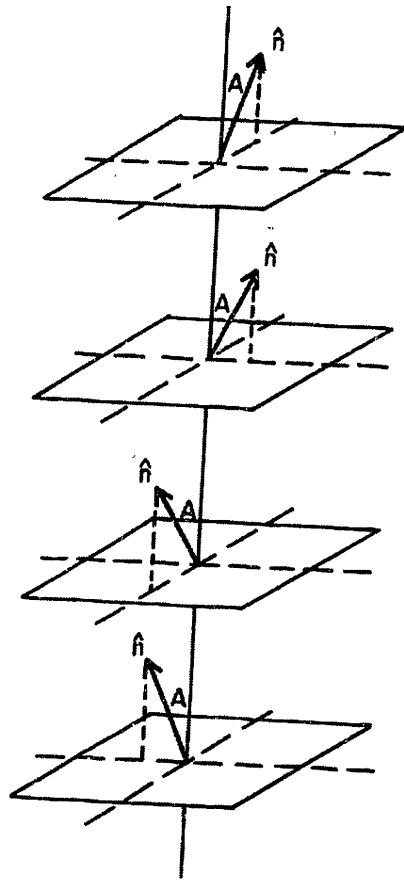


Figure 1.5 Schematic of the smectic C* phase. The planes represent the smectic layers. The director takes the same angle with respect each layer, but rotates around an axis normal to the layers. Taken from **18**.

1.4 Side-Chain LC Homopolymers

Side-chain liquid-crystalline polymers consist of a polymer main chain to which mesogens are attached as side-chains. The rigid core of the mesogen is separated from the polymer main chain via a flexible spacer, which can vary in length. The role of the spacer is to decouple the mesogen from the polymer chain, thus allowing the mesogens to form LC phases and to interact with other mesogens in a similar way as in small molecule liquid crystals. In fact, side-chain LCPs generally form thermotropic liquid crystal phases analogous to small molecule liquid crystals, e.g. nematic, smectic, and cholesteric. The choice of mesogen generally determines the types of LC phases; nematic, smectic, and cholesteric mesophases have all been observed and are directly correlated with the mesogen choice²⁴. The most common main chains used are the acrylates, methacrylates, and siloxanes²⁵, although many other types of main chains have been used, such as vinyl ethers⁶ and a substituted 1,2 and 3,4 isoprene polymers¹. The use of a siloxane backbone in SCLCPs was first reported in 1980 by Finkelmann and Rehage¹⁴, which leads to lower glass transitions temperatures. Side-chain liquid crystalline siloxane homopolymers were subsequently studied extensively, as they are readily prepared with different molecular weights and mesogens^{14, 16}. Because of the low T_g, the liquid crystalline properties of these polymers, such as electro-optic switching, may be accessed at room temperature^{13, 15}. These types of homopolymers have only recently been synthesized anionically, using methods developed in our labs concurrently with other researchers²⁶. This allows for the synthesis of block copolymers and α,ω -endfunctional siloxanes with controlled molecular weights and molecular weight distributions.

In terms of display and related optical applications, the side-chain polymer liquid crystal materials have found limited use thus far, especially when compared with their small molecule counterparts. The reason for this is that the small molecules have switching times about three orders of magnitude faster than their polymer counterparts²⁷.

1.5 SSFLCS

SSFLC stands for surface stabilized ferroelectric liquid crystal and refers generally to an effect first observed in 1980 by Clark and Lagerwall in chiral smectic C* small molecule liquid crystals²³. By confining the LC in a gap smaller than the helical pitch, the helix is unwound, the material becomes macroscopically polarized, and the SSFLC device shows bistable electro-optic switching. The pitch in the bulk Sc* phase is generally on the order of 2-3 μm ²², and hence cells of this thickness (or thinner) are needed to effect the fast bistable switching phenomena. The fast, bistable, electro-optic switching effect has been extended from small molecule Sc* liquid crystals to Sc* side-chain polymers, most successfully in siloxane SCLCPs^{13, 15}.

Researchers in the block copolymer area have found that block copolymer morphology is an alternative way to unwind the Sc* helix, if one of the blocks is a smectic C* LCP. Mao et al. have surface stabilized ferroelectric LCP phases using cylindrical block copolymer morphologies⁸ as well as in lamellar morphologies; the high voltages necessary (75V/ μm , 750V for a 10 μm cell), suggest that the presence of morphology hinders switching relative to the LC homopolymer.

In this work none of our block copolymers showed any electro-optical activity after numerous shearing and poling treatments. Voltages as high as 30V/ μm were tested

(the maximum available with our power supply) and resulted in no observable electro-optic effects in the block copolymers, although the siloxane homopolymers generally showed electro-optic activity. The details of these observations are discussed in Chapter 4.

1.6 Side-Chain LCP Elastomers

Upon light crosslinking, side-chain liquid crystalline siloxanes become room temperature LC elastomers¹⁰. Liquid crystalline elastomers have an unique combination of liquid crystallinity and elasticity, which leads to mechano-optic²⁸ and piezo-electric behavior²⁹. Figure 1.5 summarizes the types of effects that have already been observed in LC elastomers containing the smectic C* phase.

Vallerien et al.²⁹ observed piezo-electricity in crosslinked LC elastomers in both the Sc* phase and in the twisted nematic or cholesteric phase. Their samples were polydomain samples prepared by thermally crosslinking the homopolymers above the liquid crystalline clearing point in a 100 μ m LC cell. Although these samples have many liquid crystalline domains, i.e. multidomains, within the domains the mesogens are oriented parallel to the glass plates.

Brehmer and Zentel studied the ferroelectric switching of smectic C* LC elastomers and found that the nature of the crosslinking has a large effect on the mesogen mobility^{30, 31}. Specifically, crosslinking the network at the mesogen terminus greatly reduced the “free” uncrosslinked mesogen mobility compared to crosslinking the network close to the polymer main chains. The samples were LC elastomer monodomains created by first obtaining an LC monodomain of the homopolymer/photoinitiator mixture in an

LC cell by applying an alternating voltage, and then using uv radiation to crosslink the monodomain.

Küpfer and Finkelmann³² pioneered LC monodomain elastomers, termed Liquid Single Crystal Elastomers. In this work, macroscopic monodomain LC samples are prepared in a two step crosslinking process. A weak LC network is formed, a mechanical load is then applied to obtain a LC monodomain, and finally the weak LC network is further crosslinked in its aligned state to yield the LSCE.

One long term goal of this work is to extend the of PS-LCP diblock structure to triblock copolymers of PS-LCP-PS, thus creating thermoplastic LC elastomers analogous to the commercial Kraton rubbers. The synthesis of triblock materials was attempted several times using the techniques described in Chapter 2, and proved more difficult than the diblock synthesis. As the diblock materials provided a rich area of study, they quickly became the focus of this thesis, and the synthesis of triblocks was set aside in order to concentrate on materials that we could make. It turns out that *rubbery diblocks* of PS-LCP are possible by making a low Tg LCP block with high molecular weight 80-120K and the PS block relatively small 13-14K. In this case the Tg of the siloxane block was -32°C .

It should be noted that researchers have successfully made PS-PDMS-PS triblock copolymers using dichlorodimethylsiloxane as a coupling agent^{33, 34}, and by using a difunctional PDMS macroinitiator to polymerize styrene by ATRP methods^{35, 36}. Triblocks with functional siloxane blocks have not yet been reported.

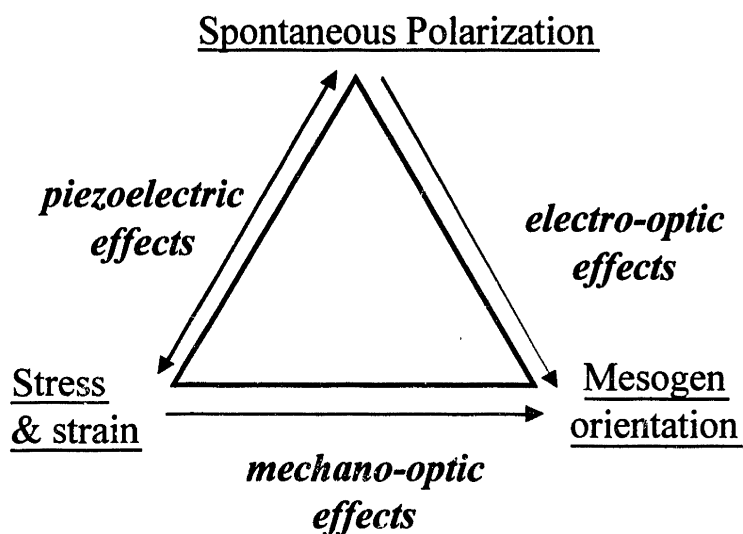


Figure 1.6 Triangular relationship between mesogen orientation, spontaneous polarization, and stress in smectic C* LC elastomers.

1.7 Amorphous-LCP block copolymers

Polymers with liquid crystalline and amorphous blocks present an unique combination of morphological order and liquid crystalline order^{1, 4, 37, 38}. These materials are of practical interest because the ability to orient mesogens with mechanical and electrical fields combined with the mechanical properties of block copolymers may lead to practical applications such as electro-optic free standing thin films, mechano-optic materials, and piezoelectric elastomers.

Researchers in our group have previously synthesized and characterized liquid crystalline block copolymers with ferroelectric mesogens using polystyrene-polymethacrylate systems³⁹. The block copolymer morphology was generally found to stabilize the smectic C* phase in the LC block, and the order-disorder transition in the block copolymer was found to be linked to the LC clearing point⁵.

Cylindrical, lamellar, spherical, and perforated layer block copolymer morphologies have all been observed in the case of amorphous – side chain liquid crystalline polymers^{5, 40}. When the liquid crystalline polymer is main chain rigid rod, then the morphologies are non-traditional, for example zig-zag lamellae⁴¹. This leads to unusual morphological phase diagrams.

Two general schemes have been used to synthesize amorphous-LCP block copolymers: 1) anionic or cationic polymerization of the amorphous block, followed by the anionic or cationic polymerization of a side chain LC monomer, and 2) formation of an AB or ABA block copolymer with a B block that can be subsequently functionalized with side-chain mesogens⁴². The mainstay of scheme 1) has been to prepare polystyrene block, add diphenylethylene, then polymerize an LC methacrylate³⁷. There appears to be some limitation on the LC block sizes using this technique^{4, 39}. A similar cationic technique using vinyl ethers has also been reported, in which an amorphous polyvinylbutylether block is cationically polymerized followed by a LC vinyl ether block^{6, 43}. In the second general scheme to amorphous-LCP block copolymers, the most popular method to date is to start with poly(styrene-*b*-(1,2 butadiene)) or poly(styrene-*b*-(1,2 isoprene co 3,4 isoprene)) block copolymers made by anionic polymerization (in some cases ABA polymers are made⁴⁴). Then, the pendant vinyl groups on the B block are converted to primary alcohols with hydroboration/oxidation and the mesogens attached by acid chloride coupling¹. This general method is termed the “polymer analogous” approach as the polymers are involved in a coupling reaction much like a small molecule would be.

The work in this thesis presents a polymer analogous scheme, in which a polystyrene-polyvinylmethylsiloxane polymer is prepared anionically, and Si-H functional mesogens are subsequently attached to the vinyl siloxane backbone. This technique gives LC blocks with exceptionally low Tg's (< -20°C) which may open up room temperature applications that rely on the mobility of the mesogens in the LCP phase.

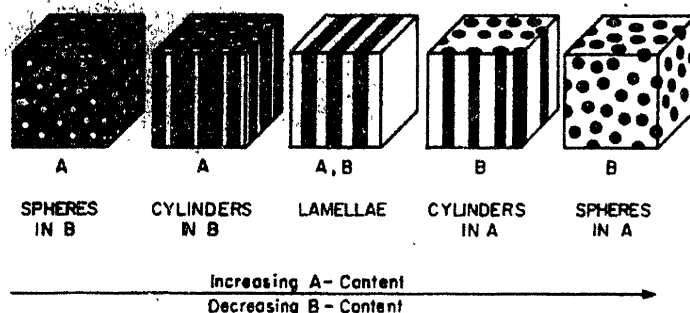


Figure 1.7 Equilibrium morphologies in AB diblock copolymers as the fraction of A block increases. Taken from A.S. Argon, R.E. Cohen, et al. ⁴⁵.

1.8 Diblock Copolymer Microphase Segregation

AB amorphous diblock copolymers microphase segregate into various geometries on the nanometer scale when the blocks are immiscible. The type of morphology formed depends on the volume fraction of the blocks; the three classical morphologies of lamellae, hexagonal cylinders, and BCC spheres, are shown schematically in Figure 1.3 as the composition of the block copolymer changes. More recently, a new morphology known as the bicontinuous double gyroid has been found intermediate between the cylinders and lamellae^{46, 47}.

The degree of microphase segregation is governed by the quantity χN , where χ is the temperature dependent ($\chi \propto 1/T$) Flory-Huggins interaction parameter between

segments of block A and block B and N is the degree of polymerization of the entire polymer (both A and B blocks included). As χN increases the material progresses from homogeneous, then through what are known as weak, intermediate, and strong segregation regimes. “Strong segregation” ($\chi N \gg 10$) refers to interfacial areas between domains that are smaller in size than the domains themselves, whereas “weak segregation” refers to broader interfaces that are characterized by a sinusoidal composition profile in a space ($\chi N \sim 10$)^{48, 49}. An example of a theoretically calculated weak segregation phase diagram⁵⁰ appears in Figure 1.4, showing the classical morphologies.

Conventional theories of polymer-polymer miscibility and block copolymer phase segregation calculate ΔG_{mix} by assuming that two amorphous blocks inter-mix to form a homogeneous melt. In the case when one of the polymers or blocks is liquid crystalline or crystalline at the temperature of interest, this assumption is not correct and the entropy and enthalpic effects due to disrupting the ordered crystalline or liquid crystalline phase must be accounted for⁵¹⁻⁵⁵. The parameter χ still maintains its meaning as the interaction parameter between the segments of the two dissimilar polymers.

AB block copolymers with an amorphous block and a crystalline, semi-crystalline, or liquid-crystalline B block microphase segregate into various morphologies in a similar (but not completely analogous) way to AB block copolymers with two amorphous blocks. In the case of side-chain LC blocks the morphologies formed have been completely analogous to two amorphous blocks, i.e., cylinders, lamellae, and spheres. In most cases, the phase diagram is skewed to one side, with lamellae being favored at lower LC contents than would be the case if both blocks are amorphous^{5, 42}.

That is, side-chain LC blocks prefer to be in a lamellar configuration as the mesogens pack easily into the lamellae. When the LC block is a rigid-rod main chain LC, the block copolymer morphologies formed are non-traditional⁴¹, as are the phase diagrams.

When an amorphous-LCP block copolymer is cooled from above its order disorder transition temperature,

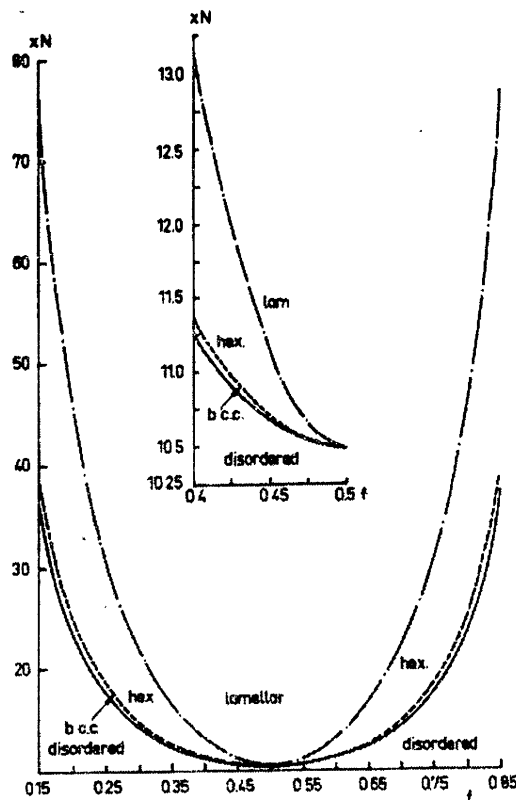


Figure 1.8 The well known Liebler weak segregation phase diagram for AB diblock copolymers, taken from **50**.

1.9 References

1. Adams, J.; Gronski, W. *Makromol. Chem., Rapid Commun.* **10**, 553-557 (1989).
2. Zashke, B.; Frank, W.; Fischer, H.; Schmutzler, K.; Arnold, M. *Polymer Bulletin* **27**, 1-8 (1991).

3. Chiellini, E.; Gallo, G.; Angeloni, A. S.; Laus, M.; Bignozzi, M.C. *Macromol. Symp.* **77**, 349-358 (1994).
4. Yamada, M.; Iguchi, T.; Hirao, A.; Nakahama, S.; Watanabe, J. *Macromolecules* **28**, 50-58 (1995).
5. Zheng, W.Y.; Hammond, P.T. *Macromolecules* **31**, 711-721 (1998).
6. Omenat, A., Hikmet, R.A.M., Lub, J. & van der Sluis, P. *Macromolecules* **29**, 6730-6736 (1996).
7. Mao, G., *et al.* *Macromolecules* **30**, 2556-2567 (1997).
8. Mao, G.; Wang, J.; Ober, C. K.; Brehmer, M.; O'Rourke, M. J.; Thomas, E. L. *Chem. Mater.* **10**, 1538-1545 (1998).
9. Zentel, R.; Reckert, G.; Bualek, S. *Makromol. Chem.* **190**, 2869-2884 (1989).
10. Finkelmann, H.; Kock, H-J.; Rehage, G. *Makromol. Chem., Rapid Commun.* **2**, 317-322 (1981).
11. Shilov, S., Gebhard, E., Skupin, H., Zentel, R. & Kremer, F. *Macromolecules* **32**, 1570-1575 (1999).
12. Meier, W.; Finkelmann, H. *Makromol. Chem. Rapid Commun.* **11**, 599-605 (1990).
13. Suzuki, T.; Okawa, T. *Makromol. Chem., Rapid Commun.* **9**, 755-760 (1988).
14. Finkelmann, H., Rehage, G. *Makromol. Chem., Rapid Commun.* **1**, 31-34 (1980).
15. Cooray, Nawalage F., Masa-aki Kakimoto, Yoshi Imai, Yoshi-ichi Suzuki, *Polymer Journal* **25**, 863-872 (1993).
16. Hsu, C.S. & Shih, L.J. *Macromol. Symp.* **98**, 883-893 (1995).
17. Blinov, L.M., and Chigrinov, V.G. *Electrooptic Effects in Liquid Crystal Materials* (Springer-Verlag, New York, 1994).
18. Collings, P.J. *Liquid Crystals: Nature's Delicate Phase of Matter* 1-129-130 (Princeton, NJ, 1990).
19. Cowie, J.M.G. *Polymers: Chemistry and Physics of Modern Materials* (Blackie Academic & Professional, London, 1991).
20. Meyer, R.B., Liebert, L., Strzelecki, L., and Keller, P. *Journal de Physique* **36**, L-69 (1975).
21. Axe, J.D.; Lines, L.E. in *Encyclopedia of Physics* 373-376 (VCH Publishing, New York, 1991).
22. Ulrich, D.C. & Elston, S.J. in *The Optics of Thermotropic Liquid Crystals* (eds. Elston, S. & Sambles, R.) 196 (Taylor and Francis, London, 1998).
23. Clark, N.A.; Lagerwall, S.T. *Appl. Phys. Lett.* **36**, 899-901 (1980).
24. Finkelmann, H. in *Polymer Liquid Crystals* (eds. Ciferri, A., Frigbaum, W.R. & Meyer, R.B.) 35-61 (Academic Press, New York, 1982).
25. Plate, N.A. & Shibaev, V.P. in *Comb-Shaped Polymers and Liquid Crystals* (ed. Cowie, J.M.G.) (Plenum, New York, 1987).
26. Hempenius, M.A., Lammertink, R.G. & Vansco, J.G. *Macromolecules* **30**, 266-272 (1997).
27. Zentel, R. in *Liquid Crystals* (ed. Stegemeyer, H.) 103-141 (Steinkopff Darmstadt, Springer, New York, 1994).
28. Kock, H.J., Finkelmann, H., Gleim, W. & Rehage, G. in *Polymeric Liquid Crystals* (ed. Blumstein, A.) 275-312 (Plenum Press, New York, 1983).

29. Vallerien, S. U.; Kremer, F.; Fischer, E.W. *Makromol. Chem. Rapid Commun.* **11**, 593-598 (1990).
30. Brehmer, M.; Zentel, R. *Macromol. Chem. Phys.* **195**, 1891-1904 (1994).
31. Brehmer, M. & Zentel, R. *Macromol. Rapid Commun.* **16**, 659-662 (1995).
32. Kupfer, J.; Finkelmann, H. *Makromol. Chem., Rapid Commun.* **12**, 717-726 (1991).
33. Morton, M., Kesten, Y., Fetters, L.J. *Polymer Preprints, ACS, Div. of Polymer Chemistry* **15**, 175-177 (1974).
34. Davies, Jones *Ind. Eng. Chem., Product Research Division* **10**, 168 (1971).
35. Nakagawa, Y., Miller, P., Cristina, P. & Matyjaszewski, K. *A.C.S. Polymer Preprints* **38**, 701-702 (1997).
36. Nakagawa, Y. & Matyjaszewski, K. *A.C.S. Polymer Preprints* **37**, 270-271 (1996).
37. Bohnert, R.; Finkelmann, H. *Macromol. Chem. Phys.* **195**, 689-700 (1994).
38. Fischer, H.; Poser, S.; Arnold, M. *Liquid Crystals* **18**, 503-509 (1995).
39. Zheng, W.Y.; Hammond, P.T. *Macromol. Rapid Commun.* **17**, 813-824 (1996).
40. Fischer, H.; Poser, S.; Arnold, M.; Frank, W. *Macromolecules* **27**, 7133-7138 (1994).
41. Thomas, E.L., Chen, J.T. & M.J.E., O'Rourke *Macromol. Symp.* **117**, 241-256 (1997).
42. Poser, S., Fischer, H. & Arnold, M. *Journal of Polymer Science* **34**, 1733-1740 (1996).
43. Omenat, A. & Lub, J. *Chem. Mater.* **10**, 518-523 (1998).
44. Sanger, J. & Gronski, W. *Macromol. Chem. Phys.* **199**, 555-561 (1998).
45. Argon, A.S., Cohen, R.E., Gebizlioglu, O.S. & Schwier, C.E. in *Crazing in Polymers* (ed. Kausch, H.H.) 300 (Springer-Verlag, New York, 1983).
46. Hajduk, D.A., *et al.* *Macromolecules* **27**, 4063-4075 (1994).
47. Schulz, M.F., Bates, F.S., Almdal, K. & Mortensen, K. *Phys. Rev. Lett.* **73**, 86-89 (1994).
48. Hamley, I.W. in *The Physics of Block Copolymers* 26-27 (Oxford University Press, Oxford, 1998).
49. Bates, F.S. & Fredrikson, G.H. *Annual Reviews of Physical Chemistry* **41**, 525 (1990).
50. Leibler, L. *Macromolecules* **13**, 1602-1617 (1980).
51. Chow, T.S. *Macromolecules* **23**, 333-337 (1990).
52. Whitmore, M.D. *Macromolecules* **21**, 1482-1496 (1988).
53. DiMarzo, E.A., Guttman, C.M. & Hoffman, J.D. *Macromolecules* **13**, 1194-1198 (1980).
54. Sones, R.A. & R.G., Petschek *Physical Review E* **50**, 2906-2912 (1994).
55. Williams, D.R.M. & Halerpin, A. *Physical Review Letters* **71**, 1557-1560 (1993).

Chapter 2 Design and Synthesis

2.1 Design of low Tg LC block Copolymers

The polymers in this project were designed to have a low Tg side-chain LC block coupled to a high Tg amorphous block. The amorphous block was chosen to be polystyrene, which has a Tg of approximately 100°C, and the side-chain LC block was chosen to be a LC siloxane, which has Tg's that range in value depending on the choice of mesogen. In this project, for example, Tg's of the LC block ranged from -32°C to -8°C. A siloxane without any mesogens attached, i.e. PDMS, has a Tg of approximately -127°C¹.

The block copolymer structure was chosen with this Tg combination so that the mesogens in the LC block are mobile at room temperature, and the glassy amorphous block can add mechanical integrity. In addition, the low Tg LC block can lead to elastomers in the case of triblock PS-LCP-PS, and to rubbery materials in the case of PS-LCP diblocks with a high volume fraction of LC block.

2.2 Early Synthetic Attempts

The first attempt at the synthesis of these block copolymers involved cationic or step growth polymerization to form an α,ω end functional Si-H backbone polymer, shown in Figure 2.1. Following polymerization and purification, the Si-H backbone is functionalized with vinyl mesogens, forming a side-chain LCP siloxane with difunctional alkyl chloride end groups. It was hoped that this difunctional LCP siloxane could be coupled to polystyrene via the alkyl chloride end groups, thus forming a PS-LCP-PS triblock copolymer.

The step growth method poses limitations on molecular weight, and the cationic method leads to the formation of cyclics which are difficult to purify and leads to a product with a broad molecular weight distribution (PDI >2). The task of then coupling these difunctional LCPs to a styrene chain appeared at least as involved as a complete anionic synthesis, discussed in the next section. Therefore, an anionic method was chosen, which leads to more well defined polymers.

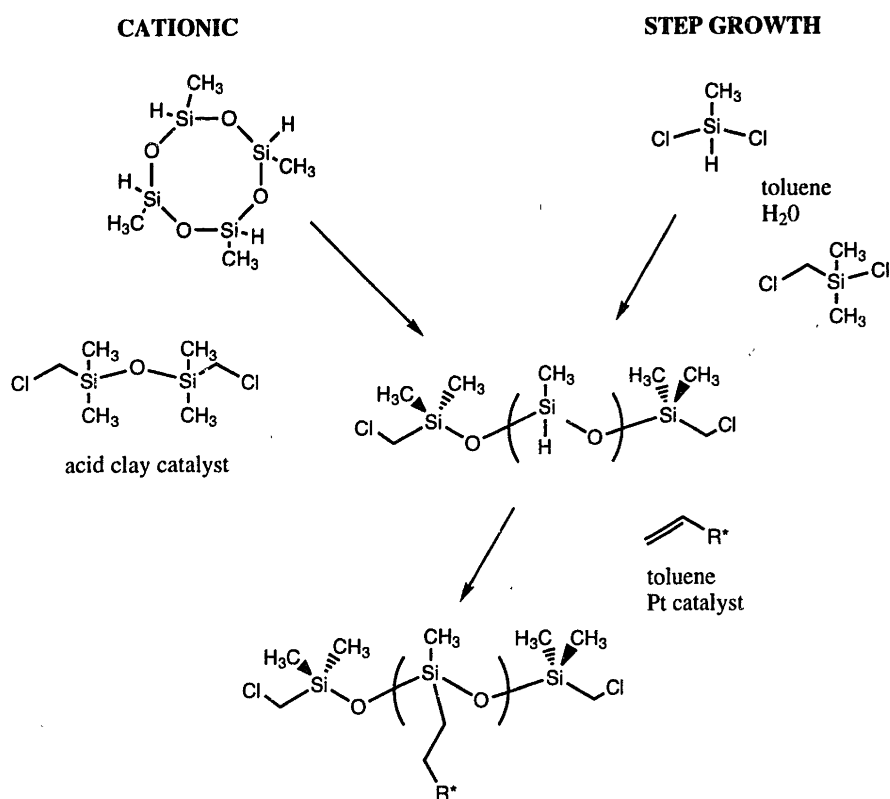


Figure 2.1 Two initial synthetic schemes towards α,ω difunctional siloxane side-chain LCPS using cationic and step-growth polymerization.

2.3 Description of Synthetic Scheme

The general synthetic scheme for the PS-LCP diblock copolymers is shown in Figure 2.2. The approach is to make a polystyrene-polyvinylmethylsiloxane (PS-PVMS) block copolymer using anionic polymerization and then to attach Si-H functional

mesogens to the siloxane block via hydrosilylation chemistry. The anionic synthesis of the polymer backbone is a variant of one of the first PS-PDMS schemes, published in 1970². The anionic polymerization of V3 combined with the attachment of Si-H mesogens to the PVMS chain is a technique developed recently in our labs concurrently with other researchers³.

In this work, two different mesogens were synthesized and attached to PS-PVMS backbones; their structures are shown in Fig 2.4. Mesogen A was chosen from the literature because of its ease of synthesis and the siloxane homopolymers made with its vinyl analogue are ferroelectric at room temperature⁴. Mesogen B was designed to give enhanced phase segregation between the PS and LCP blocks and to maintain ferroelectric properties as discussed in detail in Chapters 3 and 4. Both mesogen A and B were synthesized using the same approach, shown in Figure 2.4. A non-functional analogue to mesogen A, termed mesogen A' (Figure 2.6), was synthesized for mixing and blending studies. Finally a third mesogen, mesogen C (Figure 2.7), was synthesized and attached to a siloxane backbone, forming an LCP homopolymer. Mesogen C was not explored in detail, but preliminary results indicate that it may be a good candidate to incorporate into block copolymers.

2.4 General Procedure for Polymer Synthesis

The synthesis of the PS-PVMS backbone begins with the anionic polymerization of styrene in cyclohexane at room temperature using n-butyl lithium as an initiator. After the polystyrene block is formed (3-4hrs) and a small sample is taken for GPC analysis, hexamethylcyclotrisiloxane (D3) is added to convert the living polystyryl anion to a siloxanolate anion. In the presence of cyclohexane or any other non-polar hydrocarbon

solvent (e.g. hexane, toluene) between one to three PDMS repeats are added at the end of the polymer, regardless of the quantity of D3 added⁵. After the deep orange color of the living polystyryl anion completely disappears, trimethyltrivinylcyclotrisiloxane (V3) is added along with THF (to promote polymerization of V3 and the remaining D3). It is necessary to add THF along with the V3, as it breaks up the ion pair of siloxanolate (-) and lithium (+), which is strongly paired in cyclohexane. When D3 is not added before the V3, the living polystyryl anion attacks the double bond in the V3, and an ill defined, branched product results. The conversion of the living polystyryl anion to the siloxanolate anion was found to be slow in cyclohexane at room temperature (on order of 24hr) and required 10-15 times molar excess of D3. The final LCP blocks are random copolymers that contain 1-6wt% PDMS units, 89-100wt% functionalized mesogen repeat units and 0-5wt% unreacted PVMS repeats.

We found that by adding 1-2ml THF along with the D3 (100-200mg), the conversion of the living polystyryl anion to a siloxanolate anion became much faster at room temperature (on the order of 1hr), as shown in Figure 2.3.. However, all the polymers synthesized for this thesis were made by the scheme shown in Figure 2.2. It is anticipated that optimization of the scheme shown in Figure 2.3 will reduce the quantities of D3 and reaction times needed to convert the living polystyryl anion to a siloxanolate anion. The result of this technique is a triblock copolymer with a small PDMS block, as the D3 polymerizes in the presence of THF.

In addition to the PS-PVMS block copolymers, we have also made PVMS homopolymers with a monofunctional initiator, trimethylithiumsiloxanolate (Figure 2.8), and with a difunctional initiator, the lithium salt of 1,4-bis(hydroxydimethyl-silyl)

benzene (Figure 2.9). The difunctional initiator yields α,ω end functional polymers, whose end groups may be tailored by selecting different end capping agents. In our case, we selected a benzyl chloride end group in the hope of initiating polystyrene chains off of the LCP using atom transfer radical polymerization^{6, 7}. The ATRP technique requires full conversion of the vinyl groups along the PVMS backbone, as these can become involved in the radical polymerization. Because it was difficult to get 100% substitution of the PVMS backbone, a secondary step of functionalizing the remaining vinyl groups with hexamethyldisiloxane converted these remaining vinyl groups to small inert side-chains. A single ATRP attempt was made with one of the α,ω end functional siloxane LCPs whose unfunctionalized vinyl groups were converted to small inert side chains of hexamethyldisiloxane. The result was little to no growth of polystyrene chains off the end of the macroinitiator, and the formation of a considerable amount of homopolystyrene. ATRP was set aside due to poor first results and the additional step of converting the vinyl groups to inert groups. It is the author's opinion that further work in this area may lead to the desired triblock materials.

2.5 Instrumentation

A Waters gel permeation chromatography (GPC) system equipped with 2 Styragel HT3 columns (500-30,000 MW range), 1 Styragel HT4 column (5,000-600,000 MW range), and a UV detector (254nm) was used for molecular weight measurement relative to polystyrene standards. Tetrahydrofuran (THF) flowing at 1ml/ min was the mobile phase. NMR measurements were made with a Bruker Avance DPX400 400MHz instrument. For calculation of all polymer compositions the relaxation time D1 was set

to 15sec. Polymerizations were conducted in a Vacuum Atmospheres glove box under nitrogen.

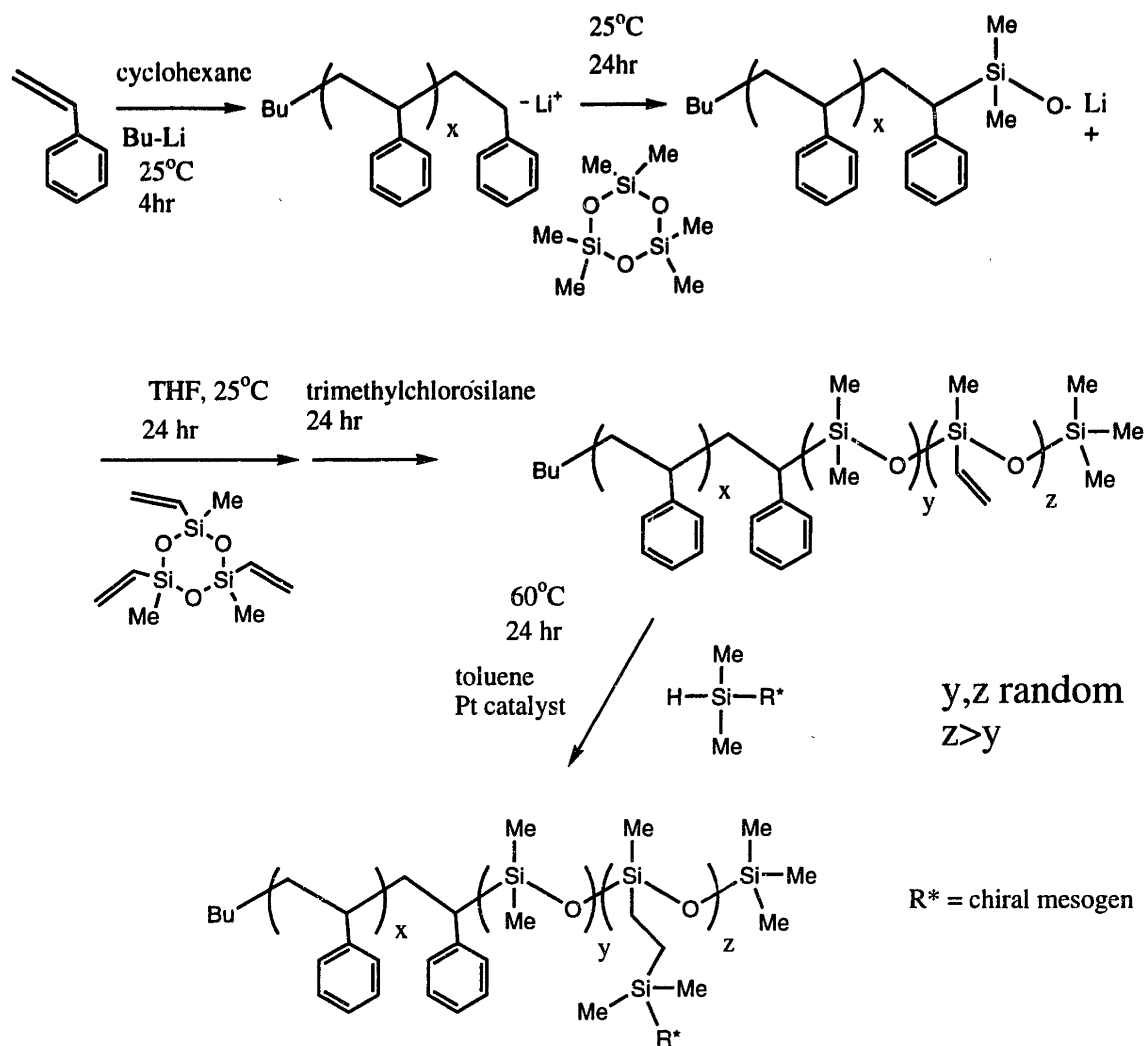


Figure 2.2 Synthetic route to polystyrene siloxane liquid crystalline block copolymers, using anionic polymerization followed by the attachment of side-chain mesogens via hydrosilylation.

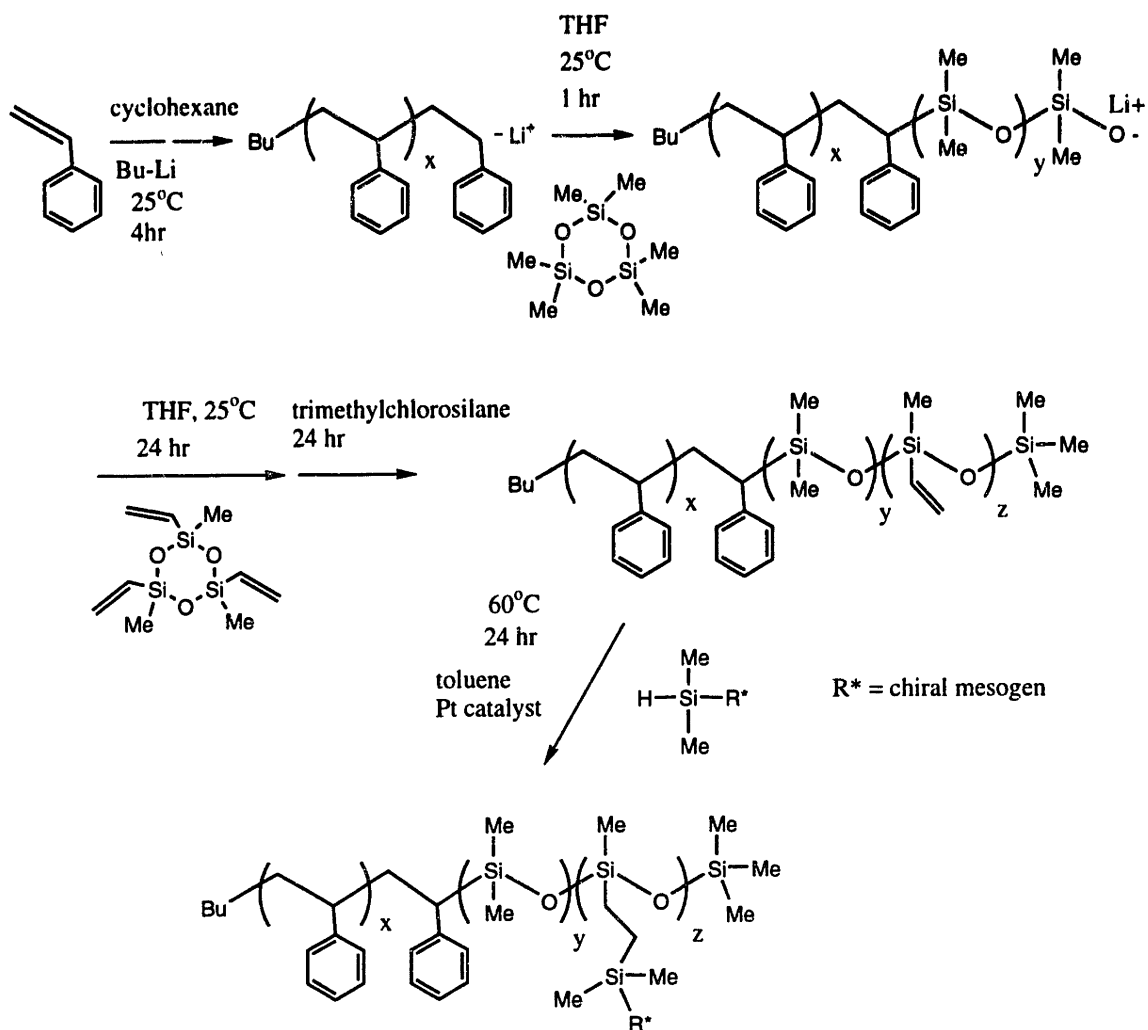
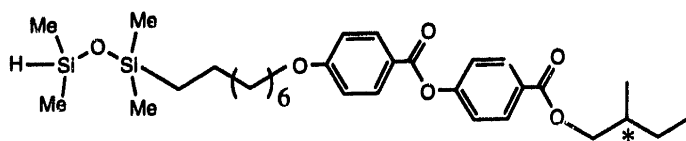


Figure 2.3 Variation of synthetic route to polystyrene siloxane liquid crystalline block copolymers. THF is added along with D3 in order to accelerate the conversion from carbanion to siloxanolate anion. Rigorously speaking, the result is a triblock copolymer with a small PDMS block as the middle block.

mesogen A



mesogen B

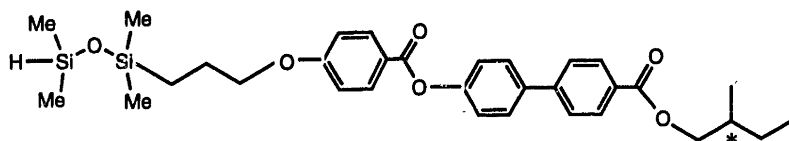


Figure 2.4 Chemical structures of two mesogens used in the PS-LCP block copolymers. Mesogen B has a shorter alkyl spacer and a more rigid core.

2.6 Synthesis of Mesogen A

(S)-2-methyl butyl 4-hydroxybenzoate (1A). To a 250 ml round bottom flask, 50 ml of benzene was added followed by 0.5 ml concentrated sulfuric acid. After this solution was mixed for several minutes, 12.3 ml S-(-)-(2)-methyl-1-butanol (113.6 mmol, 3eq) was added, followed by 5.3g (38 mmol, 1eq) of 4-hydroxybenzoic acid. 50 ml additional benzene was added, a Dean-Stark condenser was attached to the reaction flask, and the solution was brought to reflux. The solution was initially cloudy, but cleared after 20 min of reflux. The reaction refluxed an additional 48hr before cooling to room temperature. The crude reaction mixture was washed 3x with water, and the benzene was removed by vacuum. 7.46 g of clear brown viscous liquid were obtained, 95% yield. ¹H NMR dH (400Mhz, CDCL₃) .93-1.00 [m, 6 primary H], 1.26-1.34 [m, 1 secondary H], 1.48-1.57[m, 1 secondary H], 1.82-1.98 [m, 1 tertiary H], 4.08-4.23 [m, 2 Ar-COOCH₂], 6.87-6.9 [d, 2 aromatic H], 7.55-7.99 [d, 2 aromatic H]

4-(7-octenyl)benzoic acid (2A). 10.97 g (3 eq, 78.5 mmol) p-hydroxybenzoic acid, 225 ml ethanol, and 25 ml water were combined in a 500 ml round bottom flask. 10.52 g

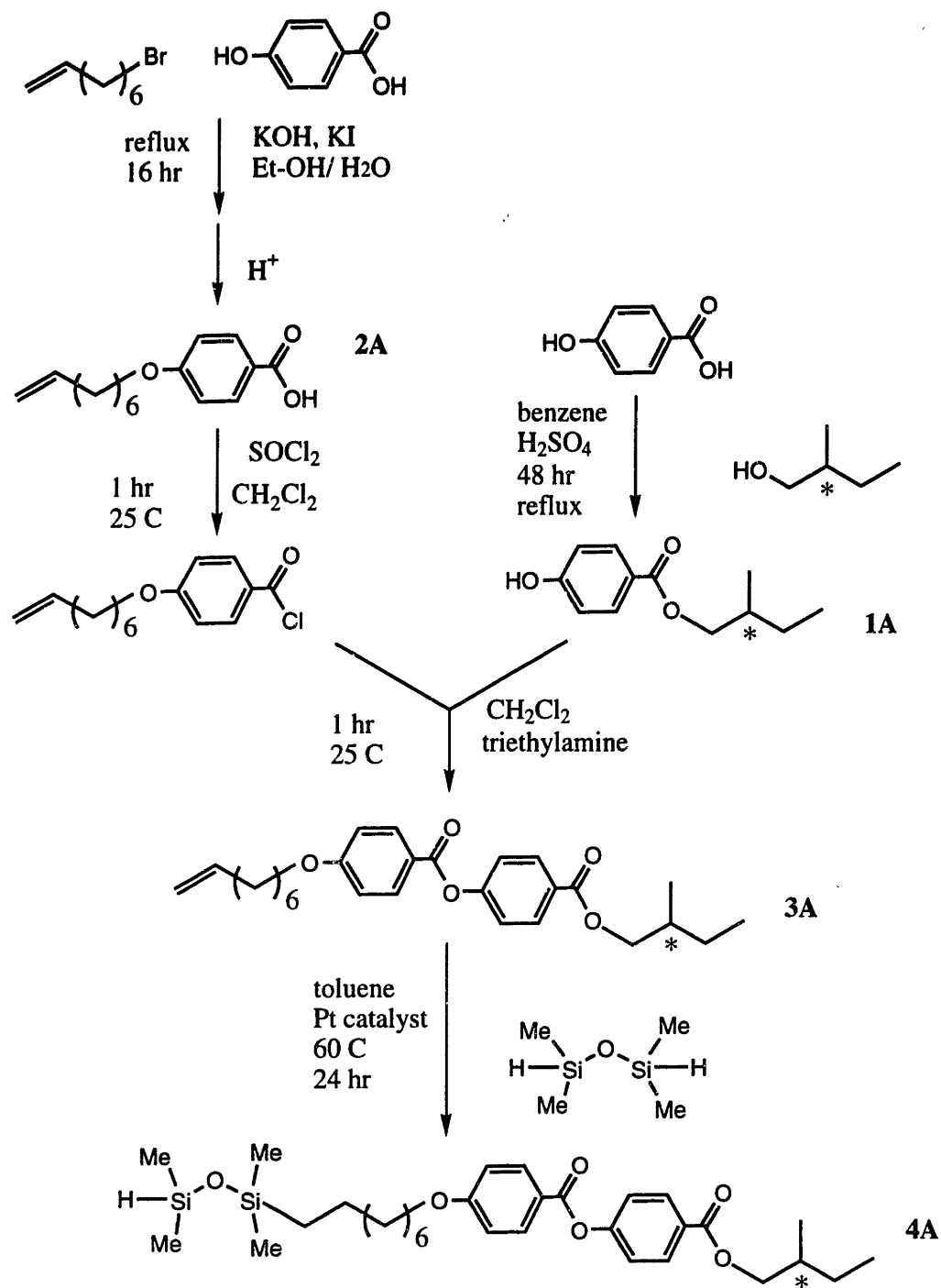


Figure 2.5 Synthetic scheme to mesogen A. Mesogens B, C, and A' were synthesized with the same general scheme.

Mesogen B was synthesized by substituting 3-bromo-1-propene for 8-bromo-1-octene in preparation of 2A, and 4'-hydroxy-4-biphenyl carboxylic acid for 4-hydroxybenzoic acid in preparation of 1A.

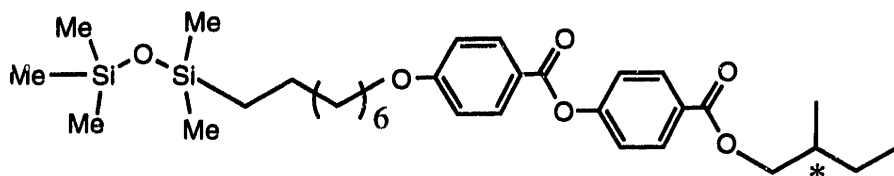


Figure 2.6 Chemical structure of mesogen A'. Synthesis is the same as for mesogen A, substituting pentamethyldisoxane for tetramethyldisiloxane in the preparation of 4A. Mesogen A' has a single Sc* to isotropic transition at 26°C.

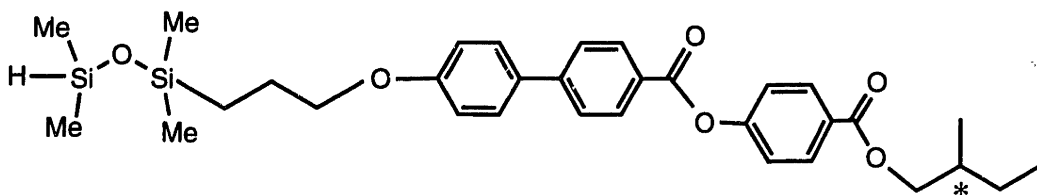


Figure 2.7 Chemical structure of mesogen C. Synthesis scheme is the same as that as that for mesogen A, substituting 3-bromo-1-propene for 8-bromo-1-octene in preparation of 2A, and 4'-hydroxy-4-biphenyl carboxylic acid for 4-hydroxybenzoic acid in preparation of 2A.

potassium hydroxide and a small scoop of potassium iodide were added to this mixture, which was brought to reflux. 5 g of 8-bromo-1-octene was then added and the mixture was allowed to reflux overnight. After cooling to room temperature, the crude reaction mixture was acidified to pH 3, white crystals precipitated, and the slurry was stirred overnight. The slurry was dumped into 600 ml of water and this mixture was stirred for an hour. 3.35 g of white crystals were collected, 51% yield, m.p. 90C. ¹H NMR dH 1.04-1.52 [m, 6 aliphatic H], 1.82-1.86 [m, 2 H, CH₂CH₂OPh], 2.10-2.08 [m, 2H, CH₂CH=CH₂], 4.03-4.04 [t, 2H, CH₂OPh], 4.96-5.05 [m, 2H, CH=CH₂], 5.83-5.85 [m, 1H, CH=CH₂], 6.94-6.97 [d, 2 Ar-H], 8.07-8.09 [d, 2 Ar-H]

(S)-2-methylbutyl 4-[4(7-octenyloxy)benzoyloxy]benzoate (3A). 3.35 g of (2A), 3 drops dimethylformamide, and 20 ml methylene chloride were added to a flask with stirring. 4.5 ml thionyl chloride were added to this mixture under a slow nitrogen purge. After 10 minutes, the initially cloudy solution cleared, becoming yellow. After 1hr of

reaction time, the solvent and excess thionyl chloride were removed by vacuum, and the remaining yellow paste (acid chloride) was further dried for 1.5hrs at 0.1mm Hg. In a separate dry flask, 2.81 g (1A), 2 ml triethylamine, and 10 ml methylene chloride were combined. The acid chloride was then dissolved in 10 ml methylene chloride and slowly added to a solution of (1A) under a slow nitrogen purge. The reaction mixture was stirred overnight at room temperature, and then washed 3 times with deionized water. After removing the methylene chloride, 4.44 g of pure product was recovered as a clear oil, 75% yield. ¹H NMR δH 0.917-1.06 [m, 6 primary H], 1.21-1.54 [m, 8 secondary H], 1.88-1.90 [m, 1 tertiary H, 2 secondary H], 2.07-2.09 [m, 2H, CH₂CH=CH₂], 4.05-4.09 [m, 2H, CH₂OPh], 4.22-4.24 [m, 2H, CH₂OCOPh], 4.95-5.08 [m, 2H, CH=CH₂], 5.81-5.92 [m, 1H, CH=CH₂], 6.99-7.01 [m, 2H, Ar-H], 7.30-7.32 [m, 2H, Ar-H], 8.13-8.18 [m, 4H, Ar-H]

Terminal Si-H Mesogen A: (S)-2-methylbutyl 4-[4-(8-(1,1,3,3-tetramethyldisiloxane)octanyloxy)benzoyloxy]benzoate (4A). 3.8 g vinyl mesogen (3A), 6 ml toluene, and 4 drops of .12M hexachloroplatinic acid in tetrahydrofuran were mixed in a dry flask and set aside. 6ml toluene and 15 ml tetramethyldiloxane were mixed in a reaction flask with stir bar and heated to 60°C. The mixture containing the vinyl mesogen and catalyst solution was added dropwise via a syringe over a 10-15 minute period to the dilsilane solution contained in the reaction flask. After 24 hr of reaction the toluene and excess siloxane were removed at room temperature by vacuum. A bright green yellow oil remained. Column chromatography in 13-1 hexane-ethyl acetate gave 3.61 g pure product, an opaque colorless viscous liquid, 72% yield. The product has a thermal transition at 21°C (endotherm on heating) as measured by

differential scanning calorimetry. ¹H NMR δH 0.10-0.19 [m, 12 Si-CH₃], 0.4-0.5 [m, 2 Si-CH₂], 1.34-1.59 [m, 12 aliphatic CH₂], 1.80-1.98 [m, 1 tertiary H, 2 secondary H], 4.05-4.09 [m, 2H, CH₂OPh], 4.14-4.70 [m, 2H, CH₂OCOPh], 4.71 [s, 1 Si-H], 6.99-7.01 [m, 2H, Ar-H], 7.30-7.32 [m, 2H, Ar-H], 8.13-8.18 [m, 4H, Ar-H]

Mesogen A': (S)-2-methylbutyl 4-[4-(8-(1,1,1,3,3-pentamethyldisiloxane)octanyloxy)benzoyloxy]benzoate (4A). 4.41g (10.1mmol) of (3A), 6ml of toluene, and 10 drops of 0.12M hexachloroplatinic acid hydrate were mixed in a holding flask. This mixture was slowly added to a reaction flask held at 60° containing 7.6ml (40.4mmol) pentamethyldisiloxane and 8ml toluene. After 24hr of reaction, the solvent was removed by vacuum, and 5.19g of crude oil obtained, 88% yield. A fraction of this crude was purified with a silica column and 33-1 hexane ethyl acetate. This material has a Sc* - isotropic transition at 26°C. ¹H NMR δH 0.10-0.19 [m, 15 Si-CH₃], 0.4-0.5 [m, 2 Si-CH₂], 1.34-1.59 [m, 12 aliphatic CH₂], 1.80-1.98 [m, 1 tertiary H, 2 secondary H], 4.05-4.09 [m, 2H, CH₂OPh], 4.14-4.70 [m, 2H, CH₂OCOPh], 6.99-7.01 [m, 2H, Ar-H], 7.30-7.32 [m, 2H, Ar-H], 8.13-8.18 [m, 4H, Ar-H]

2.7 Synthesis of Mesogen B

Mesogen B was synthesized as described below, which is essentially the same scheme used to synthesize mesogen A.

4-(3-propenyloxy)benzoic acid (2B)

34.53g (0.25mol) of 4-hydroxybenzoic acid were added to 175ml ethanol in a round bottom flask. To this solution, 28.05g (0.5mol) KOH and 2.12g of KI were added in 35ml of water. After the solution was brought to reflux, 30.25g (0.25 mol) 3-bromo-1-propene was added through an addition funnel. The solution was further refluxed for

18hr, cooled to room temperature, diluted with 300ml water, then acidified to pH 4 with HCl. The white precipitate was washed thoroughly with water. The solids were recrystallized once from ethanol. 23.0g product obtained, 51.7% yield.

(S)-2-Methylbutyl 4-hydroxybiphenyl-4'-carboxylate (1B)

75ml benzene, 10g (0.110mol) (S)-2-methyl-1-butanol, 8.14g (0.038mol) 4'-hydroxy-4-biphenyl carboxylic acid, and 0.5ml concentrated sulfuric acid were added to a round bottom flask. The reaction was refluxed 60hr with a Dean-Stark condenser, then cooled to room temperature. After washing 3x with DI water, the product was concentrated then recrystallized 2 times in a 1:1 toluene:hexane mixture. 10.79g of white solids were recovered at 76% yield.

(S)-2-methylbutyl 4-(4-(3-propenyloxybenzoyloxy))biphenyl-4'-carboxylate (3B)

3.93g (0.022mol) 4-(3-propenyloxy)benzoic acid, 3 drops DMF, and 4.81ml thionyl chloride (0.066mol) were added to a flask with stirring. The reaction was run for 30min, then the excess thionyl chloride removed by vacuum. In a separate flask, 6.26g (0.022mol) of (2B), 25ml methylene chloride, and 6ml (0.043mol) triethylamine were combined. The acid chloride was diluted with methylene chloride and added dropwise to the flask containing (2B). The reaction was run overnight at room temperature, washed with water 3 times, then recrystallized from ethanol. 8.25g of product recovered, 84.5% yield. ¹H NMR: δ = 0.98-1.07 [m, 6 aliphatic -CH₃], 1.32-1.35 [m, 1 aliphatic H], 1.56-1.61 [m, 1 aliphatic H], 1.90 [m, 1 aliphatic H], 4.19-4.26 [m, 2H, CH₂OCOPh], 4.66 [d, 2H, CH₂=CH-CH₂-OPh], 5.38-5.40 [m, 2H, CH₂=CH-], 6.05-6.12 [m, 1H, CH₂=CH-], 7.03-7.05 [m, 2H, Ar-H], 7.32-7.34 [m, 2H, Ar-H], 7.68-7.70 [m, 4H, Ar-H], 8.14-8.21 [m, 4H, Ar-H]

Terminal Si-H Mesogen B:(S)-2-methylbutyl 4-[4-(3-(1,1,3,3 tetramethyldisiloxane)propanyloxy)benzoyloxy]biphenylbenzoate (4B)

24ml toluene, 8ml (0.049mol) 1,1,3,3 tetramethyldisiloxane, and 2.02g (0.0045mol) of (3B) were added to a flask with stirring. 4 drops of a platinum catalyst in xylenes (platinum-divinyl tetramethyl disiloxane complex in xylenes, Gelest product: SIP6831.0) were added and the solution was heated at 60°C for 18hr. After cooling to room temperature, the solvent and excess disilane were removed by vacuum and lime green solids remained. Column chromatography in 10:1 hexane ethyl acetate yielded 1.85g of white solids, 72.3% yield. ¹H NMR: δ = 0.09-0.22 [m, 12H, Si-CH₃], 0.70-0.71 [m, 2H, RCH₂-Si] 0.98-1.07 [m, 6 aliphatic -CH₃], 1.32-1.35 [m, 1 aliphatic H], 1.50-1.62 [m, 1 aliphatic H], 1.80-2.1 [m, 3H, aliphatic H], 4.03-4.06 [m, 2H, CH₂OPh]. 4.19-4.26 [m, 2H, CH₂OCOPh], 4.73 [s, 1H, Si-H], 7.03-7.05 [m, 2H, Ar-H], 7.32-7.34 [m, 2H, Ar-H], 7.68-7.70 [m, 4H, Ar-H], 8.14-8.21 [m, 4H, Ar-H] FTIR: strong Si-H stretch at 2121cm⁻¹.

2.8 Synthesis of mesogen C

Figure 2.7 shows the chemical structure of mesogen C, which is a constitutional isomer of mesogen B. In mesogen C, the biphenyl unit occupies the central position of the mesogen, while in mesogen B, the biphenyl unit lies at the terminus. The reason mesogen C was synthesized was that it is expected to promote phase segregation like mesogen B, but to have more favorable electro-optic properties, since its analogue with an aliphatic spacer has been reported to possess good electro-optic properties⁸.

Mesogen C was synthesized in the same manner as A, substituting 3-bromo-1-propene for 8-bromo-1-octene in preparation of 2A (Figure 2.4), and 4'-hydroxy-4-

biphenyl carboxylic acid for 4-hydroxybenzoic acid in preparation of **2A** (Figure 2.5). Time constraints prohibited a full study of mesogen C PS-LCP block copolymers. A LCP homopolymer using mesogen C was synthesized and shows excellent electro-optic properties (Chapter 5). Mesogen C was attached to one block copolymer sample; because of the low degree of substitution in this sample (42%), no liquid crystallinity was observed.

4'-(2-propenyl)-4-biphenyl carboxylic acid (2C): 5g (23.34 mmol) 4'-hydroxy-4-biphenyl carboxylic acid, 120ml 90vol% EtOH/ 10vol% H₂O, 2.88g (51.35mmol) KOH, and a few crystals of KI were loaded into a flask and heated to reflux. 2.2ml (25.67mmol) allyl bromide were added to the cloudy, heterogeneous, refluxing mixture. Upon addition of the allyl bromide, the solution became more cloudy and white as product precipitated. After refluxing overnight, the reaction mixture was cooled and dumped into 600ml D.I. water (more white solids precipitated). The pH of the slurry was adjusted to 5.5 by the dropwise addition of HCl. Upon the acidification, more white solids precipitated. 4.44g of dry white crystals were recovered at 73% yield.

(S)-(-)-4-(2-methylbutyloxycarboxy)phenyl-4'-(3-propenyloxy) biphenyl-4-carboxylate (3C): 4.33g (2C) (17.03mmol), 5ml thionyl chloride (60mmol), 2 drops of DMF, and 25ml CH₂Cl₂ were added to a flask under a slow N₂ purge. After one hour with stirring, all the solids had not dissolved and an additional 5ml of thionyl chloride was added. Twenty minutes later, all the solids had dissolved indicating conversion to the acid chloride. After 2 more hours of reaction time, the solvent was removed by vacuum and a white yellow solid (acid chloride) remained. This solid was further dried on the vacuum line for 1hr. In a separate flask, 30ml CH₂Cl₂, 3.55g chiral phenol (**1A**),

and 2.64ml Et₃N were added. The acid chloride was dissolved in 30ml CH₂Cl₂ and added slowly to the solution containing the chiral phenol (2A). After stirring overnight, the reaction solution was washed 3x with D.I. water and once with saturated NaCl. The solvent was removed and a yellow-white solid remained. A recrystallization from warm EtOH/ CH₂Cl₂ gave 4.66g of white crystals, a 62% yield.

Terminal Si-H Mesogen C: (S)-(-)-4-(2-methylbutyloxycarboxy)phenyl-4'-(3-(1,1,3,3-tetramethyldisiloxane)propanyloxy) biphenyl-4-carboxylate (4C):

80ml toluene, 20ml 1,1,3,3-tetramethyldisilane, 4.66g of (3C), were added to a flask and heated to 60°C. 10 drops of platinum catalyst in xylenes (platinum-divinyl tetramethyl disiloxane complex in xylenes, Gelest product: SIP6831.0) were directly added to the solution. After reacting overnight, very little starting material had been converted to product as measured by TLC, and an additional 10 drops of catalyst were added. 7 hours later, the reaction still had not proceeded to conversion and 25 additional drops of catalyst were added. After stirring for two additional days, the solvent was removed by vacuum. Full conversion still had not been reached by TLC analysis. After running a column in methylene chloride, 1.94g of white solids were obtained 32% yield. ¹H NMR: δ = 0.09-0.22 [m, 12H, Si-CH₃], 0.70-0.71 [m, 2H, RCH₂-Si] 0.98-1.07 [m, 6 aliphatic -CH₃], 1.32-1.35 [m, 1 aliphatic H], 1.50-1.62 [m, 1 aliphatic H], 1.80-2.1 [m, 3H, aliphatic H], 4.03-4.06 [m, 2H, CH₂OPh]. 4.19-4.26 [m, 2H, CH₂OCOPh], 4.73 [s, 1H, Si-H], 7.03-7.05 [m, 2H, Ar-H], 7.32-7.34 [m, 2H, Ar-H], 7.68-7.70 [m, 4H, Ar-H], 8.14-8.21 [m, 4H, Ar-H] FTIR: strong Si-H stretch at 2121cm⁻¹.

2.9 PS-PVMS Block Copolymer Synthesis

All reactions were carried out in an inert atmosphere glovebox. Glassware was dried overnight at 120°C. Styrene was purchased from Aldrich, washed 1x with 2% aqueous sodium hydroxide (this turned the styrene a light yellow color), 3x with deionized water, then dried over magnesium sulfate for an hour. The magnesium sulfate was filtered off and the styrene was vacuum distilled from calcium hydride and then from phenylmagnesium chloride. Trimethyltrivinylsiloxane, hexamethyltrisiloxane, and trimethylchlorosilane were purchased from Gelest. Trimethyltrivinylsiloxane was placed over molecular sieves and degassed by gently bubbling nitrogen through for 15 minutes. The hexamethyltrisiloxane was dissolved in benzene and stirred over calcium hydride overnight. The benzene was removed by vacuum and the monomer was then sublimed at room temperature. The trimethylchlorosilane were used without further purification. All reactions were carried out in an inert atmosphere glovebox. 1.6M butyllithium in hexanes was purchased from Aldrich and used without further treatment. Cyclohexane was stirred over calcium hydride overnight, degassed by a freeze-thaw cycle under vacuum, and then distilled under vacuum. Tetrahydrofuran was treated the same way as the cyclohexane, then was distilled finally from butyl lithium.

Polymerization procedure. 3 ml cyclohexane was added to a flask with stirring, followed by 75 μ l of 1.6 M butyl lithium. After stirring for about 1 minute, 1 ml styrene was added, and the solution became bright orange. After 4 hr of reaction, a small aliquot of the reaction mixture was taken and precipitated in methanol for analysis of the polystyrene homopolymer molecular weight distribution. In a separate flask, 0.30 g hexamethyltrisiloxane was dissolved in 0.5 ml cyclohexane and this mixture was added

to the living polystyrene solution. After 24 hr, the bright orange color of the living polystyryl anion had cleared, indicating the conversion of the living polystyryl anion to a siloxanolate anion. In a separate flask, 4 ml cyclohexane, 1.5 ml trimethyltrivinyltrisiloxane and 1.5 ml tetrahydrofuran were mixed, and this mixture was added to the polymerization flask. 24 hr after this addition, 35 μ l trimethylchlorosilane was added to terminate the polymerization, and the reaction mixture was allowed to stir for an additional 24 hr to ensure complete termination. The solvents were removed by vacuum, the product redissolved in a minimal quantity of tetrahydrofuran and then precipitated into methanol. Quantitative yield of white powder. $^1\text{H NMR}$ δ 0.02-0.17 [m, Si- CH_3], 1.70-2.22 [m, br, - CHPh -], 1.44-1.57 [m,br, - CH_2CHPh -], 5.79-6.06 [m,Si- $\text{CH}=\text{CH}_2$], 6.30-6.80 [m, Ar-H], 6.90-6.73 [m,Ar-H]

Mesogen attachment to block copolymer backbone. 0.144 g polystyrene-polyvinylsiloxane polymer was dissolved in 0.5 ml toluene with stirring at 60°C. 3 drops of a 0.12M hexachloroplatinic acid solution in THF were added to this mixture, which was stirred for several minutes. Finally, 0.5 g of Si-H tipped mesogen (~ 1:1 molar equivalents of vinyl groups to Si-H mesogens) was added drop-wise in 0.5 ml of toluene. The reaction mixture was stirred for 2 days at 60°C. The toluene was removed at room temperature by vacuum, and the product was then dissolved in a minimal amount of tetrahydrofuran and precipitated into methanol three times until no residual mesogen remained as measured in TLC. 0.450 g soft white product recovered. $^1\text{H NMR}$ δ 0.05-0.11 [m, Si- CH_3], 0.40-0.60 [m, Si- CH_2], 0.95-1.05 [m, $\text{CH}_3\text{-C}$], 1.22-1.70 [m, aliphatic], 1.72-2.10 [m, aliphatic], 4.01-4.11 [m, CH_2OPh], 4.14-4.24 [m, 2H, CH_2OCOPh], 5.70-

6.10 [m, Si-CH=CH₂], 6.30-6.80 [m, Ar-H], 6.94-6.99 [m, Ar-H], 7.01-7.10 [m, Ar-H],
7.26-7.30 [d, Ar-H], 8.12-8.15 [m, Ar-H]

2.10 LCP siloxane homopolymer synthesis

Anionic synthesis of polyvinylmethylsiloxane homopolymer (PVMS1) using monofunctional initiator. 1 ml of trimethyltrivinylsiloxane in 2 ml THF was added to a solution of 2 ml THF and 280 ml lithiumtrimethylsilanolate. Lithium trimethylsilanolate is deep orange in solution. The solution became light orange/yellow when the monomer was added. After 12 hours of reaction at room temperature, 44 μ l of trichloromehtylsilane was added to terminate the polymerization. The solution was stirred an additional 12 hours to ensure termination. The product was precipitated directly into 50 ml of methanol containing 0.5 ml of triethylamine. The polymer precipitated as a second liquid phase. 0.273 g product, 28% yield, recovered. Mw=8428, Mn=6922, PDI =1.22.

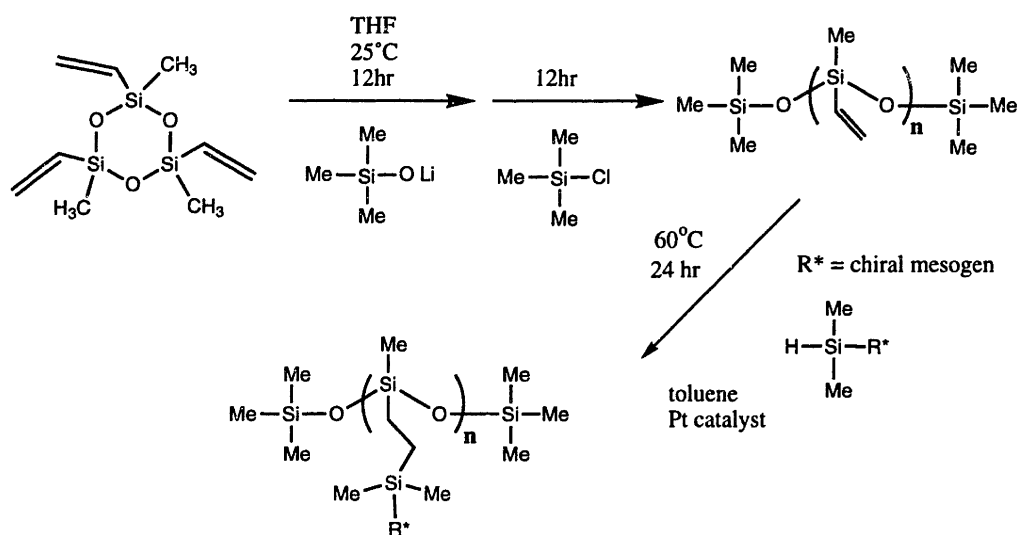


Figure 2.8 Anionic synthesis of siloxane side-chain LCP using a monofunctional initiator.

Mesogen A attachment to homopolymer backbone made with monofunctional initiator (LCPA47). 93 mg (PVMS1) ($M_w=8428$, $M_n=6922$, $PDI=1.22$) was mixed with 0.6 ml toluene and heated to 60°C. Two drops of a 0.12M hexachloroplatinic acid solution in THF were added to this mixture. In a separate vessel, 586mg Si-H tipped mesogen A was mixed with 0.6 ml toluene. This solution was added dropwise to the polymer solution containing the catalyst. 0.6 ml additional toluene used to rinse out the vessel that contained the mesogen and the wash was added to the reaction. After 24 hr of reaction, excess mesogen was removed by running the crude reaction mixture through 2.5 inches of silica gel, using toluene as the eluant. Once the excess mesogen had been removed, the product was eluted with THF, then concentrated and precipitated into methanol. Product is a white sticky paste, 0.381g recovered. GPC results: $M_w=42,823$ $M_n=34,461$ $PDI=1.24$.

Preparation of difunctional lithium silanolate initiator (DFI). 32ml dry THF, 2.314g (10.23mmol) 1,4-bis(hydroxydimethyl-silyl)benzene, and 1.160g (48.45mmol) lithium hydroxide were added to a round bottom flask and stirred for 2 days. The excess LiOH was filtered out of the solution, leaving behind the pure lithium siloxanolate in THF solution.

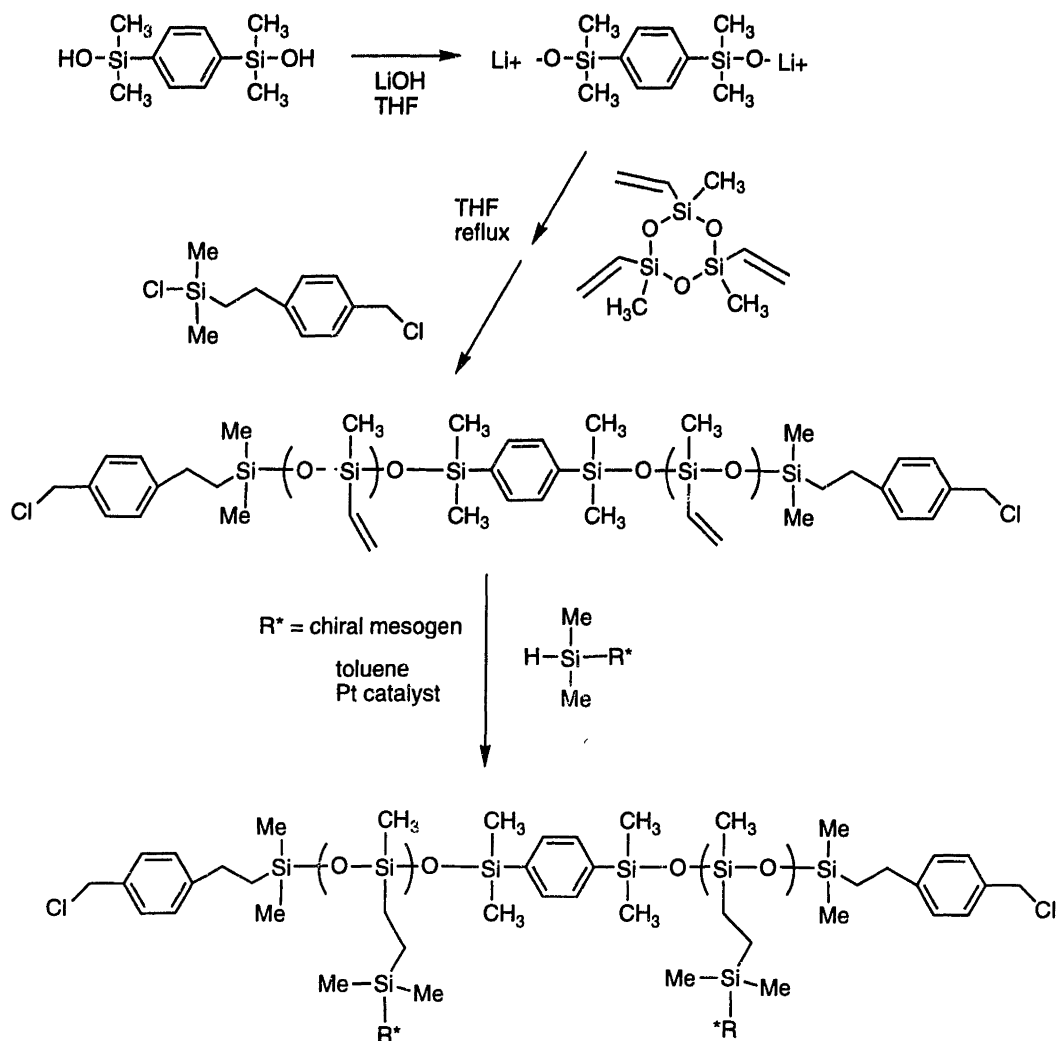


Figure 2.9 Anionic synthesis of PVMS using a difunctional initiator and endcapping agent.

Anionic synthesis of polyvinylmethylsiloxane (PVMS2) homopolymer using

difunctional initiator. 10ml trimethyltrivinylcyclotrisiloxane (V3) in 5ml THF were added to 5ml of THF solution containing the difunctional initiator (1.99 mmol initiator). The solution was refluxed overnight and then cooled to room temperature before adding 1.6ml (7.23 mmol) ((chloromethyl)phenylethyl)dimethylchlorosilane. The solution was stirred overnight, concentrated, then precipitated into methanol. 7.64g clear oil

recovered, 79% yield. GPC analysis: $M_w=12,750$; $M_n=6,900$; PDI = 1.85, NMR indicates all difunctional polymers, i.e α,ω endfunctional siloxanes. ^1H NMR δ H ppm 0.09-0.93 [m, Si- CH_3], 1.59 [m, 4H, CH_2 -Si], 2.69 [m, 4H CH_2 -Ph], 4.59 [s, 4H, Cl- CH_2 -Ph], 5.79-6.01 [m, $\text{CH}_2=\text{CH}$ -Si], 7.20 – 7.31 [m, 8H, Ar-H (from Cl- CH_2 -Ph- CH_2CH_2 -) end groups], 7.57 [s, 4H, Ar-H (from O-Si-Ph-Si-O) initiator]. NMR end group analysis estimates M_n to be 17,658 (likely too high in light of GPC analysis of this polymer and of its functional LCPB 35)

Attachment of mesogen B to difunctional PVMS (LCPB 35). 260mg mesogen B, 51mg (PVMS2), 1/2ml toluene, and 2 drops platinum catalyst in xylenes (platinum-divinyl tetramethyl disiloxane complex in xylenes, Gelest product: SIP6831.0) were added to a flask with stirring. After stirring overnight at 60°C , the toluene was removed by vacuum, the crude product was dissolved in a minimum of THF and then precipitated into methanol. 232mg of product recovered, white paste. GPC results: $M_w = 59,780$; $M_n = 38,190$; PDI = 1.84

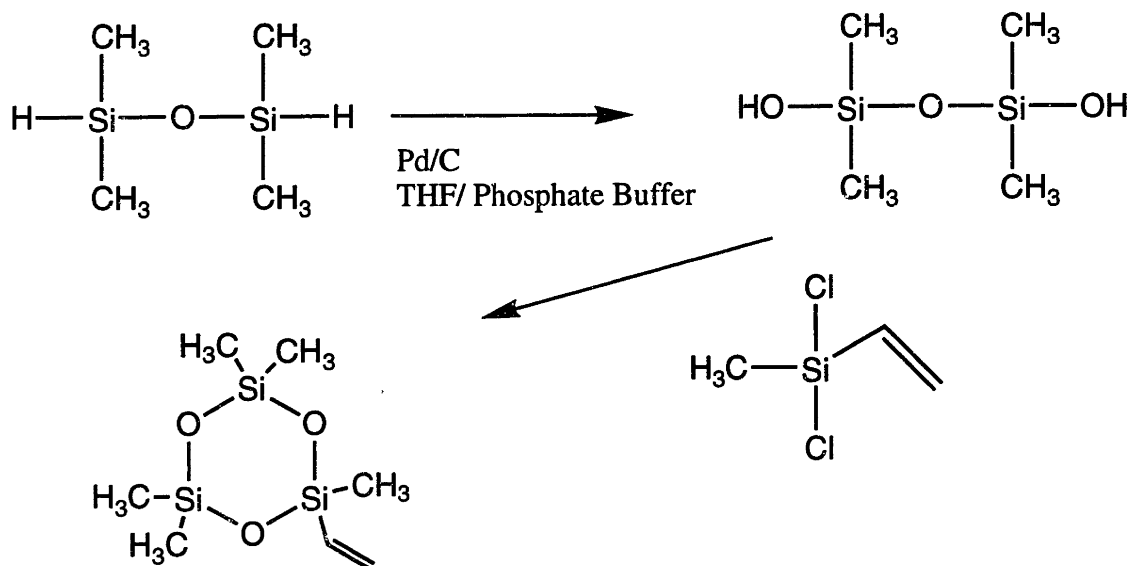


Figure 2.10 Synthesis of V_1D_2 monomer.

Synthesis of V1D2 monomer V1D2D2 monomer was synthesized as shown in Figure 2.10. The reason it was made (instead of purchasing V3 from Gelest) was that with poly V1D2 based LCPs we expected enhanced phase segregation between the LCP and the polystyrene in the block copolymer, because of the greater siloxane content. Moreover, a viable ATRP route to PS-LCP-PS triblocks would require complete substitution of the vinyl groups in the LCP prior to polymerization of styrene, and for steric reasons it would be easier to substitute poly V1D2 than poly V3. The following procedure for V1D2 synthesis was adapted from Hempenius et al³.

Tetramethyldisiloxane-1,3-diol. - A phosphate buffer containing 20ml 0.1N NaOH and 0.322g $H_2NaPO_4 \cdot H_2O$ in 500ml D.I. water was prepared. In a round bottom flask equipped with a stir-bar and bubbler, 30ml phosphate buffer, 55ml THF, and 0.635g 10wt% palladium on carbon (Aldrich 20-569,9) were added and cooled to 0°C. To this solution, 25ml tetramethyldisiloxane in 25ml THF were added slowly with stirring. Vigorous bubbling ensued upon the addition of the disilane (evolution of H_2). After the addition was complete, the mixture was stirred overnight at room temperature and the Pd/C catalyst filtered off. The solvents were removed by vacuum and white crystals remained. Recrystallization from hot hexane yielded 18.07g of white crystals, 77% yield.

Pentamethylvinylcyclotrisiloxane, V₁D₂ - 3ml Et_3N , and 70ml Et_2O were loaded into a 3-neck flask under N_2 at 0°C. Two addition funnels were fitted on the flask. In one funnel 14.1 ml (108.9 mmol) methylchlorovinylsilane and 226ml Et_2O were placed. In the other funnel, 18.07g (108.9mmol) of the siloxane diol, 30.3ml Et_3N , and 192ml Et_2O were placed. The contents of the addition funnels were then both added at a moderate rate to

the flask. Copious quantities of a white precipitate, $\text{Et}_3\text{NH}^+\text{Cl}^-$ formed immediately, forming a slurry. After stirring overnight, the white precipitate was filtered off and washed with Et_2O . The washes were combined with the filtrate. The solution was concentrated with a roto-vap, then washed three times with D.I. water and placed over MgSO_4 to dry. The product was isolated by first stripping the remaining Et_2O and Et_3N with a small vacuum pump 25" Hg for 15 minutes, then using high vacuum 0.1mm Hg with a liquid N_2 trap to capture the monomer. 6.28g clear liquid recovered, 25% yield.

Synthesis of poly V_1D_2 with a difunctional initiator (PV_1D_2):

20ml THF, 3ml of V_1D_2 monomer, and 1.75ml of a solution of difunctional initiator (prepared as described previously (**DFI**)) were added to a flask under N_2 and refluxed for 18hr. After cooling to room temperature, 500 μl of terminating agent ((chloromethyl)phenylethyl)dimethylchlorosilane was added and the solution was stirred overnight. The solution was concentrated and precipitated into 60ml of methanol. After vacuum drying, 0.751g clear oil remained. NMR revealed that all the chains to be difunctional with benzyl chloride endcapper. ^1H NMR δ H ppm 0.09-0.93 [m, Si- CH_3], 1.59 [m, 4H, CH_2 -Si], 2.69 [m, 4H CH_2 -Ph], 4.59 [s, 4H, Cl- CH_2 -Ph], 5.79-6.01 [m, $\text{CH}_2=\text{CH}$ -Si], 7.20 – 7.31 [m, 8H, Ar-H (from Cl- CH_2 -Ph- CH_2CH_2 -) end groups], 7.57 [s, 4H, Ar-H (from O-Si-Ph-Si-O) initiator]. This polymer was not detectable with the GPC 254nm UV detector or with the RI detector. However, end-group analysis from NMR estimates its M_n to be 15,800. This estimate is likely high as discussed in the synthesis of PVMS2.

Functionalization of (PV_1D_2)with meosgen C (LCPC 19): 0.392g of PV_1D_2 , 0.98 meosgen C, and 4ml of toluene were placed in a flask and heated to 60°C. 4 drops of

platinum catalyst in xylenes (platinum-divinyl tetramethyl disiloxane complex in xylenes, Gelest product: SIP6831.0) were added and the solution stirred overnight. The toluene was removed by vacuum, the crude solids dissolved in ~2ml THF and precipitated into ~25ml methanol. 1.048g product recovered, 76% yield. NMR shows approximately 69% substitution of the vinyl groups. GPC Mw = 39,096; Mn = 18,937 ; PDI = 2.06. The polymer is a sticky goo with a single Sc*- isotropic clearing point at 31.4°C.

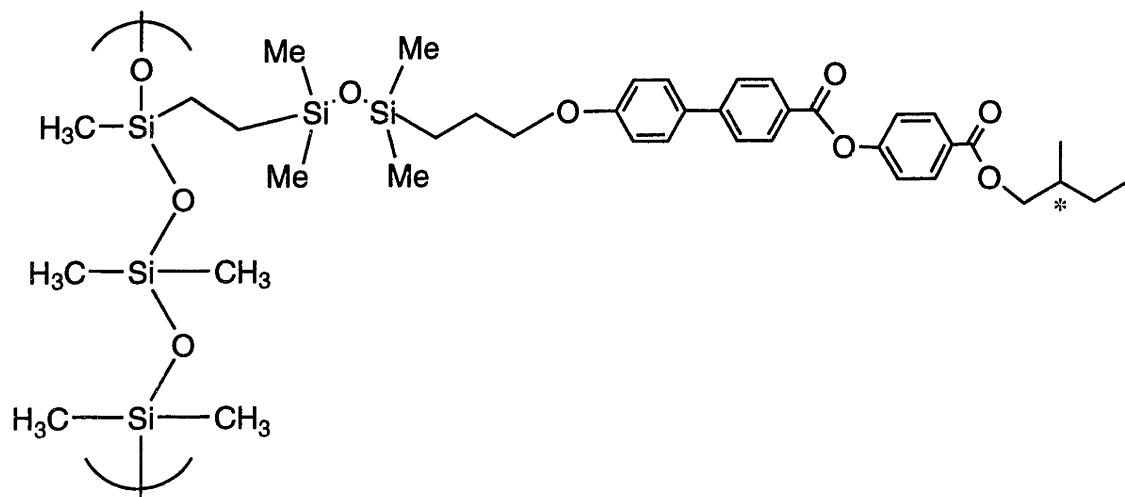


Figure 2.11 Repeat unit structure of LCPC 19. A PVMS backbone was synthesized substituting V_1D_2 monomer for V3, using a difunctional initiator and a benzyl chloride end capping agent as shown in Figure 2.8.

2.11 Summary of Materials Synthesized

The general block copolymer structure appears in Figure 2.2, and Tables 2.1 and 2.3 list all homopolymer and block copolymer samples synthesized in this study and their molecular weights. The polydispersities of the polymers are given in Tables 2.2 and 2.4 for mesogen A and B polymers respectively. Samples are labeled by the molecular weights of each block and the mesogen used, either A or B. Thus, PS 12 – LCPC 8 is a block copolymer sample with the following structure: polystyrene Mn = 12,000; liquid

crystalline siloxane (mesogen A) $M_n = 8,000$. The same system is used to label homopolymers, e.g., LCPB 35 is a liquid crystalline siloxane homopolymer (mesogen B) with $M_n 35,000$. The LCP block molecular weight in the sample label is an estimate from NMR integration, as this proved to be most accurate in light of our morphological characterization.

Table 2.1 Summary of polymers made with mesogen A.

Samples	Wt % LCP	Mn, PS GPC	Mn, siloxane GPC	Mn, siloxane NMR	% sub NMR	Mn, LCP NMR	Mn, LCP GPC
LC Homopolymer							
LCPA 47	100	--	6,900	--	92	47,300	34,500
Block Copolymers							
PS 12 - LCPA 8	40	12,000	2,600	1,500	100	8,100	15,900
PS 39 - LCPA 30	43	39,300	7,600	5,700	82	29,800	21,800
PS 13 - LCPA 81	86	13,300	27,400	16,100	73	81,100	38,100
PS 14 - LCPA 129	90	14,100	29,100	21,200	86	129,900	57,000

Table 2.2 Polydispersity index of polymers made with mesogen A.

Samples	Wt % LCP	PS block PDI	PS-PVMS PDI	PS-LCP PDI (after mesogen added)	% Substitution NMR
LC Homopolymer					
LCPA 47	100	--	1.22	1.26	92
Block Copolymers					
PS 12 - LCPA 8	40	1.03	1.05	1.18	100
PS 39 - LCPA 30	43	1.02	1.04	1.42	82
PS 13 - LCPA 81	86	1.05	1.13	1.49	73
PS 14 - LCPA 129	90	1.06	1.13	1.32	86

Table 2.3 Summary of polymers made with mesogen B.

Samples	Wt % LCP	Mn, PS GPC	Mn, siloxane GPC	Mn, siloxane NMR	% sub NMR	Mn, LCP NMR	Mn, LCP GPC
LC Homopolymer LCPB 35	100	0	6900		68	35,100	38,200
Block Copolymers							
PS 12 – LCPB 8	40	12,000	2,600	1,500	99	8,200	18,400
PS 14 – LCPB 111	89	14,100	29,100	21,200	69	111,200	82,000

Table 2.4 Polydispersity index of polymers made with mesogen B.

Samples	Wt % LCP	PS block PDI	PS-PVMS PDI	PS-LCP PDI (after mesogen added)	% substitution NMR
LC Homopolymer LCPB 35	100	-	1.85	1.84	68
Block Copolymers					
PS 12 – LCPB 8	40	1.03	1.05	1.20	99
PS 14 – LCPB 111	89	1.06	1.13	1.22	69

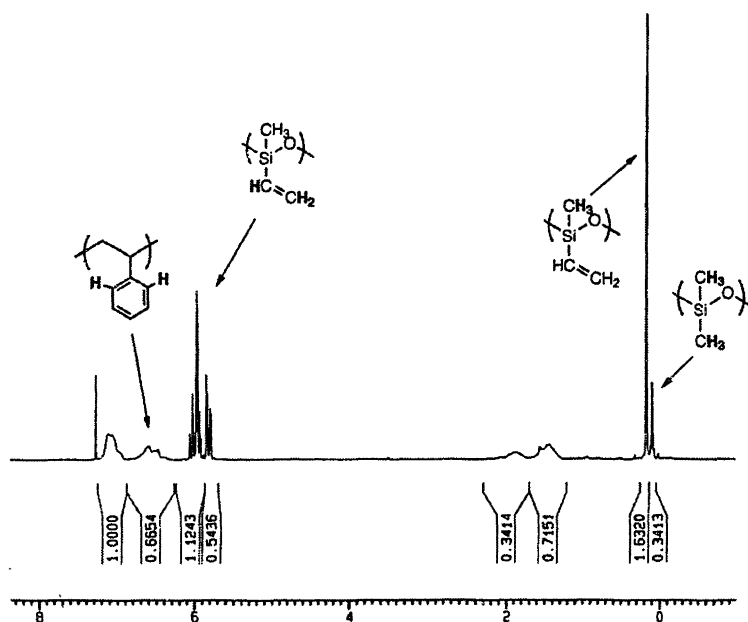


Figure 2.12 ^1H NMR spectra of PS-PVMS block copolymer before mesogen attachment. The composition of this polymer is estimated from the labeled peaks. For this sample, PS Mn GPC = 14,100; Siloxane Mn GPC = 29,100; Siloxane Mn NMR = 21,200.

The polydispersities of the block copolymers range from 1.18 - 1.49, with lower degrees of substitution generally leading to higher polydispersities. LCPB 35 has a high PDI (1.84) as it was synthesized with a difunctional initiator prepared in the lab in ambient conditions, while LCPA 47 was prepared with a initiator purchased from a supplier (Aldrich) that was prepared in inert conditions.

2.12 Molecular Weight Determination

The polystyrene molecular weight was estimated by taking a GPC of this block before the siloxane monomers were added. The GPC is calibrated with respect to polystyrene standards, hence the polystyrene block MW is known accurately. After the siloxane monomers were added and polymerized, ¹H NMR was then used to calculate the composition of the resulting PS-PVMS polymer. The time between successive pulses (D1) on the NMR instrument was set to 15 sec to improve the accuracy of the integration and resulting composition calculations. Because a small amount of D3 monomer is used to convert the living polystyryl anion to a siloxanolate anion before the addition of V3 (Figure 2.2), the siloxane block contains both methylvinyl siloxane repeats and dimethyl siloxane repeat units. Three types of repeat units are therefore considered: polystyrene repeats, polydimethyl siloxane repeats, and vinylmethyl siloxane peaks. Each of these units has distinct peaks in NMR as shown in Figure 2.12. The composition

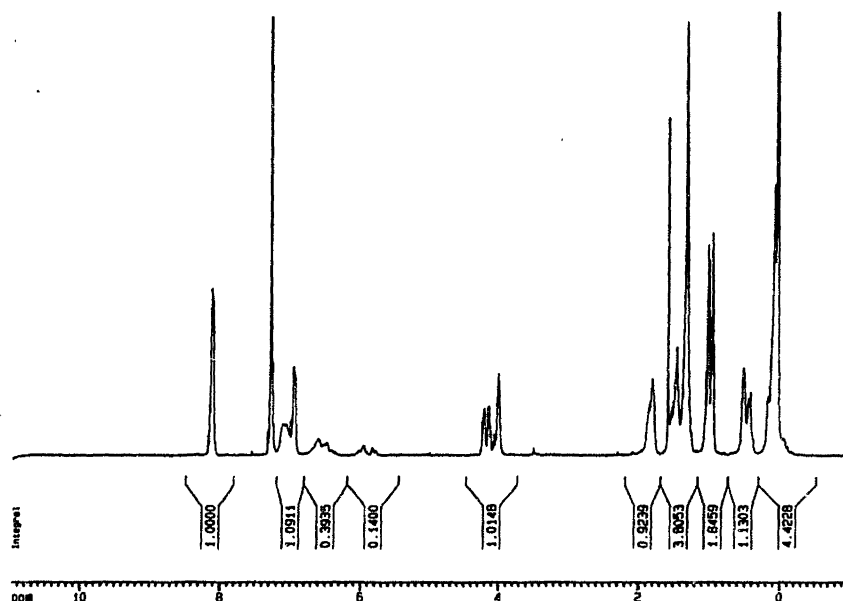


Figure 2.13 ^1H NMR spectra of PS 14 - LCPA 129 block copolymer after mesogen A attachment. The block copolymer substrate is the same as that shown in Figure 2.6.

of the PS-PVMS block copolymer is estimated from these peaks. The PS molecular weight (GPC) and the composition of the PS-PVMS block copolymer (NMR) are used to calculate a molecular weight of the siloxane block, and the average number of vinyl repeats in the siloxane block. In addition, the ratio of vinyl units to styrene units is noted, as this changes after the mesogen is attached. This ratio is taken as $2/3$ times the vinyl proton integration divided by the aromatic polystyrene protons integrated from δ 6.60 – 6.49 ppm. These two aromatic protons don't overlap with any of the mesogen protons. The other 3 aromatic protons overlap with mesogen aromatic protons, and hence are not used in the calculation. Once the mesogen has been attached to the second block and the polymer purified, NMR of this product gives the ratio of remaining vinyl units to polystyrene units. Figure 2.13 is an NMR spectra of PS14 LCPA129. As the number of polystyrene units remains the same before and after the mesogen is attached, a degree of substitution can be calculated, that is the fraction of vinyl groups that have reacted with

the mesogen. Finally, the molecular weight of the entire LCP block is taken as the sum of the siloxane block M_n before mesogen attachment and the additional molecular weight due to the mesogens. This is reported as an NMR based molecular weight estimate of the LCP block.

2.12.1 A note about molecular weight measurements

The molecular weights of the polystyrene blocks are accurate, as our GPC is calibrated with polystyrene standards, and a sample of this block was taken before the second block was formed. The molecular weights of the liquid crystalline blocks, however, are estimates based on NMR integration, and are thus less accurate than the polystyrene molecular weights. We choose to use the NMR estimates instead of the GPC estimates of the LC block lengths because they are more consistent with our TEM and SAXS morphologies. In particular, PS12 – LCPB 8 was found to have small LC cylinders embedded in a majority polystyrene matrix, which is clearly inconsistent with the GPC estimated molecular weight of the LCP block of 18,350. The NMR estimates were therefore assumed to be more accurate over the entire molecular weight range. The relaxation time D1 was set to 15sec for all NMR runs on the polymer samples.

A GPC instrument calibrated for a linear polymer is inadequate for measuring the molecular weights of a block copolymer consisting of the linear block (for which the GPC is calibrated for) linked to a comb shaped block of different chemical composition. Comparing GPC and NMR estimates of the LCP block length reveals that the GPC under-predicts *AND* over-predicts the NMR based LCP block length, depending on the sample. For those samples with large LCP blocks (NMR block size > 50K), the GPC generally under-predicts the molecular weight, the extreme case being PS 14 – LCP A

129, in which the NMR estimated LCP size is 129K, and the GPC estimate is 57K. This is in agreement with the common observation that branched polymers have intrinsic viscosities lower than a linear molecule of the same molecular weight⁹. As the LCP block becomes smaller and the fraction of PS higher in the block copolymers, the GPC over-predicts the NMR estimated molecular weight. In both PS 12 – LCPA 8 and PS 12 – LCPB 8 the GPC over-estimated the LCP block molecular weights as 15.9K (8.1K NMR) and 18.4K (8.1K NMR). The fact that PS 12 – LCPB 8 was found to have a morphology of small LC cylinders embedded in a PS matrix (Chapter 3) lends credibility to these NMR estimates and makes the GPC estimates suspect. So, as the polymer becomes less branched (smaller LCP content), the effects of the branching become less important than the block copolymer junction and chemical composition. The coils become more expanded in solution relative to a linear polystyrene block of the same molecular weight, and the GPC thus over predicts the molecular weight of the second block.

2.13 References

1. Brandrup, J. & Immergut, E.H. *Polymer Handbook*, 3rd Ed. (John Wiley & Sons, New York, 1989).
2. Saam, J.C., Gordon, D.J., and Lindsey, S. *Macromolecules* **3**, 1-4 (1970).
3. Hempenius, M.A., Lammertink, R.G. & Vansco, J.G. *Macromolecules* **30**, 266-272 (1997).
4. Suzuki, T.; Okawa, T. *Makromol. Chem., Rapid Commun.* **9**, 755-760 (1988).
5. Frye, C.L., Salinger, R.M., Fearon, F.W.G., Klosowski, J.M. & DeYong, T. *The Journal of Organic Chemistry* **35**, 1308-1314 (1970).
6. Nakagawa, Y. & Matyjaszewski, K. *A.C.S. Polymer Preprints* **37**, 270-271 (1996).
7. Nakagawa, Y., Miller, P., Cristina, P. & Matyjaszewski, K. *A.C.S. Polymer Preprints* **38**, 701-702 (1997).
8. Cooray, Nawalage F., Masa-aki Kakimoto, Yoshi Imai, Yoshi-ichi Suzuki, *Polymer Journal* **25**, 863-872 (1993).

9. Zimm, B.H. & Kilb, R.W. *Journal of Polymer Science B: Polymer Physics* **34**, 1367-1390 (1996 (first published 1959)).

Chapter 3 Morphology and Thermal Properties

3.1 Background and Related Literature

The morphology of the PS-LCP siloxanes was examined by TEM and SAXS to establish general trends and phase diagrams in the PS-LCP block copolymers, and to determine influence of block copolymer morphology on the orientation of the mesogens in LCP domains. The morphological data is combined with DSC measurements of LC clearing points and polymer Tg's to give a more complete picture of the block copolymer structure-property relationships.

In previous work on amorphous-LCP block copolymers all the traditional block copolymer morphologies have been found, although no single system has displayed all of them. Mao et al. observed all the traditional morphologies save amorphous spheres in a LCP matrix¹. However, this one “missing” morphology was observed by Fischer et al.² in a different system.

Fisher also found that the block copolymer microdomain morphology can influence the type of LC phase formed. When the LCP blocks form a continuous morphology, the LCP is in the smectic A phase. LCP spheres, however, displayed the nematic phase, possibly because the spherical shape is not compatible with a smectic packing of the mesogens. In addition, the S_A -isotropic clearing point is depressed by $\sim 20^\circ\text{C}$ relative to the homopolymer LCs, but this is not systematic in PS volume fraction².

Furthermore, there is an absence of LC cylinders in Fisher's phase diagram; the morphology transitions directly from LC lamellae to LC spheres. This is due to the strong tendency of the LCP block to stay in a lamellar configuration, and has been

observed in other smectic systems³. There are counterexamples, however, that do include the LCP cylinder morphology¹ (this thesis, page 89); in Mao's system, there was still a strong tendency for the lamellar configuration and the phase diagram is skewed to one side.

Zheng and Hammond found that the LC clearing point is linked to the ODT in PS-LCP methacrylates when the LCP block volume fraction is high, and introduced a chi-parameter explanation of this effect³. In these samples, the LC clearing point and the ODT coincide, indicating that the LC can drive phase separation in a system that might otherwise be mixed. When the LC clearing point lies below the ODT, the microphase segregated morphology forms before onset of LC order. In the LC methacrylates, the morphology generally stabilized the smectic C* phase (the clearing point temperature increases in the block copolymers relative to the LC homopolymer).

A common observation among smectic LC blocks is a decrease in the clearing point transition enthalpy (normalized to LCP content) with increasing amorphous block content^{1, 2, 4-6}. This is attributed to an interfacial effect: as the amorphous block volume fraction goes up the surface area to volume ratio of the LC domains increases.

3.2 Experimental

Sample Preparation: All polymer samples were cast from a concentrated ($\geq 10\text{wt}\%$) toluene solution onto a teflon coated sheet, then air dried for $\sim 24\text{hr}$. SAXS measurements were taken on the as cast films. The films were then vacuum dried for $\sim 18\text{hr}$ at elevated temperature prior to additional SAXS measurements. If the annealing resulted in a more well defined SAXS peak, TEM characterization was performed on

annealed samples, otherwise TEM was performed on the solvent cast samples (annealing slightly discolored the samples due to residual platinum from the synthesis). The annealing temperatures were selected from 80°C-110°C depending on the sample, and the annealing times ranged from 12 – 18hr (overnight). Polymers made with mesogen A were annealed at or above the PS Tg, and above the LC clearing point and LCP Tg. Polymers made with mesogen B had higher clearing points, and hence were annealed above both block Tg's and below the LC clearing point. Film thickness was on the order of 0.25mm.

TEM: A Reichert-Jung FC4E Ultracut E was used to ultracryotome samples of 40-50nm in thickness below room temperature. The diamond knife temperature was set at -100°C and the sample temperature set at -120°C. Films were transferred to copper grids and stained for 15 minutes with the vapor from a RuO₄ 0.5% aqueous solution. The RuO₄ stain is preferentially absorbed by the polystyrene, making these regions appear dark in the TEM images. Samples were then observed with a JEOL 200CX electron microscope operating at 200kV.

SAXS: A Siemens 2-D SAXS detector placed 130cm from the sample was used to detect the scattering of Cu K α . X-Rays at 40kV and 24mA.

DSC: A Perkin-Elmer DSC-7 with liquid nitrogen cooling system was used for low temperature DSC. All scans were conducted at a heating/ cooling rate of 20°C/min.

OM: A Leica Optical Microscope equipped with a Mettler FP82HT hot stage/ FP90 controller was used to observe samples under crossed polarizers at different temperatures.

GPC: A Waters gel permeation chromatography (GPC) system equipped with 2 Styragel HT3 columns (500-30,000 MW range), 1 Styragel HT4 column (5,000-600,000

MW range), and a UV detector (254nm) was used for molecular weight measurement relative to polystyrene standards. Tetrahydrofuran (THF) flowing at 1ml/ min was the mobile phase.

NMR: ^1H NMR measurements were taken with a Bruker Avance DPX400 400MHz instrument using CDCl_3 as a solvent.

3.3 Results and Discussion

The general structure of the PS-LCP block copolymers is shown in Figure 2.2. Two series of polymers were prepared, each series with a different mesogen. The structures of the mesogens are shown in Figure 2.3. Mesogen B has a shorter aliphatic spacer length and a more rigid core than Mesogen A. The final LCP siloxane block contains three types of repeat units: PDMS (1 - 6wt% of LCP block), functionalized mesogen repeats (89-100wt% of LCP block), and unreacted PVMS repeats (0-5wt% of LCP block). Tables 3.1 and 3.4 summarize the block copolymer structures synthesized with both mesogens, and illustrate the range of block sizes and total block copolymer molecular weights that have been made. There were no apparent practical limits on block sizes; large (~120,000 Mn) and small (~8,000 Mn) LCP blocks were successfully prepared.

3.4 Mesogen A polymers

The first series of samples, those made with mesogen A and appearing in Table 3.1, range in total molecular weight from 20,000 – 144,000 with weight fractions of liquid crystal from 0.4 – 0.9. The thermal properties of these samples are given in Table 3.2.

Table 3.1 Molecular weight characterization of polymers made with mesogen A.

Samples	Wt % LCP	Mn, PS GPC	Mn, siloxane GPC	Mn, siloxane NMR	% sub NMR	Mn, LCP NMR	Mn, LCP GPC
LC Homopolymer							
LCPA 47	100	--	6,900	--	92	47,300	34,500
Block Copolymers							
PS 12 – LCPA 8	40	12,000	2,600	1,500	100	8,100	15,900
PS 39 – LCPA 30	43	39,300	7,600	5,700	82	29,800	21,800
PS 13 – LCPA 81	86	13,300	27,400	16,100	73	81,100	38,100
PS 14 - LCPA 129	90	14,100	29,100	21,200	86	129,900	57,000

Table 3.2 Thermal properties of polymers made with mesogen A. Values taken from DSC heating scans at 20°C/min heating rate.

Sample ID	Wt % LCP	% Sub. NMR	PS Tg °C	LCP Tg °C	Smectic Clearing Pt. °C	ΔH clearing J/g	ΔH clearing J/g LCP
LCPA 47	100	92	-	-24	90	6.71	6.71
PS 12 – LCPA 8	40	100	-	-	-	-	-
PS 39 – LCPA 30	43	82	84	-35	43	0.17	0.38
PS 13 – LCPA 81	86	73	70 (84)	-34	60	3.46	4.01
PS 14 – LCPA 129	90	86	61 (89)	-32	79	5.59	6.20

Numbers in (parenthesis) are PS Tg's of PS-PVMS block copolymers measured before the mesogens are attached to the PVMS block.

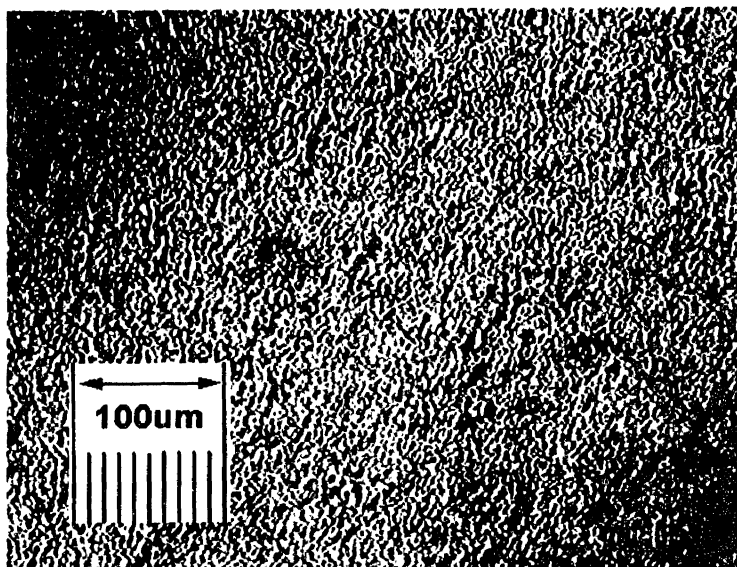


Figure 3.1 OM image of PS 39 – LCPA 30 taken between crossed polarizers at room temperature.

When a liquid crystalline phase did exist in the mesogen A polymers, it showed a single LC transition, a smectic C*– isotropic clearing point that was detected in DSC and observed in OM. The OM textures of the polymers were all sandy, fine grained smectic textures; an illustrative example appears in Figure 3.1 for PS 39 – LCPA 30. In addition, a smectic spacing of $\sim 36\text{\AA}$ was maintained in all the LCPA block copolymers and homopolymers. Figure 3.2 is an illustrative DSC scan showing the two Tg's and the single liquid crystalline clearing point of sample PS 14 – LCPA 129. All but one (PS 12 – LCPA 8) of the block copolymer samples in this series have two distinct Tg's and a single liquid crystalline transition, a smectic C* clearing point. The exception, sample PS 12 – LCPA 8, has no observable Tg's or clearing points, nor is it birefringent in OM. In addition, this sample has no smectic SAXS peak. Thus we conclude that the blocks in PS 12 – LCPA 8 are miscible with each other due to their low MW, whereas

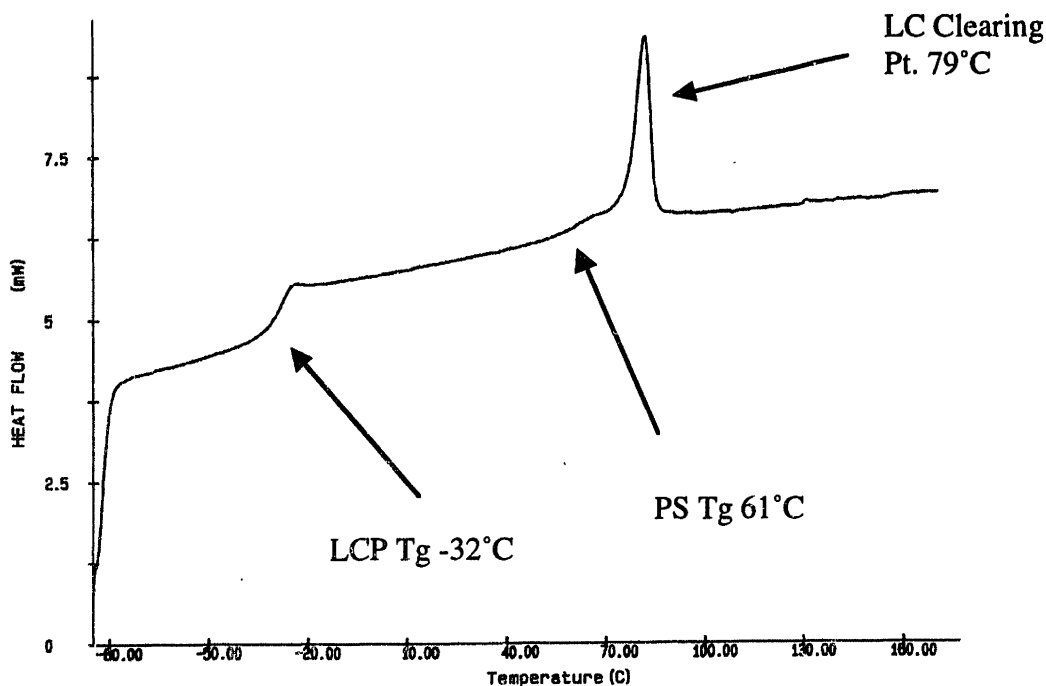


Figure 3.2 DSC heating trace at 20°C/min of PS 14 - LCPA 129 showing two Tg's and a single smectic liquid crystalline clearing point.

the other samples are all microphase segregated. All the clearing points are below the polystyrene Tg, except in the case of PS 14 – LCPA 129 which has a clearing point 18°C higher than the polystyrene Tg. The Tg of the homopolymer LCPA 47 was measured to be 10°C higher than the Tg's of the LCP blocks in the homopolymers. All scans were done at 20°C/ min, but the homopolymer run was collected on a different DSC instrument than the other samples. The measured discrepancy is likely due to differences in instrumental calibration/ setup, or to differences in degree of substitution along the polymer backbones.

As the polystyrene content increases in this series, the liquid crystalline clearing point decreases from 90°C in the homopolymer to 43°C in PS 39 – LCPA 30. In addition, the polystyrene Tg is plasticized by the LC block by as much as 30°C in PS 14 –

LCPA 129, while the T_g of the liquid crystal block remains constant at ~ -35°C. These trends suggest some degree of phase mixing which destabilizes (lowers the clearing point) the LCP phase and plasticizes the polystyrene.

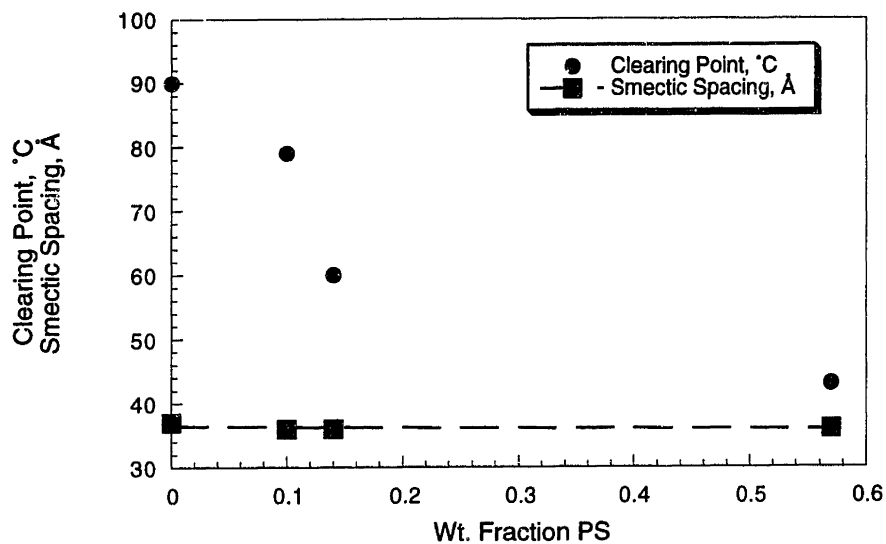


Figure 3.3 Clearing point (°C) and smectic d-spacing (Å) vs. wt. fraction PS in LCPA block copolymers.

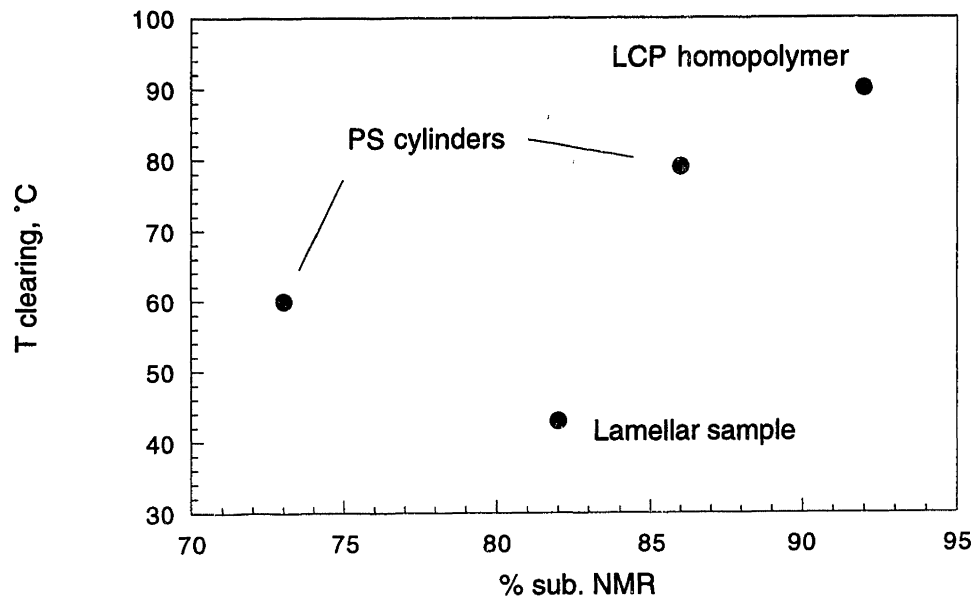


Figure 3.4 Clearing point (°C) vs. % mesogen substitution in the LCP block.

The 2nd column of Table 3.4 shows SAXS measurements of the smectic layer spacing in these samples. The smectic spacings don't change more than an angstrom (relative to a pure LC homopolymer), except for PS 12 – LCPA 8, which has no liquid crystalline peak and no indication of a birefringent LC phase in OM. In light of the thermal data, the SAXS data show that LCP domains maintain the same smectic spacing while their clearing point is lowered either by differences in degrees of substitution of mesogen along the backbone, or by geometrical/ packing effects of the microdomains.

This clearing point depression is illustrated in Figures 3.3 & 3.4. Figure 3.3 shows a plot of clearing point (°C) and smectic d-spacing (Å) vs. wt. fraction PS, while Figure 3.4 shows a plot of clearing point (°C) vs. % substitution of the mesogen along the

polymer backbone. The important fact that these plots illustrate is that the lamellar sample, PS 39 – LCPA 30, has a clearing point that is depressed by $\sim 50^{\circ}\text{C}$ with respect to the LCP homopolymer, and that this depression cannot be attributed to degree of substitution. That is, the morphology is responsible for the depression. Mao et al. also observed a similar depression of the clearing point by $\sim 20^{\circ}\text{C}$ in lamellar samples; when the morphology shifted to LC cylinders the clearing point then went 4°C above the homopolymer¹. The large depression of clearing point in the lamellar sample is related to packing/ surface effects, and the depression of clearing point in the other two samples likely stems from the differing degrees of substitution of the mesogen along the polymer backbone.

Similar melting point depression phenomena have been observed in lamellar polystyrene-polyethylene oxide block copolymers as the polystyrene volume fraction increases⁷. In this case, the blocks are strongly segregated and the melting point depression phenomena is related to constraining the PEO crystallites to progressively smaller lamellae. As the polystyrene volume fraction increases, the contribution of surface free energy to the total energy of the crystallite increases because the surface area to volume ratio of the crystallites is becoming larger. The greater surface free energy contribution depresses the melting point which is defined as the temperature at which the free energy of a polymer chain in the crystallite is equal to that in a pure liquid.

These trends are in contrast to what was observed in polystyrene-polymethacrylate side chain liquid crystalline block copolymers³, where the polystyrene block stabilized the smectic C* phase relative to the homopolymer by as much as 15°C . This stabilization was attributed to a lamellar geometry combined with sharp interface

between the domains. In many cases, however, the amorphous coil has little effect on the phase transition temperatures of the LC block^{5, 8}.

Table 3.3 SAXS and TEM observations of mesogen A containing polymers.

Sample ID	Wt % LCP	SAXS smectic d spacing Å	SAXS morphology Spacing, Å	TEM morphology Spacing, Å
LCPA 47	100	37	-	-
PS 12 – LCPA 8	40	-	-	-
PS 39 – LCPA 30	43	36	286	Lam, 240
PS 13 – LCPA 81	86	36	Not observed	PS disordered cylinders, 275
PS 14 – LCPA 129	90	36	279	PS disordered cylinders, 230

When discussing the clearing point depression in mesogen A block copolymers, it is important to consider the fact that the degree of mesogen substitution along the polymer backbone AND the molecular weight of the LCP block can have a strong effect on the clearing point. The clearing point will increase with molecular weight (using 100% substituted LCP homopolymers) up to a critical value before leveling off. It is generally considered that for side chain siloxane LCPs this critical MW is about 10 repeat units⁹; all of our samples have DPs greater than this, and hence MW can be ruled out as a primary factor in the depression of LC clearing point. The variability in % substitution, however, must be considered.

The last column of Table 3.2 shows the clearing point enthalpies for mesogen A polymers normalized per gram of LCP, which decrease with increasing amorphous block content. Figure 3.5 is a plot of normalized clearing point enthalpy (J/ g LCPA) vs. weight fraction of polystyrene. A drop in normalized clearing point enthalpy relative to the LC homopolymer is a common observation in amorphous – smectic LCP block copolymers^{1, 2, 4-6}. In these cases the drop in the clearing point enthalpy of the LC

block with increasing PS content is attributed to a destabilization of the LC phase by the presence of an interface. The decrease in enthalpy may also be tied to the % substitution in the LCP block. Figure 3.6 plots the normalized clearing point enthalpy vs. % substitution, and illustrates that for the lamellar sample PS39 – LCPA30 the large drop in clearing point enthalpy cannot be attributed to % substitution, but is instead related to the morphology.

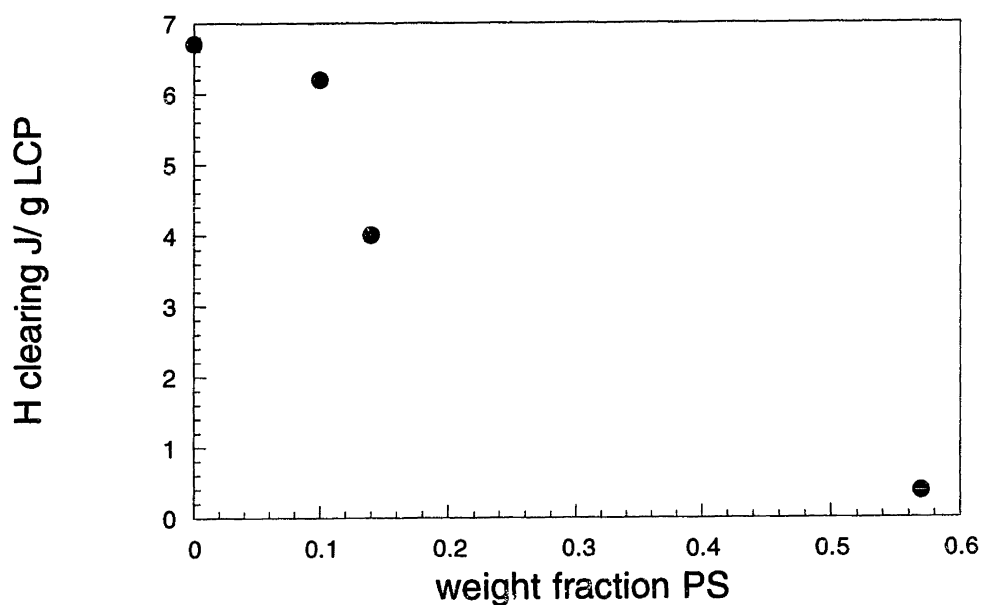


Figure 3.5 Normalized clearing transition enthalpy ($S_c^* - I$) in PS-LCP block copolymers vs. wt. fraction PS.

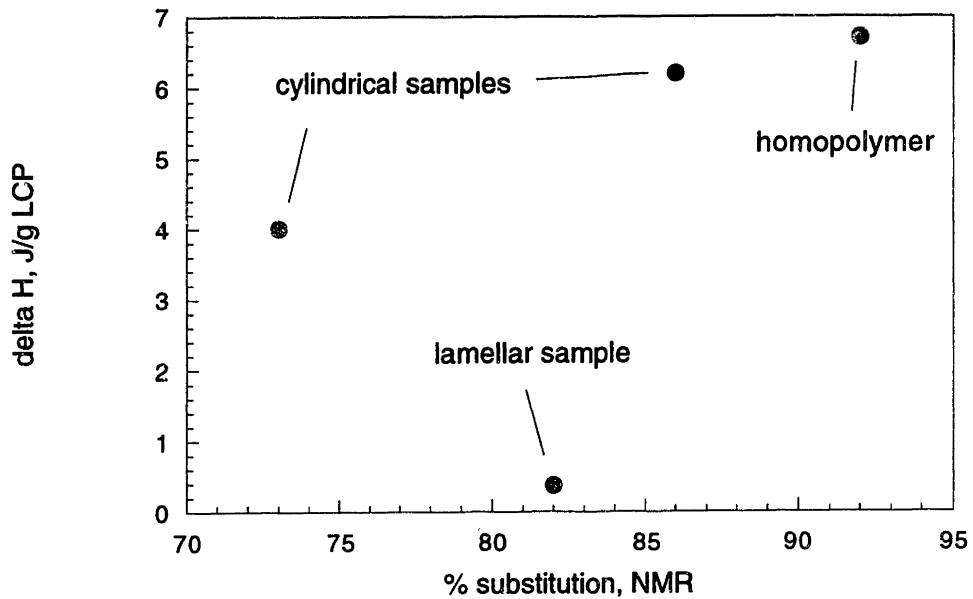


Figure 3.6 Normalized clearing point enthalpy vs. % mesogen substitution in LCPC block copolymers.

When cast from toluene and dried, all the samples in the mesogen A series showed diffuse SAXS scattering in the region of morphological dimensions, 100Å-500Å, and the liquid crystalline samples had a clear smectic peak at 36Å. The samples were then annealed for 18hr above or at the T_g of the polystyrene and SAXS traces were measured again.

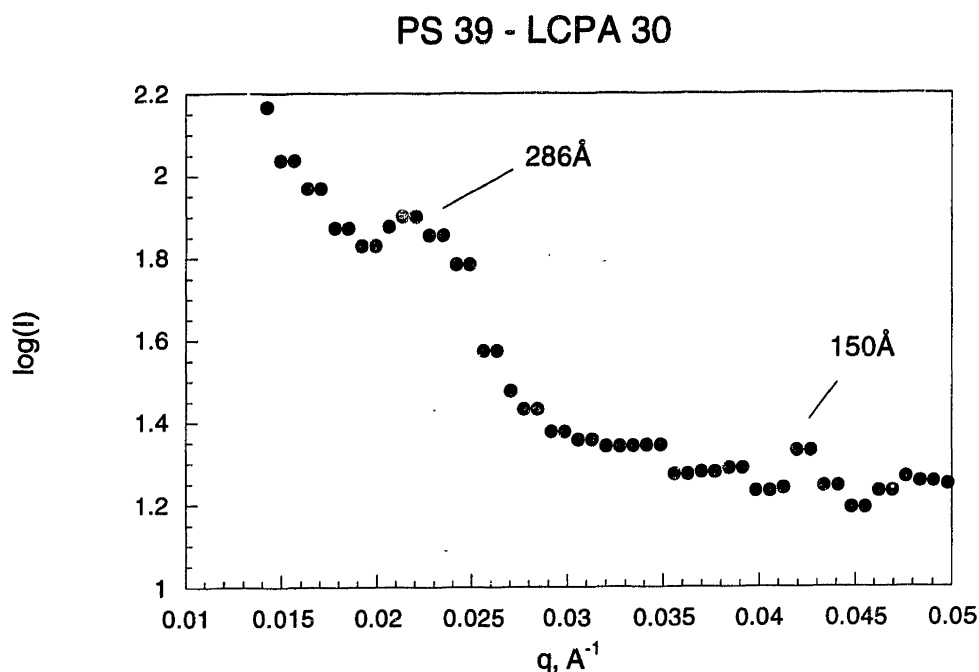


Figure 3.7 1D SAXS plot of $\log(I)$ vs. q (\AA^{-1}) for PS 39 - LCPA 30. Sample was toluene cast, then annealed at 80°C for 24hr. A first order peak at 286\AA and a second peak at 150\AA are observed. The morphology of the sample is lamellar as observed in TEM (Figure 3.5).

After annealing for 12hr at 80°C , PS 39 - LCPA 30 showed a strong first order SAXS peak and a smaller second order peak, as shown in Figure 3.7. The annealing temperature 80°C is approximately the T_g of the PS in this sample and above the LC clearing point of 43°C . This 286\AA SAXS peak, shown in Figure 3.7, agrees reasonably well with the lamellar morphology (240\AA d spacing) observed in TEM and shown in Figure 3.8.

A striking feature of this TEM image is the three areas of contrast. It appears as if the stain is preferentially absorbed at the interface between the blocks, and that this interface is about $1/3$ the width of the "pure" LCP lamellae.

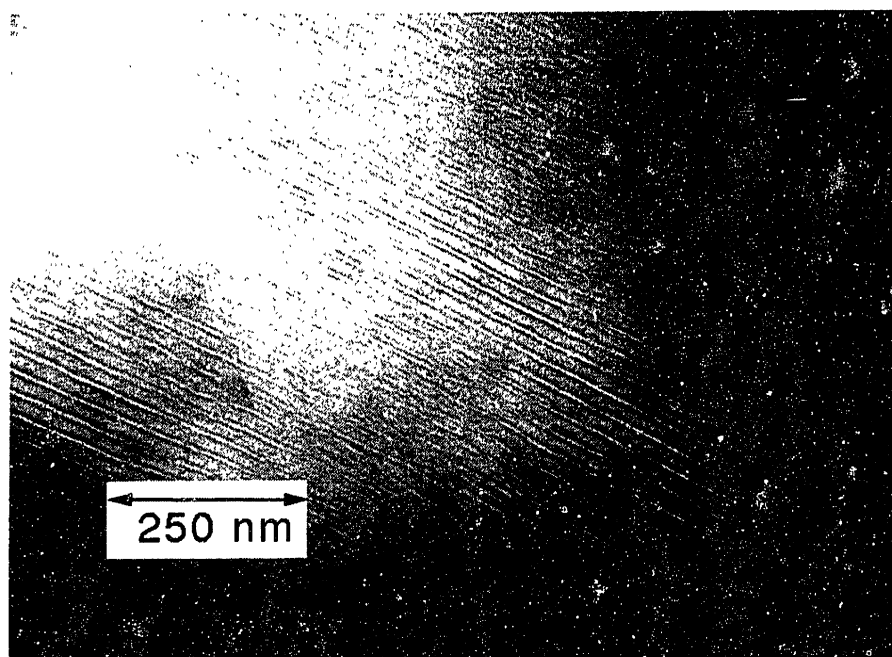


Figure 3.8 TEM image of PS 39 - LCPA 30.

Polystyrene is selectively stained by RuO_4 , making these regions dark. Three areas of contrast appear, one for the LCP rich regions, one for the PS rich regions, and one for the interface.

There are a number of plausible reasons for the three areas of contrast. This interfacial region may have a high concentration of pure polystyrene which is rejected from the LCP phase upon its transition to a smectic LC at 43°C . The polystyrene region solidified at $\sim 84^\circ\text{C}$, thus locking in any LCP that was incorporated into this phase. Another explanation is a decrease in density at the interface, which could make it easier for the ruthenium to diffuse into this region. In any case, it is likely that when the LC phase formed at 43°C upon cooling from the annealing temperature of 80°C the “liquid crystallization” of the siloxane region perturbed the interface in such a way as to result in selective staining. The ODT is known to be greater than 135°C in this sample, as oscillatory shear performed at 135°C led to aligned lamellae as discussed in section 3.6.

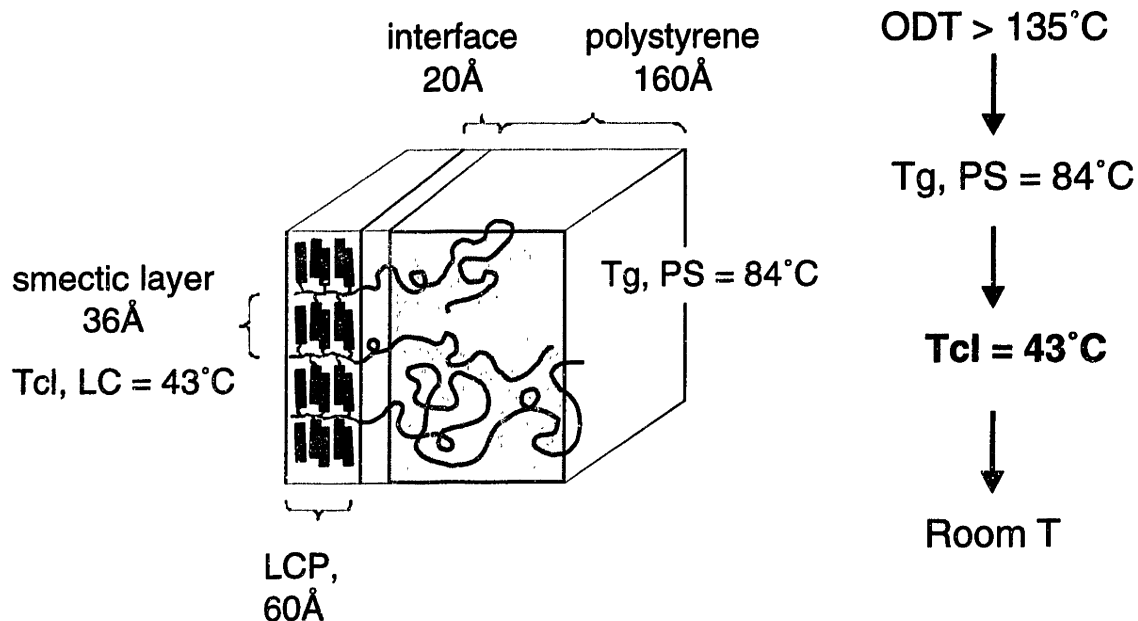


Figure 3.9 Schematic of the morphology, and temperature path for morphology development in sample PS 39 - LCPA 30. The dimensions are estimates from the TEM image shown in Figure 3.6.

Figure 3.9 presents a schematic image of the lamellar morphology observed in PS 39 – LCPA 30, as well as the temperature path for morphology development. This image depicts the “interfacial” region in which there is preferential staining as shown in Figure 3.8, and highlights the fact that the LC phase formed $\sim 40^\circ C$ below the glass transition temperature of the PS region. The polystyrene rich region likely contains some amount of LCP, as its T_g is plasticized to $84^\circ C$. The mesogens are drawn parallel to the lamellae such that the smectic layers are perpendicular to the lamellae. This configuration was confirmed by SAXS measurements on a sheared sample of PS 39 – LCPA 30; experimental details of the shearing are given in an appendix of this chapter.

The information in Figure 3.9 can be compared to the expected domain sizes for a perfectly segregated lamellar morphology with no interfacial width. If L is the total width of the PS domain, LCP domain, and the interface taken together, then $\phi_{LC} L$ is the

expected width of the LC domain in a perfectly segregated situation and $\phi_{PS} L$ is the expected width of the polystyrene domain. Assuming that the density of LCPA is 1.12 (the paste consistency of LCPA made a density measurement difficult, while LCPB has a density of 1.12 as measured by immersion in salt water) and that of polystyrene is 1.05¹⁰, ϕ_{LC} of PS 39 – LCPA 30 is 0.41, only slightly smaller than the weight fraction of LC, 0.43. This allows calculation of $\phi_{LC} L$ and $\phi_{PS} L$, which can be compared to the widths measured from TEM. These results are displayed in Table 3.4, which suggests that some of the LCP has mixed in to the PS phase, the estimate of ϕ_{LC} is too large, or that the polystyrene domains have been swollen in size by the ruthenium. It is interesting that the TEM measured interfacial width of 20Å is in good agreement with that measured by Hashimoto et al using SAXS for strongly segregated systems^{11, 12}.

Table 3.4 Comparison of TEM measured domain dimensions and theoretical domain dimensions for perfect segregation in PS 39 - LCPA 30.

Dimension	Size Å
L Total width	240
l_{PS} PS domain width	160
l_{LC} LCP domain with	60
$l_{interface}$ interfacial width	20
$\phi_{LC} L$	98
$\phi_{PS} L$	142

The last two samples, PS 13 – LCPA 81 and PS 14 – LCPA 129 are also clearly phase segregated, as seen in TEM (Figures 3.10 and 3.11). In both cases the morphology appears as somewhat disordered cylinders of polystyrene in a matrix of liquid crystal

polymer, with the higher molecular weight sample, PS 14 – LCPA 129 having better defined phase boundaries and a higher degree of order than the lower molecular weight sample.

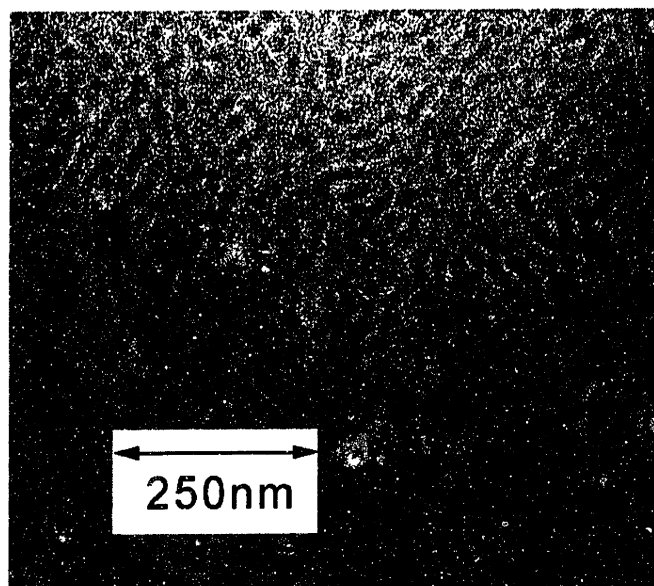


Figure 3.10 TEM image of PS 13 - LCPA 81

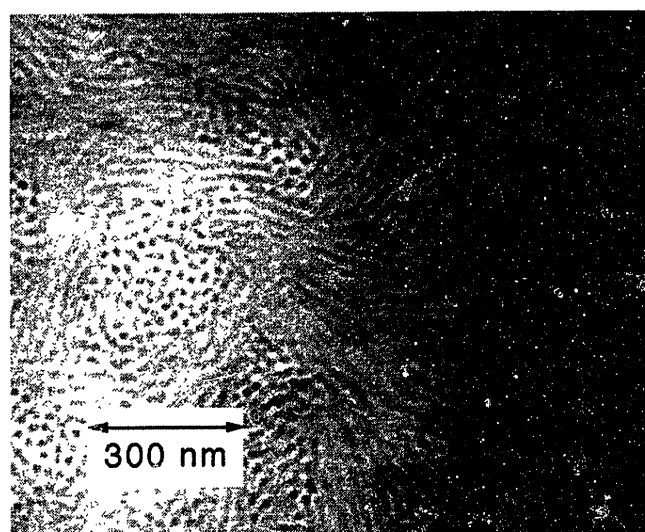
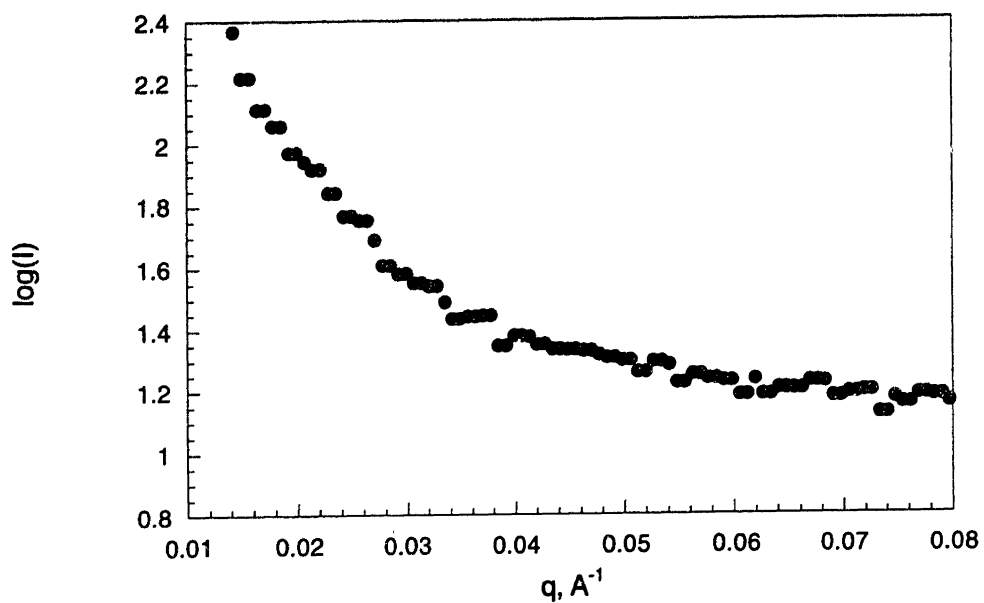


Figure 3.11 TEM image of PS 14 - LCPA 129

PS 13 - LCPA 81



PS 14 - LCPA 129

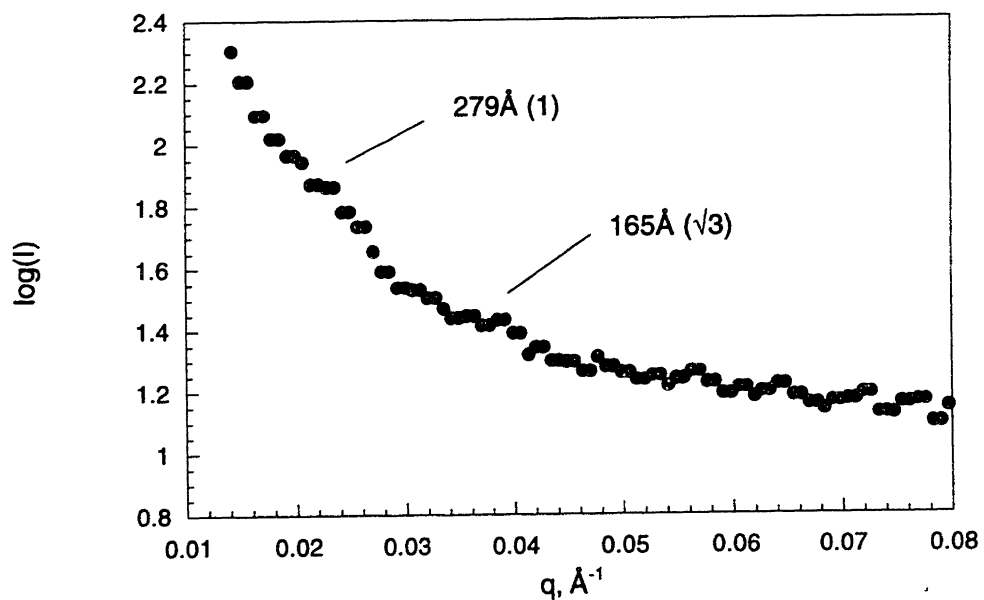


Figure 3.12 1D SAXS profiles of PS 13 - LCPA 81 and PS 14 - LCPA 129. Samples were cast from toluene and annealed at 90°C for 12 hr prior to X-ray measurements.

The SAXS scattering agrees with these observations, as PS 13 – LCPA 81 shows diffuse scattering in the range of interest (Figure 3.12) , and PS 14 – LCPA 129 has distinct shoulders at 279Å and 165Å, suggesting that these cylinders are weakly ordered on a hexagonal lattice (Figure 3.11). Both samples contain between 85-90wt% LCP block; if both blocks were amorphous, we would expect a spherical morphology. The packing of the smectic mesogens could explain the persistence of a cylindrical morphology at these high LCP contents. Another reason cylinders may be favored is that mixing between the PS and the LCP in the amorphous PS-rich domains leads to a greater weight fraction of material in these domains (relative to a strongly segregated system). Finally, the molecular weight estimate based on NMR for the LCP block size may be high.

Figure 3.13 presents a crude block copolymer phase diagram based on experimental observation for mesogen A containing polymers. The physical properties of all these polymers correlate well with TEM observations; samples with disordered polystyrene cylinders embedded in a continuous soft liquid crystalline siloxane matrix were soft and rubbery, and samples consisting of alternating layers of polystyrene and liquid crystalline siloxane were rigid and glassy.

The lamellar sample, PS 39 – LCPA 30, is well ordered over a long range, while the cylindrical samples, PS 13 – LCPA 81 and PS 14 – LCPA 129, are not. One possible explanation for our observations is that the lamellar sample is simply more strongly segregated (i.e., further above the phase line in the phase diagram), while the disordered cylindrical samples lie close to the boundary between miscible blocks and microphase

segregation. This would explain why the higher molecular weight cylindrical sample appears more ordered than the lower molecular weight material.

Because LCPA and polystyrene are somewhat miscible, it is likely that the high LCP content PS-LCPA block copolymers have an ODT close to their LC clearing points, similar to the finding of Zheng and Hammond³ for samples with large LCP volume fractions. The LC clearing points of PS 13 – LCPA 81 and PS 14 – LCPA 129 are 79°C and 60°C respectively. If it is the case that the ODT is close to the clearing point, it would be difficult to achieve an ordered structure by annealing; in order to anneal above the Tg's of both blocks one is forced to anneal close to the ODT, where the driving force for order formation is low. Thus, a disordered morphology is likely kinetically “frozen in” during the initial formation of the microdomains. A series of annealing studies at different temperatures revealed that annealing right below the LC clearing point does enhance order in these block copolymers, but it remained difficult to achieve a well ordered sample with a distinct Bragg reflection in SAXS. In addition, diffuse boundaries between the domains also contribute to the lack of a distinct Bragg reflection.

These arguments are supported by Hashimoto et al.¹³, who found that near the ODT in a low MW cylindrical sample (polystyrene cylinders) of polystyrene-block-polyisoprene that the kinetics of order formation are slow (8hr). In this case, it was possible to obtain an ordered sample 10°C below the ODT; in our case however, it was not possible to obtain such a well ordered sample in this time frame, likely because of the higher molecular weight of our samples and to the smectic structure in the LCP block.

Similarly disordered cylindrical morphologies without a strong SAXS diffraction peak have also been observed by Gido and co-workers¹⁴. In this case, the polymers were

A₂B simple graft “Y” architecture block copolymers, rather than the amorphous-liquid crystalline block copolymers discussed here. When the branched system was the continuous phase, the block copolymer exhibited only short range order and disordered cylinders. This observation in a strongly segregated system is explained by packing and curvature effects arising from the unique polymer architecture.

The last two samples in the series, PS 13 – LCPA 81 and PS 14 – LCPA 129, are elastomeric in nature; when stretched, they retract back to their original dimensions. The elastomeric nature of our samples is likely due to the combination of a low T_g (~ -30°C) and large molecular weight of the liquid crystalline block (80,000-120,000); the polystyrene blocks act as physical elements which add mechanical integrity and toughness. These elastomers break at ~40% strain, and exhibit fully recoverable deformation to 8-10% strain. Under crossed polarizers these samples are highly birefringent, and the color and intensity of light passing through the polarizer are changed when the sample is stretched. Moreover, the optical texture returns to its original state after the sample retracts to its initial dimension. A more thorough discussion of these effects is given in Chapter 5.

Block Copolymer Phase Diagram, Mesogen A

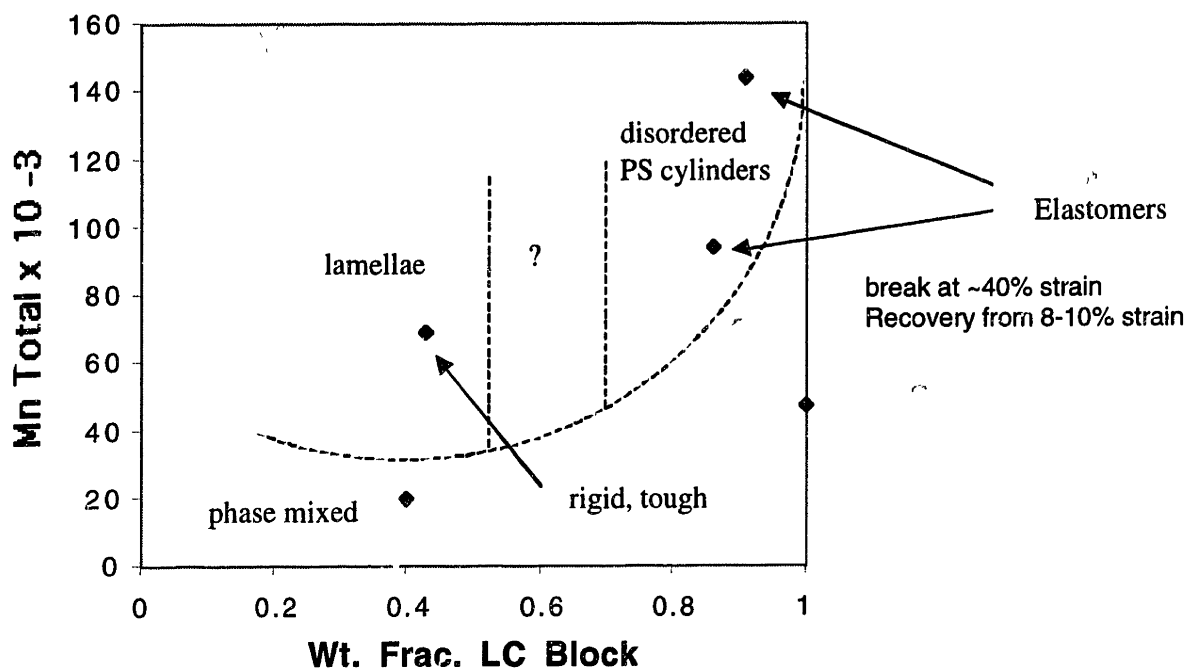


Figure 3.13 Experimentally determined phase diagram for polymers made with mesogen A.

It was initially surprising that miscibility was an issue in these systems, as siloxanes are highly immiscible with polystyrene and the liquid crystallinity of the siloxane block was expected to *further* insure the immiscibility of the blocks. It should be noted that polystyrene is known to be miscible with polycarbonate derivatives and with PPO¹⁵, which have aromatic, ester, and ether functional groups as do the mesogens in this study. In addition, our own studies revealed that mesogen A is partially miscible with polystyrene and plasticizes polystyrene, lowering its T_g. A more detailed account of blends and mixtures of PS, LCP, and PS-LCP block copolymers appears in Chapter 5. Finally, there are examples of miscible polymer pairs where one of the polymers is crystalline (PEO) and the other polymer is amorphous (PMMA)⁷. So the fact that one of

the blocks is crystalline or liquid crystalline and the other block is amorphous does not insure that the two polymers are immiscible.

3.5 Mesogen B polymers

To introduce a higher degree of segregation, we designed mesogen B, which has a shorter spacer and a more rigid mesogen unit (see Figure 2.4). Two block copolymer samples were prepared with mesogen B, using the same block copolymer substrates as in PS 12 –LCPA 8 and PS 14 – LCPA 129. This gives a direct comparison of two PS – LCP block polymers that differ only in the mesogen attached to the siloxane block. Tables 3.5 and 3.6 show the molecular weight characterization and the thermal properties of polymers made with mesogen B.

Table 3.5 Molecular weight characterization of mesogen B polymers.

Samples	Wt % LCP	Mn, PS GPC	Mn, siloxane GPC	Mn, siloxane NMR	% sub NMR	Mn, LCP NMR	Mn, LCP GPC
LC Homopolymer LCPB 35	100	0	6900		68	35,100	38,200
Block Copolymers							
PS 12 – LCPB 8	40	12,000	2,600	1,500	99	8,200	18,400
PS 14 – LCPB 111	89	14,100	29,100	21,200	69	111,200	82,000

Table 3.6 Thermal properties of polymers made with mesogen B. Values taken from DSC heating scans at 20°C/ min.

Sample ID	Wt % LCP	% sub NMR	PS Tg °C (substrate)	LCP Tg °C	LC transitions °C	ΔH clearing J/g	ΔH clearing J/g LCP
LCPB 35	100	68	-	-9	Sc* 54 Sa 145 I	5.46	5.46
PS 12 – LCPB 8	40	99	89	-8	?	-	-
PS 14 – LCPB 111	89	69	82 (89)	-5	Sc *150 I	5.13	5.89

Numbers in (parenthesis) are Tg's of PS in PS-PVMS blocks before mesogen attachment.

The most remarkable difference between these two series of polymers (mesogen A vs. mesogen B) is that the mesogen B containing polymers have a greater tendency to phase segregate into ordered morphologies. Whereas PS 12 – LCPA 8 is phase mixed by all measures, PS 12 – LCPB 8 is clearly phase segregated, with small liquid crystalline cylinders hexagonally packed in a polystyrene matrix (Figure 3.13). The degree of mesogen substitution in both PS 12 – LCPA 8 and PS 12 – LCPB 8 polymers is close to 100% so we can conclusively say that mesogen B yields siloxane blocks that are less miscible with polystyrene blocks than LCP siloxanes made with mesogen A. The χ parameter is therefore higher for B-PS than for A-PS.

Figure 3.14 shows 1D and 2D SAXS scattering plots for PS 12 – LCPB 8, and Figure 3.15 shows a TEM image of the hexagonally packed cylinder morphology. The 2D SAXS pattern shows that the mesogens are aligned parallel to the long axis of the cylinders and that the cylinders lie in the plane of the film. The 1D $\log(I)$ vs. q (nm^{-1}) plot shows a single first order reflection at 180\AA . The strongly segregated morphology was present prior to annealing, although the SAXS peak became more well defined with annealing at 110°C , and the cylinders became oriented in the film direction. Figure 3.16 is a schematic image of an LC cylinder in PS 12 – LCPB8, drawn approximately to scale, showing how the smectic layers are perpendicular to the cylinder axis. The cylindrical sample has a smectic spacing of 33\AA , 2\AA larger than that measured in the LCP homopolymer, suggesting that the smectic C^* phase may have been converted to a smectic A phase. A tilt angle of 20.0° in the smectic C^* phase (with $d = 31\text{\AA}$) would lead

to a corresponding smectic A phase with $d = 33\text{\AA}$. This is a tilt angle consistent with those measured in the literature for smectic C^* LCs¹⁶.

On the other side of the composition range, we have a similar result. PS 14 – LCPB 111 has a morphology of hexagonally packed polystyrene cylinders in a liquid crystalline matrix (Figure 3.18). The toluene cast PS 14 – LCPB 111 showed no Bragg reflection in SAXS; after annealing at 110°C however, a first order peak at 286\AA formed in addition to higher order reflections that agree with a hexagonally packed cylindrical morphology (Figure 3.17).

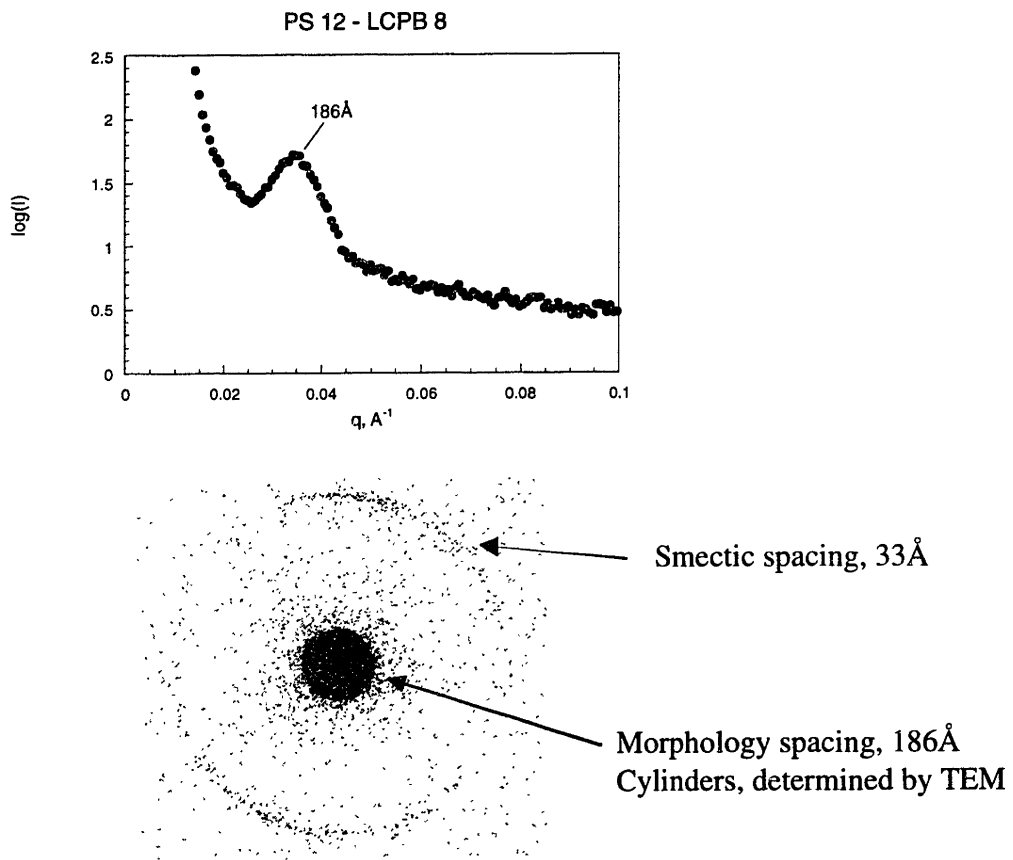


Figure 3.14 1D and 2D SAXS patterns of PS 12 - LCPB 8 after casting from toluene and annealing at 110°C .

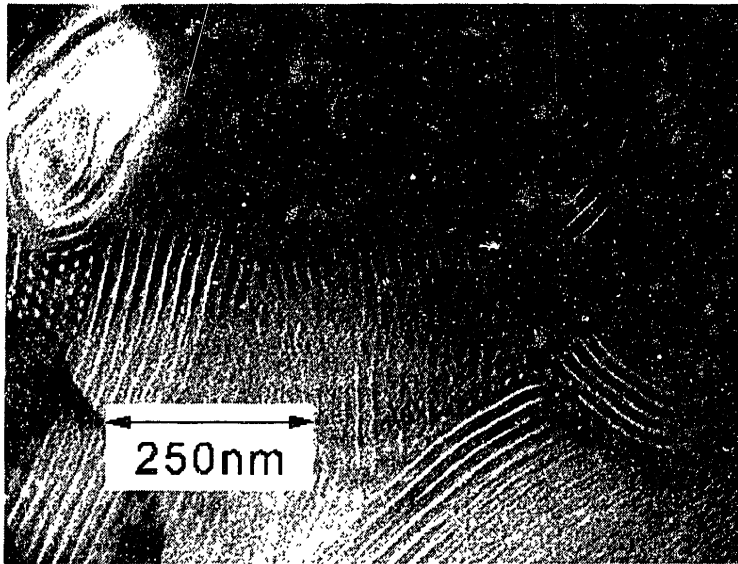


Figure 3.15 TEM image of PS 12 - LCPB 8. The sample was toluene cast and annealed at 110°C overnight. The RuO₄ stain is preferentially absorbed by the polystyrene, making these regions appear dark in the image. Also note the small grain sizes in this sample.

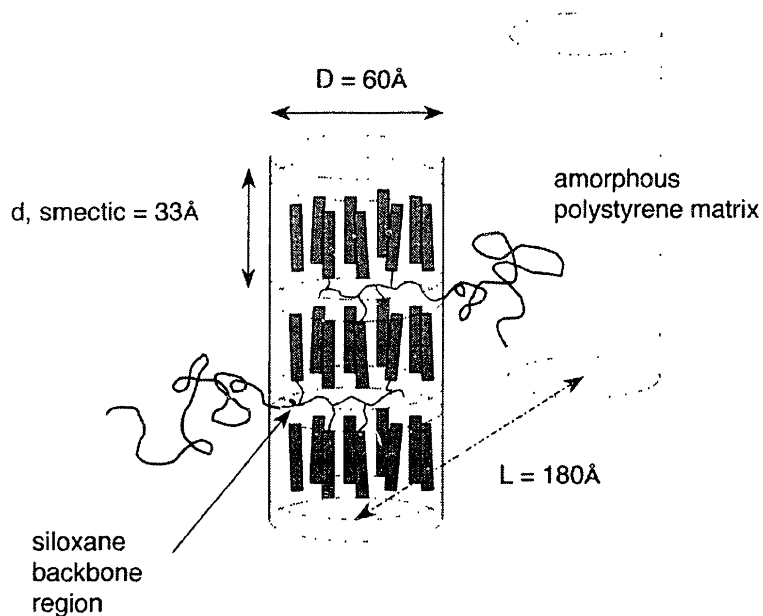


Figure 3.16 Schematic illustration of LCP cylinder morphology in PS 12 - LCPB 8. The cartoon is drawn approximately to scale.

The PS 14 – LCPB 94 first order SAXS peak (Figure 3.17) is stronger and more distinct than the shoulder observed in PS 14 – LCPA 129 (Figure 3.12). In addition, the phase boundaries observed in PS 14 – LCPB 111 are much more distinct than in PS 14 – LCPA 129 (Figure 3.11), suggesting stronger phase segregation in the mesogen B containing block copolymer.

It should be noted that PS 14 - LCPB 111 has a 69% substitution of mesogen groups, while PS 14 - LCPA 129 has an 86% substitution. Therefore, the comparison between these samples is less satisfactory than in the case of PS 12 – LCPA 8 and PS 12 – LCPB 8, both of which have mesogen substitutions close to 100%. However, one would expect that further LC substitution in PS 14 – LCPB 111 would increase the LCP MW, only furthering phase segregation.

The thermal properties of the polymers made with mesogen B appear in Table 3.5. PS 12 – LCPB 8 is weakly birefringent in OM and a clearing point is difficult to detect in both OM and DSC. However, the distinct smectic peak at 33Å in X-ray scattering shows that this sample is liquid crystalline. PS 14 – LCPB 111 is highly birefringent in OM, having a typical grainy polymer smectic texture at room temperature in OM. This polymer clears at 150°C, very close to the homopolymer clearing point LCPB 35 of 145°C. The homopolymer LCPB 35 has two thermal transitions, a smectic C* - smectic A transition at 54°C (not observable in OM, but distinct in DSC) and a smectic A – isotropic clearing point at 145°C. The smectic clearing points and the siloxane T_g in the mesogen B polymers are both higher than those observed with mesogen A.

PS 14 - LCPB 111

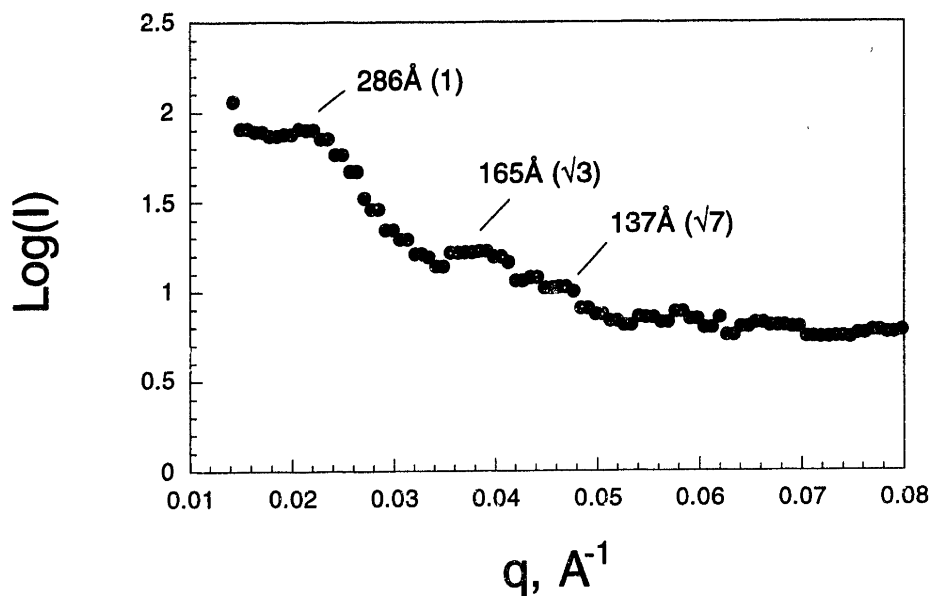


Figure 3.17 1D SAXS plot for PS 14 - LCPB 111

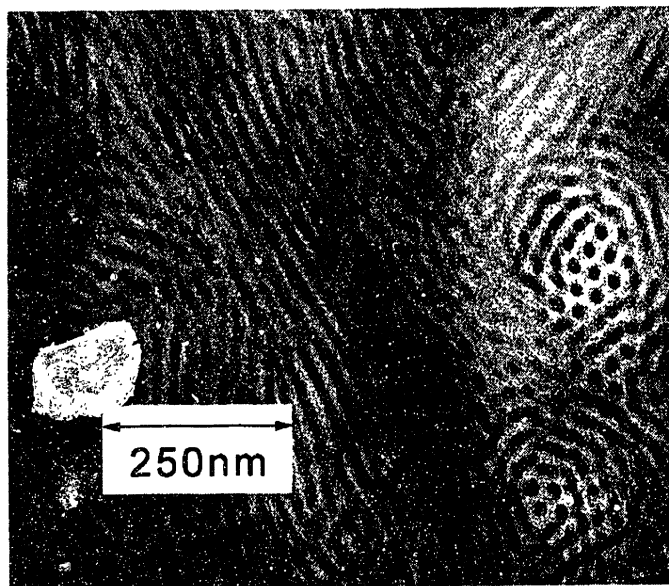


Figure 3.18 TEM image of PS 14 - LCPB 111. The sample was toluene cast and annealed at 110°C overnight. The RuO_4 stain is preferentially absorbed by the polystyrene, making these regions appear dark in the image.

Table 3.7 Summary of SAXS and TEM observations of mesogen B containing polymers.

Sample ID	Wt % LCP	SAXS smectic d spacing Å	SAXS Morphology Spacing, Å	TEM Morphology, Spacing, Å
LCPB 35	100	31	-	
PS 12 – LCPB 8	40	33	180	LCP hex. packed cylinders 155 (D cyl. 60)
PS 14 – LCPB 111	89	32	286	PS hex. packed cylinders 260 (D cyl. 125)

Moreover, the smectic clearing points do not become depressed with decreasing LCP content, and the polystyrene block Tg is less depressed than in the case of mesogen A. In fact, the LC clearing point is 5°C higher in PS 14 – LCPB 111 than in the homopolymer LCPB 35, similar to PS-LC methacrylate systems studied previously³. In the context of TEM and SAXS data this thermal data further supports the claim that mesogen B containing block copolymers are more strongly phase segregated than polymers made with mesogen A. Also, the clearing point trends we observe for mesogen A and B are in agreement with previous observations of liquid crystals¹⁷. Specifically, increasing mesogen rigidity and aspect ratio leads to higher clearing points, and in the case of liquid crystalline polymers, to both higher Tg's and clearing points.

The fact that mesogen B polymers have a higher clearing point than mesogen A polymers may be linked to the enhanced phase segregation; the higher clearing points indicate a higher enthalpic penalty disruption of the LCP phase. If we assume that the entropy of mixing between mesogen A siloxanes and mesogen B siloxanes with polystyrene is roughly equal, then the increased enthalpic penalty for disrupting mesogen B siloxanes could account for the stronger segregation, i.e. χ is larger for the B-PS interaction.

The physical properties of polymers made with mesogen B are quite different from mesogen A polymers, due to the higher Tg of the mesogen B siloxanes. While PS

14 – LCPA 129 is elastomeric, PS14 – LCPB 111 forms a pliant tough material that is easy to bend but difficult to stretch.

3.6 Appendix: Oscillatory shear of PS39 – LCPA 30

In order to determine the orientation of the smectic layers with respect to the lamellae in PS 39 – LCPA 30, a sample was oriented in an oscillatory shear apparatus prior to SAXS measurements. The polymer (a few mg) was placed between the quartz plates of a Linkham CSS 450 shear cell held 550 μ m apart. The sample was sheared at 100% strain, 0.5Hz, and 135°C, well above the LC clearing point (43°C) and the PS T_g (70°C). After cooling to 40°C the plates were separated and the sample was removed for SAXS analysis.

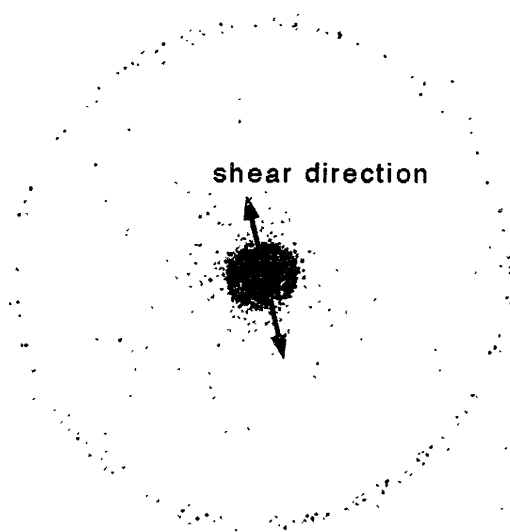


Figure 3.19 2D SAXS pattern of oriented sample of PS 39 - LCPA 30.

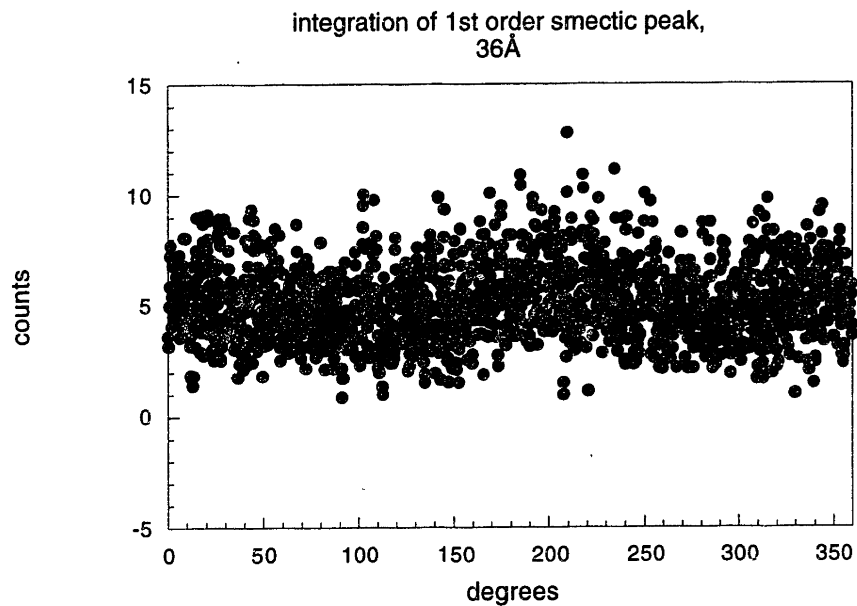
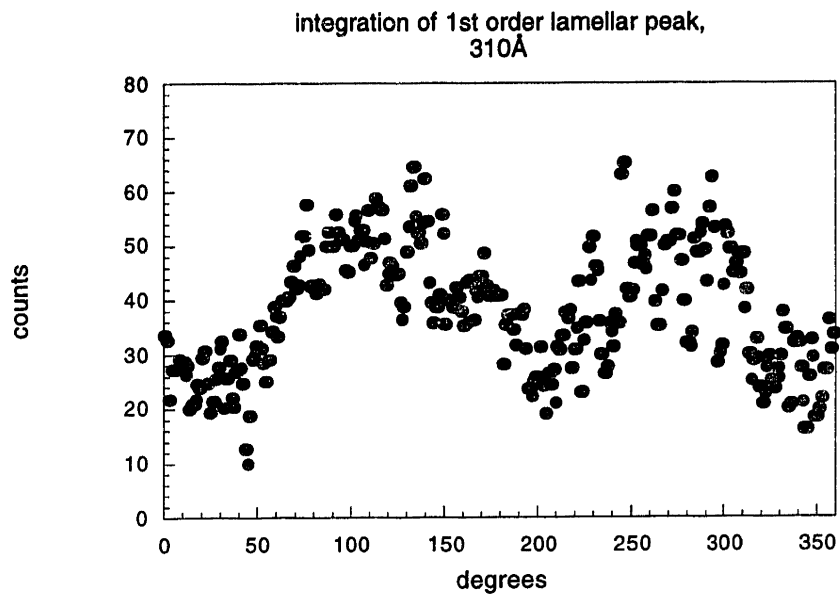


Figure 3.20 Integration of 1st order lamellar peak and 1st order smectic peak in the 2D SAXS pattern of PS 39 – LCPA 30 shown in Figure 3.18

The 2D SAXS data appear in Figure 3.19, and show that the lamellae orient perpendicular to the quartz plates and in the direction of shear. The smectic peak does not show the same degree of orientation as the morphology peak; integration of these

two rings, however, does show that on average the smectic layers lie perpendicular to the lamellae. Figure 3.20 shows the integrations of the morphological peak and the smectic peak and that the maxima are 90° out of phase with each other, establishing the structure shown schematically in Figure 3.9.

3.7 Chapter 3 Summary

This chapter presented a comparison of the thermal properties and morphology of two series of PS-LCP block copolymers, each series with a different smectic C* mesogen in the LCP block. The most important finding was that mesogen B containing PS - LCP materials have a greater tendency to phase segregate into well ordered morphologies than mesogen A materials. In other words, $\chi_{PS-LCPA} < \chi_{PS-LCPB}$. In addition, the more rigid mesogen (Mesogen B) led to higher clearing points and Tgs of the LCP block.

Finally, in PS-LCPA block copolymers, a lamellar morphology was found to depress the clearing point by 50°C relative to the LCPA homopolymer, a fact which can be attributed to a combination of (1) confining the LCP into lamellar sheets ~60Å in width, and (2) mixing of the LCP block into the PS rich domains, which plasticized the PS Tg to 84°C.

3.8 References

1. Mao, G., *et al. Macromolecules* **30**, 2556-2567 (1997).
2. Fischer, H.; Poser, S.; Arnold, M.; Frank, W. *Macromolecules* **27**, 7133-7138 (1994).
3. Zheng, W.Y.; Hammond, P.T. *Macromolecules* **31**, 711-721 (1998).
4. Adams, J.; Gronski, W. *Makromol. Chem., Rapid Commun.* **10**, 553-557 (1989).
5. Yamada, M.; Iguchi, T.; Hirao, A.; Nakahama, S.; Watanabe, J. *Macromolecules* **28**, 50-58 (1995).
6. Omenat, A. & Lub, J. *Chem. Mater.* **10**, 518-523 (1998).
7. Chow, T.S. *Macromolecules* **23**, 333-337 (1990).
8. Bohnert, R.; Finkelmann, H. *Macromol. Chem. Phys.* **195**, 689-700 (1994).
9. Plate, N.A. & Shibaev, V.P. in *Comb-Shaped Polymers and Liquid Crystals* (ed. Cowie, J.M.G.) (Plenum, New York, 1987).

10. Brandrup, J. & Immergut, E.H. *Polymer Handbook, 3rd Ed.* (John Wiley & Sons, New York, 1989).
11. Hahimoto, T., Todo, A., Itoi, H. & Kawai, H. *Macromolecules* **10**, 377 (1977).
12. Hashimoto, T., Shibayama, M. & Kawai, H. *Macromolecules* **13**, 1237 (1980).
13. Hashimoto, T., *et al.* *Polymer* **39**, 1573-1581 (1998).
14. Pochan, D.J., *et al.* *Macromolecules* **29**, 5091-5098 (1996).
15. Shaw, M.T. *Journal of Applied Polymer Science* **18**, 449-472 (1974).
16. Blinov, L.M., and Chigrinov, V.G. *Electrooptic Effects in Liquid Crystal Materials* (Springer-Verlag, New York, 1994).
17. Gray, G.W. in *Polymer Liquid Crystals* (eds. A., C., W.R., K. & R.B., M.) 1-33 (Academic Press, New York, 1982).

Chapter 4 Electro-Optic and Mechano-Optic Properties of LC Homopolymers and Block Copolymers

4.1 Background and Motivation

The ability of scientists to control the orientation of the director in LC materials lies behind a wide range applications, from high modulus, high strength LC polymers (e.g. Kevlar) to LC displays and related electro-optic applications. The PS-LCP block copolymers synthesized in this work are unique materials in that they exhibit a thermotropic liquid crystalline phase within a film forming polymer that may be processed to achieve orientation. In particular, the LC phase in the block copolymers is the smectic C* phase, which is known to be ferroelectric.

It is well known that in order to observe electro-optic switching in ferroelectric smectic C* liquid crystals, the LC phase must be confined in a space smaller than the pitch of the LC¹. Because the block copolymer morphology of the PS-LCP diblocks forces the LCP block into domains on the nanometer scale, it is of interest to test these materials for electro-optic switching behavior², noting that the pitch of the typical chiral small molecule LC is on the order of a few microns³. It is also important to compare the switching behavior of the block copolymers to their homopolymer analogues in order to gauge the advantages and disadvantages of the block copolymers.

In addition to electro-optic effects, we can also expect mechano-optic effects in the PS-LCP materials, especially in the elastomeric samples. In this case we examine the response of the director of the liquid crystal to the application of a mechanical field. A preliminary study of the response of PS 14 – LCPA 129 to stretching and release was examined under an optical microscope equipped with crossed polarizers. In addition,

stretched samples were examined with SAXS to establish how the mesogens and smectic layers orient with respect to the stretch direction.

Finally, piezoelectricity in smectic C* elastomers has been observed before⁴. Piezoelectric measurements on well aligned samples of the PS-LCP block copolymers is a logical next step in exploring the applications of these polymers.

4.2 Experimental

All of the LC homopolymers and PS-LCP block copolymers were tested for electro-optic activity in 4-5 μ m thick ITO glass LC cells. A Leica Optical Microscope equipped with a Mettler FP82HT hot stage/ FP90 controller was used to observe samples in LC cells under crossed polarizers at different temperatures and applied voltages. Voltages as large as ± 120 V were applied with a HP 6827A Bipolar Power Supply/ Amplifier. Mechano-optic effects were observed in the elastomeric sample of PS 14 – LCPA 129 (~0.25mm thick) as it was stretched and released, and SAXS was conducted with the same instrumentation as described in section 3.2.

Electro-optic cells were prepared in two different ways depending on the viscosity of the sample. All the LC siloxane homopolymers were easily loaded into pre-fabricated 4 μ m LC cells (Displaytech, Inc.; Longmont CO) with a rubbed polyimide alignment layers (both top and bottom rubbed in the same direction). We note that the polyimide alignment layers in the purchased cells were not effective in forming lc monodomains in the small molecules, lc polymers, or lc block copolymers.

Samples were placed on a glass slide in an oven at ~120°C, and then the LC cell was placed directly on top of the sample so that the liquid polymer could enter the cell by capillary forces. When the samples were too viscous to be loaded with this technique,

cells were prepared by sandwiching small (mg) quantities of sample between ITO coated glass slides along with 5 μ m fiber spacers (from EM Industries; Hawthorne, NY).

Samples prepared with this method were manually sheared below the LC clearing point and above the polystyrene T_g to get alignment of the morphology and the mesogens.

4.3 Results and Discussion

The only samples that had electro optical activity in the range of $\pm 30\text{V}/\mu\text{m}$ were the liquid crystalline homopolymers. Both sample preparation methods were used successfully for the LC homopolymers, i.e., switching was observed using the 4 μ m pre-fab cells in addition to the sandwich technique. LCPA 47 was active from room temperature up to its clearing point, and LCPB 35 began showing electro-optic activity at 65°C. A third LC homopolymer LCPC 19 was active at room temperature up to its clearing point. None of the samples showed any electro-optical activity as prepared. Only after slowly cooling ($\sim 1^\circ\text{C}/\text{min}$) from the isotropic state with an applied voltage ($\sim 20\text{V}/\mu\text{m}$), did the resulting LC show any electro-optic activity. In all cases, polydomains of liquid crystalline material, larger than the initial domains, were observed after this poling treatment. So when switching was observed, it was observed to occur within the many domains of LC, which were on the order of 10-100 μm in dimension.

Figure 4.1 shows the switching of LCPA 47 at room temperature. The switching was bistable, that is, when the field is removed the orientation of the mesogens within the domains and hence domain colors remain the same. Moreover, the colors of the domains could be changed by the application of the reverse voltage. The white line in the figure points to the same domain. The long needle domain morphology formed only after cooling from the isotropic state with an applied voltage of +80V. The speed of the

switching at room temperature was measured to be 100ms by Prof. Noel Clark (University of Colorado, personal correspondence). This agrees well with measurements on the analogous siloxane with a purely hydrocarbon spacer⁵.

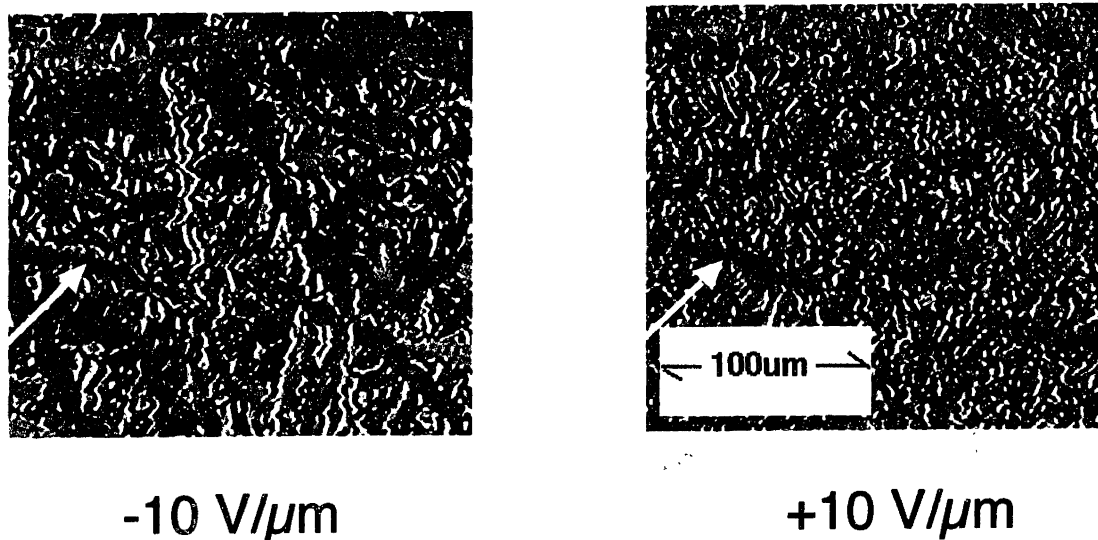


Figure 4.1 Ferroelectric bistable electro-optic switching of LCPA 47 at room temperature. The white arrow points to the same domain in both images.

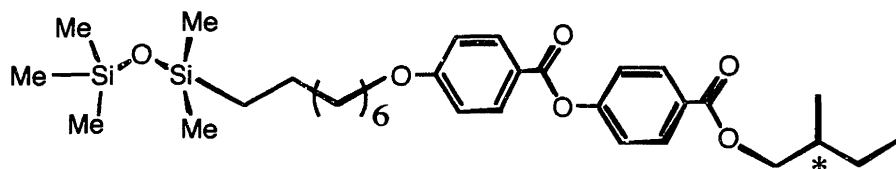


Figure 4.2 Chemical structure of mesogen A', which has a Sc* to isotropic transition at 26°C

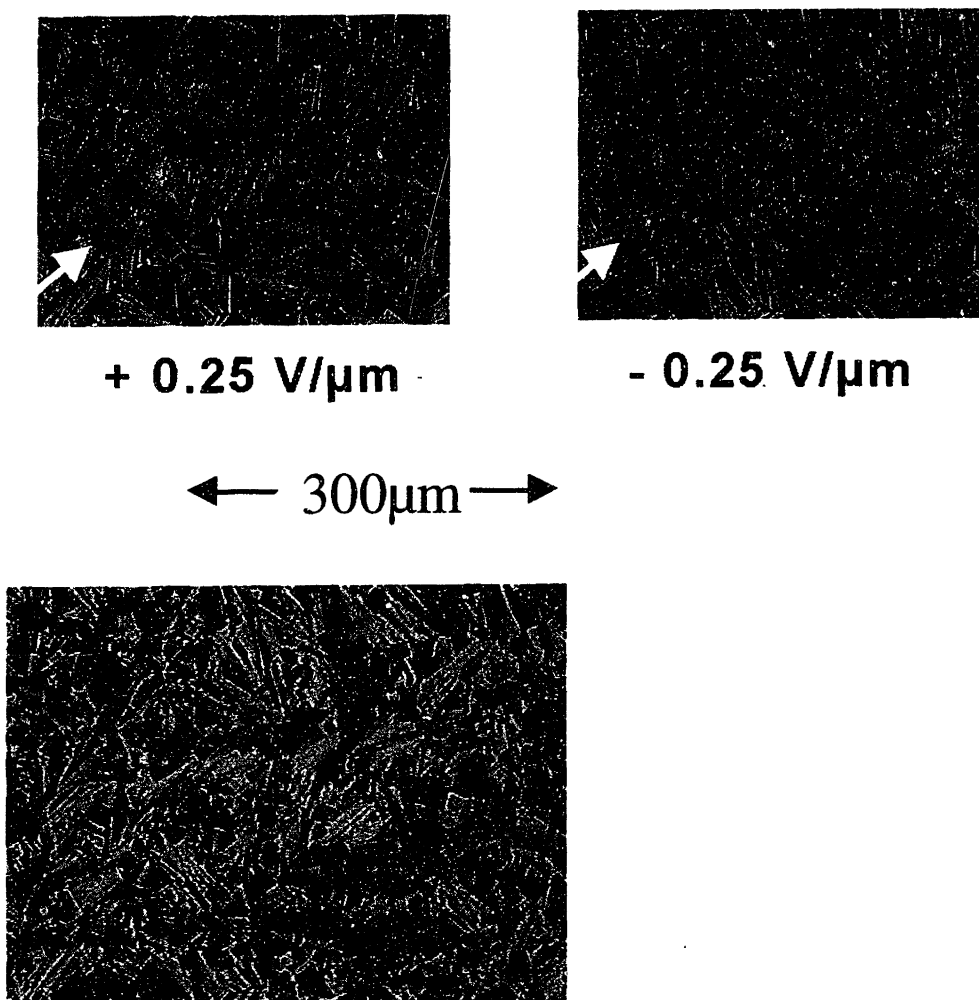
Figure 4.3 shows room temperature electro-optic switching of small molecule mesogen A', which is analogous to mesogen A but has no Si-H functionality. The chemical structure of mesogen A' is shown in Figure 4.2. The voltage required for the switching of the small molecule mesogen is about 40 times smaller than for the LCP. The white arrow in the image shows the same domain and how it changes from light to

dark by the application of the voltage. During switching each domain switched color from light to dark through a very well defined circular motion illustrated in Figure 4.2. This motion is the direct result of the mesogens switching their alignment from one state to another via a 180° rotation about a vector normal to the smectic layer. It is interesting that even in the case of the small molecule LC, the polyimide alignment layers in the cell did not effect the formation of monodomains. The liquid crystalline texture is that of large focal conic fans, characteristic of smectic phases. As discussed in Chapter 5, blending the small molecule mesogen A' with a PS-LCP block copolymer may lead to electro-optic effects in the blended system at more accessible voltages.

The electro-optic switching of LCPA 47 and Mesogen A' illustrates why liquid crystalline polymers have generally found little use in electro-optic applications. For the polymer LCs, the voltages required are larger, the switching times slower (in the case of ferroelectrics, by a factor of 1000), the synthesis more involved, and loading the cells is more difficult because of the higher viscosity of the polymer. In terms of ferroelectric display elements, LCPs may offer some advantages in terms robustness and ease of manufacture, but these have been outweighed by the general difficulty of making reliable smectic LC devices.

The most prevalent LC displays are based on nematic small molecules in a twisted geometry, and have switching times on the order of tens of ms. Bistable ferroelectric displays based on small molecules have switching times on the order of $50\mu\text{s}$ - $100\mu\text{s}$ (about two orders of magnitude faster than nematic switching). Despite the advantages of faster switching times and bistability, commercialization of this technology has not been widespread, as there are problems in 1) obtaining well oriented

defect-free display elements, and 2) maintaining this orientation in the presence of mechanical shock and temperature variations⁶.



during switching

Figure 4.3 Room temperature bistable switching of small molecule mesogen A' at room temperature. The white arrow points to the same domain, which switches from light to dark. Domains switch from light to dark in a well defined circular pattern.

Researchers have found that side-chain polymer smectic C* based ferroelectric LC devices can increase the robustness of the FLC devices and ease their manufacture⁷. The switching times of smectic C* polymer based devices are on the order of tens to hundreds of ms at room temperature⁸, slower than their small molecule analogues, but about the same order of magnitude as the TN small molecule displays.

Electro-optic effects in LCPB 35 were observed above 65°C up to the clearing point of ~150°C. In this case, the application of voltage appeared to result in the formation of new domains with a purple color. In this temperature range we believe the material is in the smectic A state, and bistable electro-optic switching is not possible. That is, in the absence of an applied voltage, the texture returns to its native state. Voltages of 3V/μm effected the first discernable change in the texture, at voltages of 10V/μm and higher the maximum change was observed. These values are close to the voltages required for LCPA 47 to switch. It is important to note that electro-optic phenomena observed in LCPB 35 do not constitute a switching phenomena as observed in LCPA 47, but a transient reorientation effect that disappears in the absence of an electric field. The type of behavior is known as “electroclinic” and is described as the field induced tilt of the mesogens by the application of voltage, resulting in a Sa – Sc* transition⁹.

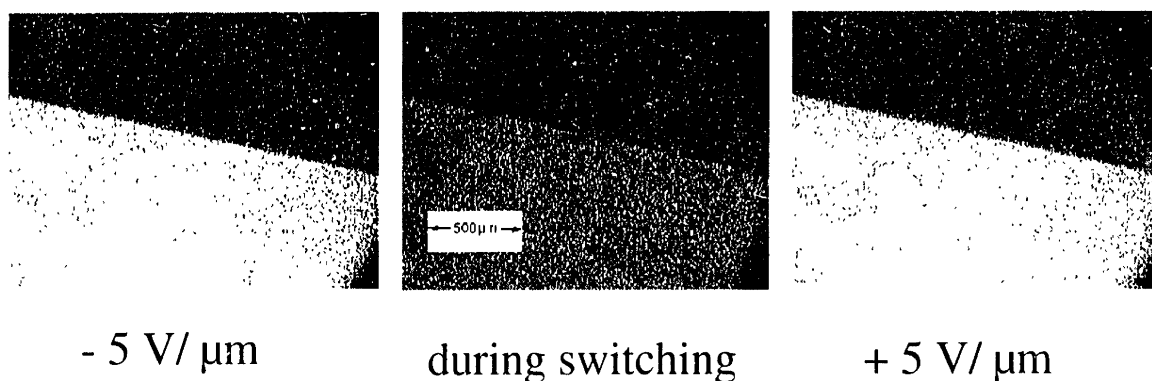


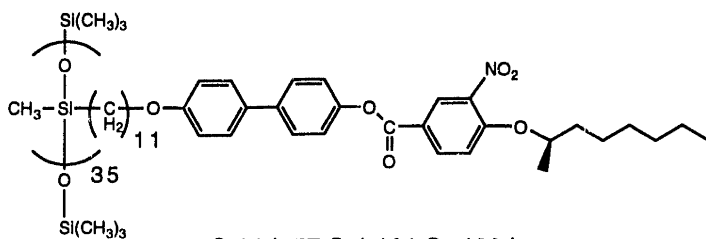
Figure 4.4 Room temperature bistable switching of LCPC 19. Positive and negative voltages result in a region that is uniformly brighter than regions with no voltage. In the images above the light regions are treated with ITO, the dark regions are untreated.

Figure 4.5 shows room temperature switching of LCPC 19. This material formed a fine grained smectic texture that was easily modulated by the application of $5\text{V}/\mu\text{m}$ fields. In this case, the switching was bistable, when the voltage was removed, the light region remained light. There are many small domains, and the dark domains become light and the light domains become dark during switching. The line across the images in Figure 4.4 is the boundary between the ITO region of the LC cell and the untreated portion of the cell. The lighter regions in the image are ITO treated, and the darker images are untreated. Like all the other LC homopolymers examined in this work, no switching was observed in the cell as prepared; only after slowly cooling from the isotropic state with an applied field did the cell become active. It is interesting to note that after the cell had been tested and set aside the material in the ITO regions was visibly different (lighter, more opaque) to the naked eye than the material in the non-ITO regions.

None of the block copolymers showed any electro optical switching activity, even after attempting many different shearing treatments, poling procedures, etc.. It appears

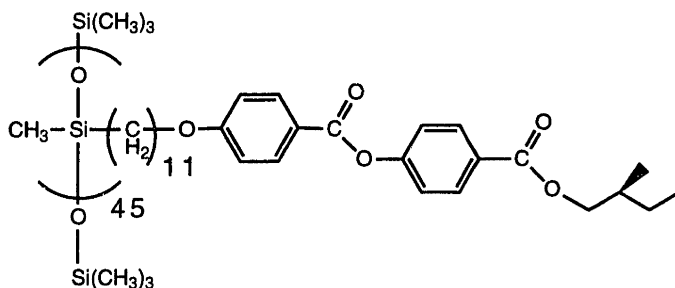
to us that the morphology may be a hindrance in achieving electro-optic switching for the samples we synthesized. In the case of the block copolymers, the sandwich technique was generally used. Two block copolymer samples, PS 14 – LCPA 129 and PS 39 – LCPA 30, were loaded into the 4 μ m cells by the capillary technique as well, but switching was not observed. We note that 30V/ μ m that was used to test the PS-LCP siloxanes is considerably less voltage than the 75V/ μ m reported by Mao et al.²so, our materials might switch at higher voltages.

The reason why our particular block copolymer samples did not show any electro-optic activity while Mao et al.² were successful in their demonstration of ferroelectric switching is likely due to the large difference in spontaneous polarization between the LCPs used by the two research groups. Figure 4.5 gives the spontaneous polarization (nC/ cm², measured 10°C below the S_C* - S_A transition) of two siloxane LCPs functionalized with mesogens analogous to mesogen A in this thesis and to Mao et al.'s mesogen . The LCP similar to those used in this thesis has a Ps of 8 nC/ cm², compared to a Ps of 420 nC/ cm² for the LCP analogous to Mao's, who used a 1,2-butadiene backbone instead of a siloxane backbone. The implication is that in order to observe bistable ferroelectric switching in a amorphous-S_C* block copolymer, the mesogen must be chosen to effect a large (order of 100s nC/ cm²) spontaneous polarization in the LCP block. The reason for the differences in spontaneous polarization has to do with the strength of the dipole in the mesogen and its placement with respect to the chiral center⁹.



G 21 k 57 S_C^* 161 S_A 183 i
Zentel, R., *Polymer*, 33, 4040-4046, 1992

Ps,
 n_C / cm^2
420



S_C^* 70 S_A 125 i
Suzuki, T., Okawa, T., *Makromol. Chem., Rapid Commun.* 9, 755-760, 1988

8

Figure 4.5 Spontaneous polarization of two LCP siloxanes taken from the literature. These LCPs are analogous to LCP blocks used in this thesis and in Mao et al.'s demonstration of switching in amorphous-LCP block copolymers¹⁰.

In addition to a low spontaneous polarization, there are a number of other reasons that can explain the lack of switching in our particular block copolymers. In the mesogen A series, the block copolymer PS 39 – LCPA 30, the LC lamellae are on the order of 60Å in thickness (Figure 3.9). The fact that the LC phase is confined in this small thickness likely reduces the mobility of the mesogens in the presence of an electric field. Moreover, any switching of the mesogens requires some rearrangement of the siloxane backbone, which is anchored to the PS lamellae through a covalent bond. In addition, the block copolymer morphology inherently presents orders of magnitude more surface to the LC material than a simple ITO cell presents to a LCP homopolymer. This large quantity

of surface may anchor the mesogens and large voltages would be necessary to overcome the surface forces.

4.4 Mechano-optic and X-Ray stretching investigation of mesogen A elastomers

Free standing films of PS 14 – LCPA 129 and PS 13 – LCPA 81 are elastomeric in nature; when stretched, they retract back to their original dimensions. The elastomeric nature of our samples is likely due to the combination of a low Tg ($\sim -30^{\circ}\text{C}$) and large molecular weight of the liquid crystalline block (80,000-120,000); the polystyrene blocks act as physical elements which add mechanical integrity and toughness. These elastomers break at $\sim 40\%$ strain, and are fully recoverable up to 8-10% strain. Under crossed polarizers these samples are highly birefringent, and the color and intensity of light passing through the polarizer are changed when the sample is stretched (Figures 4.6 and 4.7). Moreover, the optical texture returns to its original state after the sample retracts to its initial dimension.

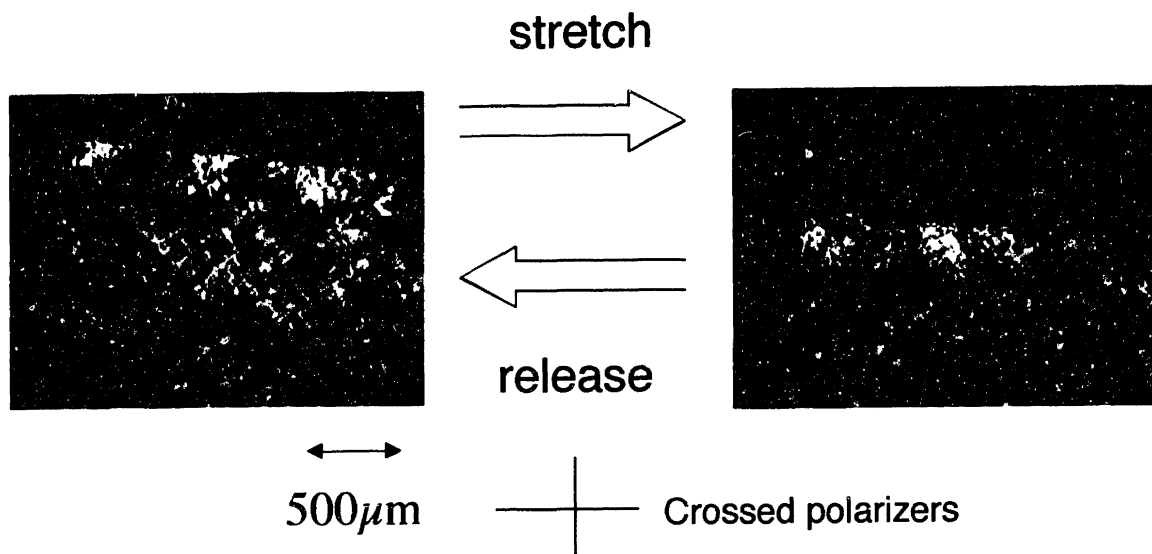


Figure 4.6 Mechano-optic effect in PS 13 - LCPA 81, on stretching to 12.5% strain. The LC domains in this polydomain sample change color on stretching.

Figure 4.6 shows one region of a 0.25mm thick free standing film (unoriented, polydomain LC film) under crossed polarizers as it is stretched and released. The direction of stretch is in the direction of one of the polarizers. As the film is stretched, color changes are observed in different regions. When the film is released, the optical texture returns back to its initial state. Most of the optical changes upon stretching happen within the first 1% of the stretch and that beyond this there is little change in the texture, that is to say the most important and measurable reorientation of the mesogens happens within the initial part of the stretch.

In select portions of the film light is extinguished upon stretching, as shown in Figure 4.7. The simultaneous observation of color changes and extinction in different regions of the films can be explained by perpendicular alignment of the mesogens with respect to the stretch direction.

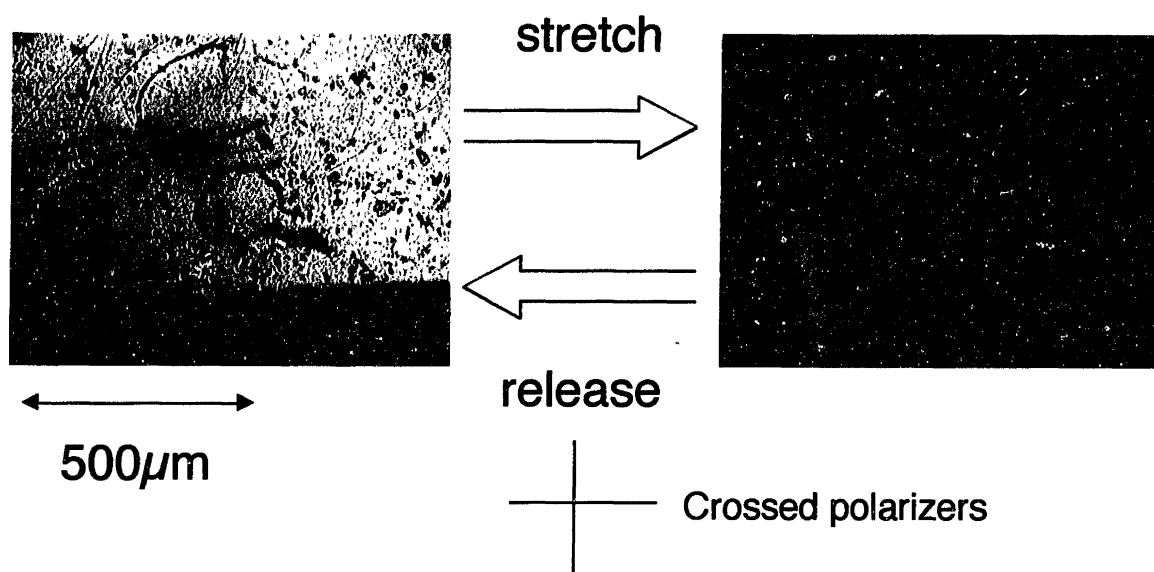


Figure 4.7 Optical microscope image of a mechano-optic effect in PS 14 - LCPA 129. The 0.25mm film was stretched to 8% strain between crossed polarizers; the result is the extinguishing of light.

To determine the mesogen orientation on stretching, polydomain (unoriented) samples of PS 14 LCPA 129 and PS 13 LCPA 81 were stretched and examined with SAXS in their stretched state. Figure 4.8 shows a schematic of this experiment and the resulting scattering patterns if the mesogens are oriented a) perpendicular to the stretch and b) parallel to the stretch direction. Figure 4.9 shows the SAXS pattern and the 2 theta integration around the smectic peak in a sample of PS 13 LCPA 81 that has been stretched to 20% strain. The data indicates that on average the smectic layers are parallel to the stretch direction and hence the mesogens are perpendicular to the stretch direction. Similar results were obtained for PS 14 LCPA 129. In principle, the orientation of the polystyrene cylinders with respect to the stretch direction can also be determined with this technique. In this case, however, the SAXS peak corresponding to the cylinders was not well defined, thus prohibiting an analysis of the cylinder orientation.

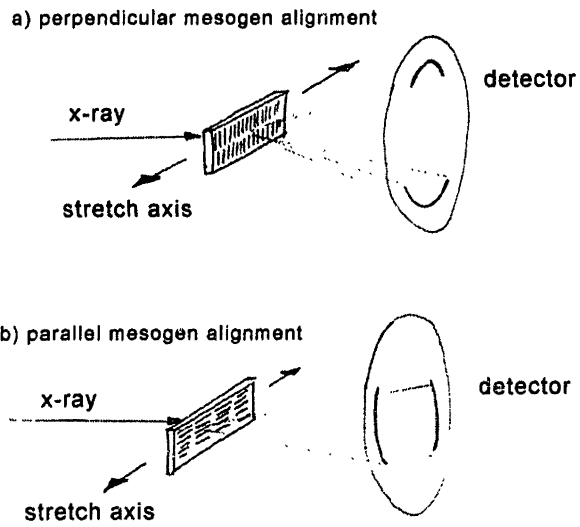


Figure 4.8 Schematic of SAXS stretching experiments showing scattering pattern when mesogens are aligned a) perpendicular and b) parallel to the stretch direction.

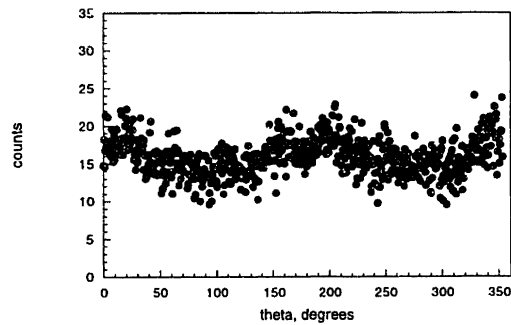
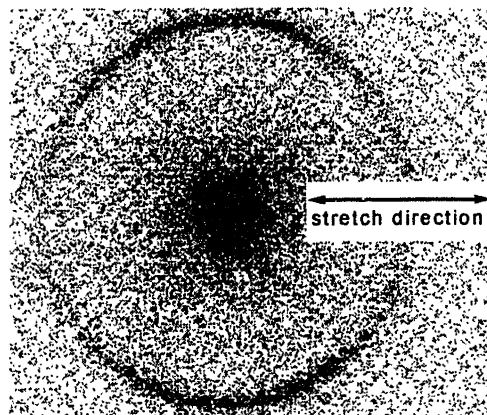


Figure 4.9 SAXS scattering pattern and integration around the smectic peak in a stretched sample (20% strain) of PS 13 LCPA 81. The results indicate that the mesogens reorient perpendicular to the stretch direction.

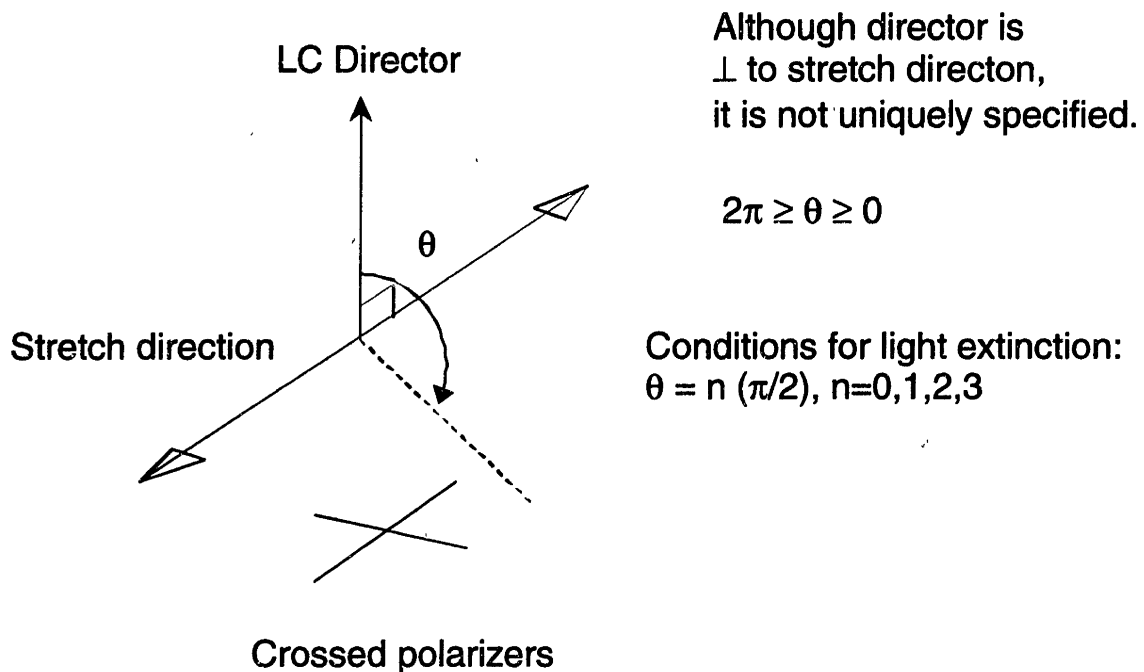


Figure 4.10 Schematic illustrating that mesogen orientation perpendicular to the stretch direction is not uniquely specified. The angle theta in the figure can take any value between 0 and 2π .

A perpendicular alignment of the mesogens with respect to the stress can explain our mechano-optic observations. In the macroscopic sample there were generally different color changes in different regions as the sample was stretched (Figure 4.6), while some regions, fewer in number, extinguish light (Figure 4.7). In the case of perpendicular alignment, the director is not uniquely specified by stretching, i.e. the angle theta in Figure 4.10 can take on any value. Thus, as the sample is stretched the director within each LC domain of the sample adopts a perpendicular alignment, but each domain maintains a unique value of theta.

In contrast to the perpendicular alignment of mesogens with the stretch direction, a parallel alignment of mesogens uniquely specifies the director and the optical axis, and we would expect light to be extinguished macroscopically by the crossed polarizers as it is stretched. This is the principle behind “nematic liquid single crystal elastomers” where a mechanical field uniformly aligns the mesogens in the stretch direction, resulting in macroscopic optical properties of a single crystal¹¹. This single-crystal orientation is usually a pre-requisite for a sample to have useful optical properties.

Kock et al. found that when nematic siloxane elastomers are stretched, both parallel and perpendicular alignment of the mesogens (w.r.t. the stretch direction) arise, depending on the spacer lengths¹². Spacers with three methylene units led to a perpendicular orientation, while spacers with four units yielded parallel orientation.

The orientation behavior of these nematic elastomers is thus rather sensitive to the specific LCP system under study, a theme which also occurs for smectic LCPs. For example, our stretching results differ from those of Zentel et al.¹³, who found that in smectic C* crosslinked elastomers, the mesogens orient parallel to the stretch direction. This situation is difficult to imagine topologically, since siloxane main chains would have to be oriented perpendicular to the stretch direction to accommodate the mesogens in their smectic layers. However, there are other examples of LCPs in which smectic mesogens align parallel to a shear field¹⁴, implying that the polymer backbone aligns perpendicular to the draw direction.

In smectic LCPs, the polymer main chains are generally considered to be perpendicular and somewhat confined between the smectic layers⁸, which leads to antagonism between mesogen alignment and polymer main chain alignment. In general,

the orientation of mesogens in smectic LCPs with respect to mechanical and shear flow fields is exceptionally system dependent, due to the delicate balance between the propensity of the mesogens and the polymer main chains to orient with respect to applied fields. For example, two chemically different smectic A LCPs can have opposite orientation behavior when drawn as fibers from melt^{14, 15}. This situation is further complicated when the smectic LCP forms one block of a block copolymer and the block copolymer domains are also subject to orientation.

Osuji et al.¹⁶ studied the orientation behavior of amorphous – smectic A block copolymers subjected to oscillatory shear. Above the clearing point of the LCP block, the sample behaved as a standard block copolymer and the cylinders oriented in the direction of shear. On the other hand, samples sheared below the LC clearing point had cylinders oriented traverse to the flow direction and smectic layers perpendicular to the flow direction. This behavior was attributed to competing orientation tendencies of the cylinders and the smectic layers, which led to a compromise in which neither element dominated. That is, the resulting orientation did not reflect the preferred orientation either an amorphous-amorphous block copolymer (cylinders in flow direction), or the LCP homopolymer analogue (smectic layers parallel to flow direction).

The observation that above the LC clearing point the block copolymer morphology dominates the orientation behavior is supported by fiber-drawing experiments on two different sets of amorphous-smectic A block copolymers^{14, 15}. Fibers drawn from the isotropic melt had the morphological elements oriented in the direction of the fiber, with the smectic layers generally perpendicular to these elements.

This was found to be the case even when the LCP homopolymer aligned with the smectic layers in the draw direction.

4.5 Chapter 4 Summary

The two main points of this chapter have been:

- (1) Ferroelectric electro-optic switching in the PS-LCP block copolymers is severely hindered relative to their LCP homopolymer counterparts.
- (2) LC elastomers are possible with diblock copolymers provided the LCP block has a high weight fraction (>0.8), high molecular weight ($\sim 100,000$), and low T_g (-30°C).

In addition, when the elastomeric materials are stretched, the mesogens orient perpendicular to the stretch direction such that the smectic layers and the siloxane main chains are parallel to the stretch direction. When the elastomeric samples were examined between crossed polarizers with an optical microscope, the optical texture of the sample was reversibly modulated by the application and release of strain, and in some cases light could be extinguished by the application of the strain.

4.6 References

1. Clark, N.A.; Lagerwall, S.T. *Appl. Phys. Lett.* **36**, 899-901 (1980).
2. Mao, G.; Wang, J.; Ober, C. K.; Brehmer, M.; O'Rourke, M. J.; Thomas, E. L. *Chem. Mater.* **10**, 1538-1545 (1998).
3. Ulrich, D.C. & Elston, S.J. in *The Optics of Thermotropic Liquid Crystals* (eds. Elston, S. & Sambles, R.) 196 (Taylor and Francis, London, 1998).
4. Vallerien, S. U.; Kremer, F.; Fischer, E.W. *Makromol. Chem. Rapid Commun.* **11**, 593-598 (1990).
5. Suzuki, T.; Okawa, T. *Makromol. Chem., Rapid Commun.* **9**, 755-760 (1988).
6. Schadt, M. in *Liquid Crystals* (ed. Stegemeyer, H.) 195-226 (Springer, New York, 1994).
7. Sekiya, T., et al. *Liquid Crystals* **14**, 1255-1267 (1993).

8. Zentel, R. in *Liquid Crystals* (ed. Stegemeyer, H.) 103-141 (Steinkopff Darmstadt, Springer, New York, 1994).
9. Blinov, L.M., and Chigrinov, V.G. *Electrooptic Effects in Liquid Crystal Materials* (Springer-Verlag, New York, 1994).
10. Mao, G.; Wang, J.; Ober, C.K.; O'Rourke, M.J.; Thomas, E.L.; Brehmer, M.; Zentel, R. *Polymer Preprints* **38**, 374-375 (1997).
11. Kupfer, J.; Finkelmann, H. *Makromol. Chem., Rapid Commun.* **12**, 717-726 (1991).
12. Kock, H.J., Finkelmann, H., Gleim, W. & Rehage, G. in *Polymeric Liquid Crystals* (ed. Blumstein, A.) 275-312 (Plenum Press, New York, 1983).
13. Zentel, R.; Reckert, G.; Bualek, S. *Makromol. Chem.* **190**, 2869-2884 (1989).
14. Yamada, M.; Iguchi, T.; Hirao, A.; Nakahama, S.; Watanabe, J. *Macromolecules* **28**, 50-58 (1995).
15. Yamada, M., *et al.* *Macromolecules* **32**, 282-289 (1998).
16. Osuji, C., Zhang, Y., Mao, G., Ober, C.K. & Thomas, E.G. *Macromolecules* **32**, 7703-7706 (1999).

Chapter 5 Blends and Homopolymer LC Properties

5.1 Context and Background

Blending small molecule liquid crystals in order to fine tune properties is a common practice in LC technology. Commercial LC displays generally use mixtures of small molecule mesogens to give the appropriate properties, such as a large temperature range of operation and good voltage transmission characteristics¹. Another application example is the blending of a small molecule chiral LC into a nematic LC matrix (either polymeric or monomeric), forcing the LC phase into a twisted nematic or cholesteric phase².

There may be advantages to blending a small molecule mesogen into PS-LCP diblocks, if the small molecule preferentially swells the LCP domains in the block copolymer. This would reduce the viscosity of the LCP phases and potentially enhance or enable electro-optic effects in the blends.

Along these lines small molecule mesogen A' (structure shown in Figure 4.2 and in Figure 2.5) was blended with homopolymer LCPA 47, homopolystyrene, and block copolymer PS 39 – LCPA 30. In addition LCPA 47 was blended with homopolystyrene, to compare the thermal properties of such a mixture to the block copolymers discussed in Chapter 3.

5.2 Mixtures of polystyrene with small molecule mesogen A'

This study was undertaken to determine the miscibility of the small molecule LC mesogen A' with polystyrene, with the ultimate objective of blending the small molecule

LC with the block copolymers and isolating the small molecule in the smectic LC siloxane microphase of the polymer. The small molecule LC by itself is a viscous liquid crystal at room temperature with a smectic C* to isotropic clearing point at 26°C, and the polystyrene standard has Mn = 29,000 and a Tg of ~104°C. All thermal measurements were made at 20°C/ min on the DSC. Samples were melt blended inside DSC pans for known times/ temperatures. SAXS was conducted on samples that were cast from toluene.

DSC runs were conducted before and after annealing a sample containing 47wt% polystyrene and 53wt% mesogen A' for 1hr at 125°C. The results are displayed in Table 5.1. After annealing, the PS Tg was depressed to 30°C from 107°C, and the mesogen A' clearing point decreased slightly from from 32°C to 31°C. The clearing point of the mesogen in this mixture is ~ 4°C higher than the clearing point of the pure mesogen, probably because the mixture has a slightly different thermal conductivity and heat capacity than the pure mesogen, or due to instrumental calibration. In addition, the clearing point enthalpy per gram of LC material decreased from 5.61J/g (no annealing) to 3.57 J/g after annealing. Assuming that the normalized enthalpy is proportional to the weight of liquid crystalline phase present in the mixture, we can estimate the composition of the two phases in the annealed sample to be 33wt% pure LC and 67% plasticized PS, where the PS phase contains 71% PS, 29% mesogen A'.

Table 5.1 Thermal data before and after annealing a mixture of polystyrene (47wt%) and mesogen A' (53wt%).

	PS Tg °C	Sc*-I clearing point °C	ΔH J/g mesogen A'
Before annealing	107	31.8	5.61
After annealing at 125°C for 1hr	30	30.6	3.57

This evidence shows that the small molecule mesogen A' is partially miscible with polystyrene, acting as a plasticizer. The small molecule is not completely miscible with the polystyrene at the concentration tested, however, as regions of the material exhibit LC ordering, as shown in both DSC and SAXS. The small molecule mesogen A' has a single smectic SAXS peak at 33\AA , and the mixture of polystyrene and the small molecule displayed a single smectic SAXS peak at 33\AA . Thus we have liquid crystalline regions that are in equilibrium with a mixture of polystyrene and the liquid crystal, illustrated schematically in Figure 5.1. It is important to note that in this instance, we didn't see any of the clearing point depression effects that were observed in the block copolymers.

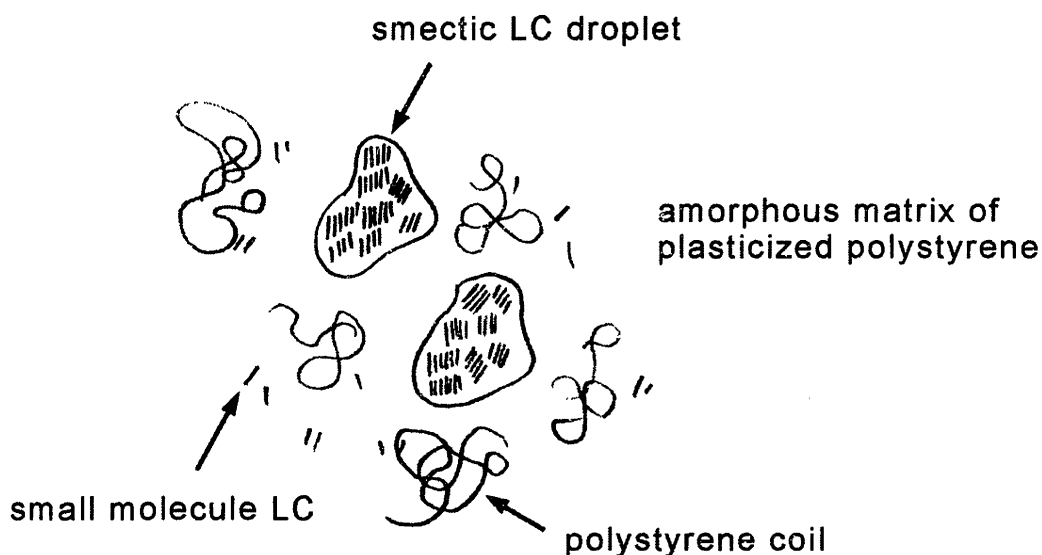


Figure 5.1 Schematic of polystyrene blended with mesogen A', forming a 2 phase system with LC droplets in equilibrium at room temperature with plasticized polystyrene.

5.3 Mixtures of polystyrene with LCPA 47

In this study, a 50/50 mixture of polystyrene 29K (anionic standard) and LCPA 47 was prepared and annealed at 125°C for 5hrs and then for 1.5 days. After 5hrs, both the T_g of PS and the LC clearing point remained unchanged; very little mixing and

plasticization of the PS occurred. The sample was further annealed for 1.5 days at 125°C, which depressed the PS Tg to 86°C, and the LC clearing point remained approximately the same at 90°C. The results are given in Table 5.2. Thus, LCPA 47 homopolymer does plasticize polystyrene by 15°C after a long annealing treatment, the kinetics of mixing between the polymers being slow. The clearing point enthalpy per gram of LCP decreases from 7.32 J/g to 5.26 J/g, also suggesting some mixing between the PS and the LCP. The LC clearing point, however, remains the same; the clearing point depression effect observed in the block copolymers does not appear in the homopolymer case.

Thus we can conclude that the clearing point depression phenomena observed in the mesogen A block copolymers is facilitated by the block copolymer architecture, which enhances the tendency of the blocks to mix and introduces large interfacial areas between domains. The covalent link between the two blocks is responsible for the increased tendency of the blocks to mix relative to their homopolymer analogues, a fact which is well documented experimentally and theoretically. In 1969 Meier showed that for an AB block copolymer “the critical molecular weights required for domain formation are greater (~2.5x) than required for phase separation of a simple mixture of the component blocks.³”

Table 5.2 Thermal properties of a 50/50 mixture of polystyrene and LCPA 47 before and after annealing treatments.

	PS Tg °C	Sc*-I clearing point °C	ΔH J/g LCP A 47
Before annealing	107	90.1	7.32
Anneal 5hr at 125°C	107	91.7	6.71
Anneal 30hr at 125°C	86	90.0	5.26

5.4 Mixtures of *Ic* siloxanes with small molecule mesogen

In this study, a mixture containing 51 wt% mesogen A' and 49% LCPA 47 was prepared and annealed in order to determine the miscibility of the small molecule mesogen A' and its polymer analogue. The results indicate complete miscibility between the components, as the mixture exhibits a single broad LC clearing range located between the clearing points of the pure components, as shown in Figure 5.2.

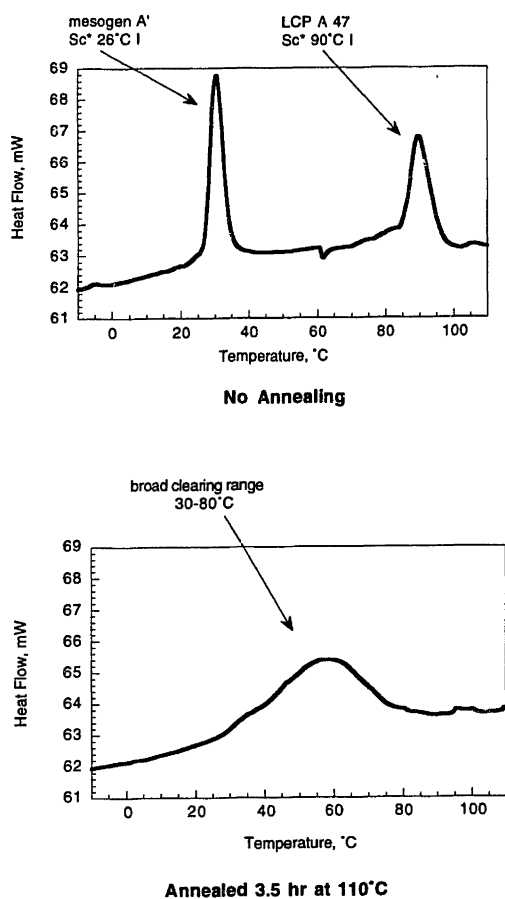


Figure 5.2 DSC heating traces illustrating the miscibility of mesogen A' and its polymer analogue LCPA 47.

5.5 Mixtures of ps-lcp block copolymers with small molecule mesogen

Sample PS 39 - LCPA 30 is a good block copolymer candidate to mix with mesogen A' as the LCP lamellae are small $\sim 60\text{\AA}$ (Figure 3.5) and swelling them with a small molecule would increase the mobility of the mesogens and thus make them more responsive to electric-fields. A solution of mesogen A' and PS 39 - LCPA 30 was cast from toluene onto a teflon film and the solvent evaporated overnight, yielding a film containing 77wt% block copolymer and 23wt% small molecule. Solution casting was chosen to insure that the small molecule is dispersed uniformly throughout the film. The DSC and SAXS measurements were made on this film, and the results are shown in Table 5.3. The addition of the small molecule further plasticized the polystyrene Tg to 43°C (from 84°C) and increased the LC clearing point to 58°C (from 43°C). In addition, the SAXS d spacing was reduced slightly from 286\AA to 274\AA . These results indicate that the small molecule mesogen A' partitions into both microphases of the block copolymer structure, plasticizing the polystyrene and in this case increasing the clearing point of the LC phase. The increase in LC clearing point is surprising because we expect that the addition of a small molecule LC to a LCP with a higher clearing point would result in a mixed phase with a clearing point intermediate between the two pure components, as in the case of LCPA 47 and mesogen A'.

It is possible that the addition of the small molecule modified the nature of the interface between the PS and the LCP phases in addition to changing the relative sizes and compositions of both phases, and these changes led to an increase in the LC clearing point.

After attempting many poling and alignment treatments, this mixture of PS 39 – LCPA 30 and mesogen A' did not show any electro-optic activity ($\pm 30\text{V}/\mu\text{m}$). We can speculate that a large quantity of the mesogen A' went into the polystyrene phase, and the remaining small molecule LC that went into the LCP phase did not increase the mesogen mobility enough to effect switching. Although in this case there was little benefit to blending the small molecule LC with the block copolymer, this avenue of exploration may still prove fruitful, as it is an experimentally facile way to modify the properties of the block copolymer.

Table 5.3 Thermal data and SAXS measurements of a mixture of mesogen A' and PS 39 – LCPA 30 compared to the pure block copolymer PS 39 – LCPA 30.

		PS Tg °C	LC clearing pt. °C	SAXS d, Å
PS 39 – LCPA 30		84	43	286
PS 39 – LCPA 30	77wt%	43	58	274
Mesogen A'	23wt%			

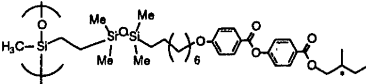
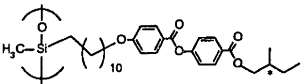
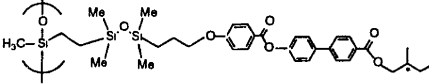
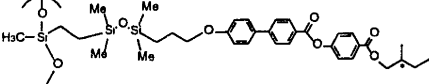

5.6 Thermal properties of LC homopolymers and small molecule mesogens

In this section, the properties of the various LC siloxane homopolymers synthesized are compared and discussed in the context of their structure. In addition, the LC properties of the small molecule mesogens before and after functionalization with tetramethyldisilane are examined and compared to their polymer analogues.

Figure 5.2 shows the three LC homopolymers synthesized for this work in addition to two examples taken from the literature. The polymers cited from the literature have aliphatic spacers, while those we synthesized contain an aliphatic/ disiloxane spacer.

Two conclusions can be drawn from Figure 5.2: 1) clearing points of the LCPs are lowered by the inclusion of a disiloxane spacer and 2) clearing points are raised by increasing the rigidity of the terminal group of the mesogen. These trends are in agreement with examples from the liquid crystalline literature^{4, 5}.

The fourth entry in the table deserves special comment, especially when compared to the third and fifth. We believe that the clearing point of this particular polymer is exceptionally low relative to the others because its low degree of substitution.

<u>Polymer structure</u>	<u>#Repeats</u>	<u>Clearing Pt. °C</u>
	72	97
	n/a	122-128 Ref. I
	50	145
	29	31
	38	241 Ref. II

I. Suzuki et al., *Macromol. Chem. Rapid Commun.* 9 755-760 (1988)

II. Cooray et al. *Polymer Journal*, 25, 863-872 (1993)

Figure 5.3 Table of some smectic C* LC siloxane homopolymers and their smectic clearing points.

Compounds without references were synthesized for this project, compounds with references were synthesized by other researchers, as indicated.

The backbone of LCPC 19 is based on poly D2V1, so the 69% substitution of the vinyl groups in this polymer must be adjusted to a 23% substitution rate when compared to the

other polymers in the table. We expect that if LCPC 19 were based on V3 and had comparable degrees of substitution to LCPA 47 and LCPB 35, its clearing point would be higher. Table 5.4 summarizes the LC and thermal properties of all the mesogens A, B, and C, as they progress from a vinyl terminated compound, to an Si-H terminated compound, to the final side-chain LCP. The important trend is that the attachment of tetramethyldisiloxane to the terminus of the mesogen lowers the clearing point. The clearing point then goes up on the transition from the small molecule to the LCP. These effects are illustrated in Figure 5.3 which shows how the clearing points change as the synthesis progresses.

Table 5.4 LC properties of mesogens and LC homopolymers.

compound	Thermal transitions in °C, transition enthalpies in (J/g)
Vinyl mesogen A	K 19.7 (1.84) Sc* 41.7 (8.56) I
Si-H mesogen A	Sc* 22.3 (5.36) I
LCPA 47	G -24 Sc* 90.0 (8.30) I
Vinyl mesogen B	K 101.5 (85.5) Sc* 153.6 (3.30) Sa 192.7 (2.01) I
Si-H mesogen B	Sc* 68.4 (3.77) I
LCPB 35	G - 8.5 Sc* 53.7 (1.32) Sa 145.0 (5.46) I
Vinyl mesogen C	K 127.8 (52.8) Sc* 204.3 (10.23) I
Si-H mesogen C	Sc* 85.2 (0.609) I
LCPC 18	Sc* 31.4 (4.27) I

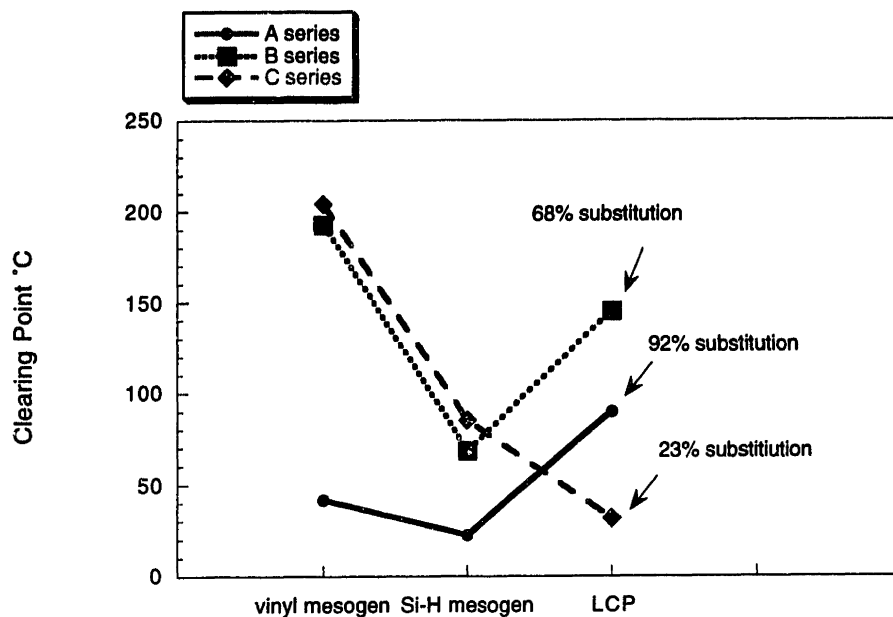


Figure 5.4 LC clearing points of materials as they progress from vinyl mesogen to Si-H tipped mesogen, and finally to the side chain liquid crystalline siloxane homopolymer.

The increase in clearing point after attaching the mesogen to the polymer backbone by 68°C and 77°C (mesogens A& B respectively) is in good agreement with previous studies on nematic siloxanes in which the clearing point increased by ~70°C on transition from monomer to polymer⁶. Attaching the mesogen to a polymer backbone restricts the motion of the mesogen and leads to a higher clearing point.

5.7 Chapter 5 Summary

The main points of this chapter have been that:

- (1) Mesogen A as a small molecule is a good plasticizer for polystyrene, reducing its T_g to 43°C in a 50/50 blend. The homopolymer LCPA plasticizes polystyrene to a lesser extent, reducing its T_g to 86°C in a 50/50 blend. These observations suggest a favorable enthalpic interaction between PS and LCPA which is corroborated by the observation of phase mixing in a low MW PS LCPA sample.

- (2) The disiloxane spacer reduces the clearing point in LCP siloxanes by about 30°C relative to aliphatic spacers.

5.8 References

1. Collings, P.J. *Liquid Crystals: Nature's Delicate Phase of Matter* 1-129-130 (Princeton, NJ, 1990).
2. Meier, W.; Finkelmann, H. *Makromol. Chem. Rapid Commun.* **11**, 599-605 (1990).
3. Meier, D.J. *J. Polymer Sci.: Part C* **26**, 81-98 (1969).
4. Hempenius, M.A., Lammertink, R.G. & Vansco, J.G. *Macromolecules* **30**, 266-272 (1997).
5. Gray, G.W. in *Polymer Liquid Crystals* (eds. A., C., W.R., K. & R.B., M.) 1-33 (Academic Press, New York, 1982).
6. Stevens, H., Rehage, G. & Finkelmann, H. *Macromolecules* **17**, 851 (1984).

Chapter 6 Conclusions and Future Directions

6.1 Conclusions

A synthetic scheme was developed that allows for the synthesis of diblock copolymers containing polystyrene and side-chain liquid crystalline siloxane blocks. A wide variety of properties and morphologies are accessible by changing the side-chain mesogen in the siloxane block and the block MW's in the block copolymer. Increasing the volume fraction of liquid crystal block, for example, changes the mechanical properties from hard and brittle to rubbery and elastomeric. Those block copolymers with low T_g ($\sim -30^\circ\text{C}$) and high weight fraction liquid crystal blocks (>0.8) formed liquid crystalline elastomers, the morphology being PS cylinders in an LCP matrix. Small angle X-Ray measurements on these samples indicate that the mesogens orient perpendicular to the stretch direction when stretched. The mesogen reorientation on stretching was observed in optical microscopy as changes in optical texture, and in some cases as an extinguishing of light. Block copolymers with large weight fraction liquid crystal blocks (0.8), large MW ($\sim 100\text{K}$) and with a T_g of -9°C were not rubbery at room temperature, and formed brittle films that did not stretch when pulled.

Two series of block copolymers were prepared, each with a different smectic C* mesogen. Miscibility between polystyrene blocks and liquid crystalline siloxane blocks was not expected, but was observed in the case of the less rigid mesogen with low molecular weight blocks. This is due to a favorable interaction between the mesogen and polystyrene. In fact, it was shown that mesogen A as a small molecule is a good plasticizer for polystyrene.

In addition to block copolymers, a series of liquid crystalline side-chain siloxane homopolymers were prepared. The more rigid mesogen led to higher clearing points and T_g 's in the homopolymers, and incorporation of a disiloxane spacer into the mesogens of siloxane LCPs was found to decrease the clearing point relative to aliphatic spacers. In addition, low degrees of mesogen substitution along the siloxane backbone were found to considerably lower the clearing point.

Electro-optic switching was facile in the LC homopolymers. In fact, all of the LCP homopolymers synthesized showed electro-optic activity, while none of the block copolymer samples did ($\pm 30V/\mu\text{m}$). It appears that mesogen mobility is reduced in the block copolymers due to the anchoring of the siloxane chains to the polystyrene domains through a covalent bond. This supports the notion that the main chain in side-chain LCP siloxanes must rearrange to accommodate electro-optic switching of mesogens. The large surface areas between the LCP and amorphous domains may also play a role in reducing the mobility of the mesogens. A comparison of the work in this thesis to the work of Mao et al.¹ suggests that in order to observe bistable ferroelectric electro-optic switching in amorphous-LCP block copolymers, the LCP homopolymer must possess a high spontaneous polarization (order of 100's of nC/cm^2).

6.2 Future Directions

A continued exploration of PS-LCP siloxane diblock polymers with different mesogens and block lengths may answer many questions that this work has left open, and may lead to useful new information and conclusions. There are examples mesogens that have good electro-optic properties and also contain a bromine or chlorine functionality likely to raise χ and thus drive phase segregation^{2, 3}.

Another natural extension of this work would be the synthesis of PS-LCP-PS triblocks with siloxane LCP middle blocks, as the resulting materials should have attractive elastomeric properties combined with liquid crystallinity. Two other groups have made PS-LCP-PS triblocks^{4, 5}, but the middle LC blocks had a T_{gs} of ~120°C and 30°C prohibiting elastomeric properties at room temperature. The synthetic technique employed by Sanger et al. involves polymer analogous reactions to a polystyrene-poly(1,2-butadiene)-polystyrene block copolymer. Poser et al. use a similar scheme, except they successfully couple living diblock copolymers using terephthalic acid dichloride prior to functionalizing the triblock with mesogens. These authors report difficulty using dichlorodimethylsilane as a coupling agent, and had success with terephthalic acid dichloride. Terephthalic acid dichloride would be a poor choice of a coupling agent for the siloxane system (used for this thesis), however, since it would result in the formation of silylesters which are exceptionally susceptible to hydrolysis.

The synthesis of PS-LCP-PS triblocks was attempted for this thesis using two methods: 1) the coupling of living diblocks to form triblocks by the addition of a coupling agent, dichlorodimethylsilane, and 2) using a LCP macroinitiator with benzyl chloride end groups to initiate the polymerization of styrene via ATRP. Both methods have been used to make PS-PDMS-PS triblocks⁶⁻⁹, but proved experimentally difficult, as discussed in Chapter 2. It is the author's opinion that both of these methods are viable for making PS-LCP-PS block copolymers with siloxane middle block using poly V3 as the middle block.

Finally, piezo-electric measurements on well ordered samples of the PS-LCP block copolymers can be performed to determine if the PS-LCP diblocks have piezo-

electric properties similar to those found in side chain LCP elastomers with the Sc* LC phase^{10, 11}.

6.3 References

1. Mao, G.; Wang, J.; Ober, C.K.; O'Rourke, M.J.; Thomas, E.L.; Brehmer, M.; Zentel, R. *Polymer Preprints* **38**, 374-375 (1997).
2. Cooray, N.F.; Kakimoto, M.; Imai, Y.; Suzuki, Y. *Macromolecules* **27**, 1592-1596 (1994).
3. Hsiue, G-H; Chen, J-H *Macromolecules* **28**, 4366-4376 (1995).
4. Poser, S., Fischer, H. & Arnold, M. *Journal of Polymer Science* **34**, 1733-1740 (1996).
5. Sanger, J. & Gronski, W. *Macromol. Chem. Phys.* **199**, 555-561 (1998).
6. Nakagawa, Y. & Matyjaszewski, K. *A.C.S. Polymer Preprints* **37**, 270-271 (1996).
7. Nakagawa, Y., Miller, P., Cristina, P. & Matyjaszewski, K. *A.C.S. Polymer Preprints* **38**, 701-702 (1997).
8. Morton, M., Kesten, Y., Fetters, L.J. *Polymer Preprints, ACS, Div. of Polymer Chemistry* **15**, 175-177 (1974).
9. Davies, Jones *Ind. Eng. Chem., Product Research Division* **10**, 168 (1971).
10. Vallerien, S. U.; Kremer, F.; Fischer, E.W. *Makromol. Chem. Rapid Commun.* **11**, 593-598 (1990).
11. Brehmer, M.; Zentel, R. *Macromol. Chem. Phys.* **195**, 1891-1904 (1994).

THESIS PROCESSING SLIP

FIXED FIELD: ill. _____ name _____

index _____ biblio _____

► COPIES: Archives Aero Dewey Eng Hum
Lindgren Music Rotch Science

TITLE VARIES: ► _____

NAME VARIES: ► Joseph

IMPRINT: (COPYRIGHT) _____

► COLLATION: 130 2

► ADD: DEGREE: _____ ► DEPT.: _____

SUPERVISORS: _____

NOTES:

cat'r:	date:
DEPT: Chem. Eng	page: F49
YEAR: 2000	DEGREE: Ph. D.
NAME: MONTGOMERY, Alaron	